Denudation history and internal structure of the Front Range and Wet Mountains, Colorado, based on apatite-fission-track thermochronology

Shari A. Kelley[1] and Charles E. Chapin[2]

[1]*Department of Earth and Environmental Science, New Mexico Institute of Mining and Technology, Socorro, NM 87801*
[2]*New Mexico Bureau of Geology and Mineral Resources, New Mexico Institute of Mining and Technology, Socorro, NM 87801*

Abstract

An apatite fission-track (AFT) partial annealing zone (PAZ) that developed during Late Cretaceous time provides a structural datum for addressing questions concerning the timing and magnitude of denudation, as well as the structural style of Laramide deformation, in the Front Range and Wet Mountains of Colorado. AFT cooling ages are also used to estimate the magnitude and sense of displacement across faults and to differentiate between exhumation and fault-generated topography. AFT ages at low elevationX along the eastern margin of the southern Front Range between Golden and Colorado Springs are from 100 to 270 Ma, and the mean track lengths are short (10–12.5 μm). Old AFT ages (> 100 Ma) are also found along the western margin of the Front Range along the Elkhorn thrust fault. In contrast AFT ages of 45–75 Ma and relatively long mean track lengths (12.5–14 μm) are common in the interior of the range. The AFT ages generally decrease across northwest-trending faults toward the center of the range. The base of a fossil PAZ, which separates AFT cooling ages of 45– 70 Ma at low elevations from AFT ages > 100 Ma at higher elevations, is exposed on the south side of Pikes Peak, on Mt. Evans, on Mt. Logan, in Waterton Canyon, and on Crow Hill. The elevation of the base of the PAZ ranges from ~ 3,500 m on Mt. Evans to ~ 1,700 m at the mouth of Waterton Canyon. The distribution of the AFT ages > 100 Ma, which lie within the PAZ, is used to document that the eastern and western margins of the Front Range were thrust laterally over the adjoining basins, while the center of the range was uplifted with respect to the margins.

An abrupt change in structural style along the eastern margin of the Front Range occurs between Golden Gate and Von Bibber Canyons, just north of Golden, Colorado. To the south, east-verging thrusts and > 100 Ma AFT ages characterize the margin. To the north, southwest-verging back thrusts and 50–80 Ma AFT ages prevail along the margin. The PAZ is not present in the northeastern Front Range, even at elevations as high as the summit of Longs Peak (4,346 m). We interpret the difference in structural style and cooling history in the northern Front Range to be in part related to the thermal effects of pluton emplacement along the Colorado Mineral Belt during Laramide deformation and in part due to dramatic changes in the thickness in the Late Cretaceous Pierre Shale between Golden and Boulder.

AFT ages from the northern Wet Mountains are typically 140–300 Ma, with older ages at high elevation. The AFT age and track-length data in the northern Wet Mountains are characteristic of samples within the PAZ. The lack of exposure of Laramide cooling ages below the PAZ, as seen in the Front Range, implies that lateral movement above thrust faults rather than vertical uplift was the dominant style of Laramide deformation in this area. AFT ages in the southern Wet Mountains vary from about 230 Ma for Proterozoic rocks collected a short distance below the summit of Greenhorn Mountain to approximately 30 Ma at the lowest elevation. The low elevation samples reflect cooling during middle Cenozoic time.

Preservation of the Late Cretaceous PAZ along the eastern margin of the southern Front Range and northern Wet Mountains, as well as the lack of late Cenozoic cooling ages, indicates that the east-facing escarpment of these ranges is due to erosional exhumation of Laramide structure rather than late Cenozoic faulting. Middle Cenozoic cooling is recorded in the AFT length data of the Front Range and Wet Mountains, and this signal becomes progressively stronger toward the south. The AFT data from surface samples are not sensitive to late Cenozoic epeirogenic uplift; the AFT data do not indicate significant differential uplift between the frontal ranges and the High Plains in late Cenozoic time, except perhaps at the south end of the Wet Mountains.

Introduction

Two long-standing controversies in Southern Rocky Mountain geology, the style and mechanics of Laramide deformation and the timing and magnitude of Cenozoic uplift, are investigated in this paper using apatite fission-track thermochronology. Apatite fission-track (AFT) data from the Front Range and the Wet Mountains in Colorado (Fig. 1) are used to evaluate the relative importance of Laramide mountain flank thrusting and questions concerning the development of the east-facing topographic escarpment along the frontal ranges of northern and central Colorado. The Front Range and the Wet Mountains are ideal places to examine using this thermochronologic tool. Several streams have carved deep canyons into the ranges, providing access for cross-strike traverses and significant topographic relief for age-elevation traverses. Total relief in the ranges exceeds 2.6 km. Preservation of a Late Cretaceous apatite partial annealing zone (PAZ) in the southern Front Range and in the Wet Mountains, which was originally discovered by Naeser (1979a), adds a particularly useful structural datum (Fig. 2). The base of the fossil PAZ is interpreted to represent the position of the ~ 110 °C isotherm at the time that Colorado was at sea level in Late Cretaceous time. This marker has since been disrupted by Laramide and post-Laramide tectonic and thermal events. The Rocky Mountain erosion surface, which in places is capped by the late Eocene Wall Mountain Tuff (McIntosh and Chapin 2004 this volume), is a second structural datum. The fossil PAZ,

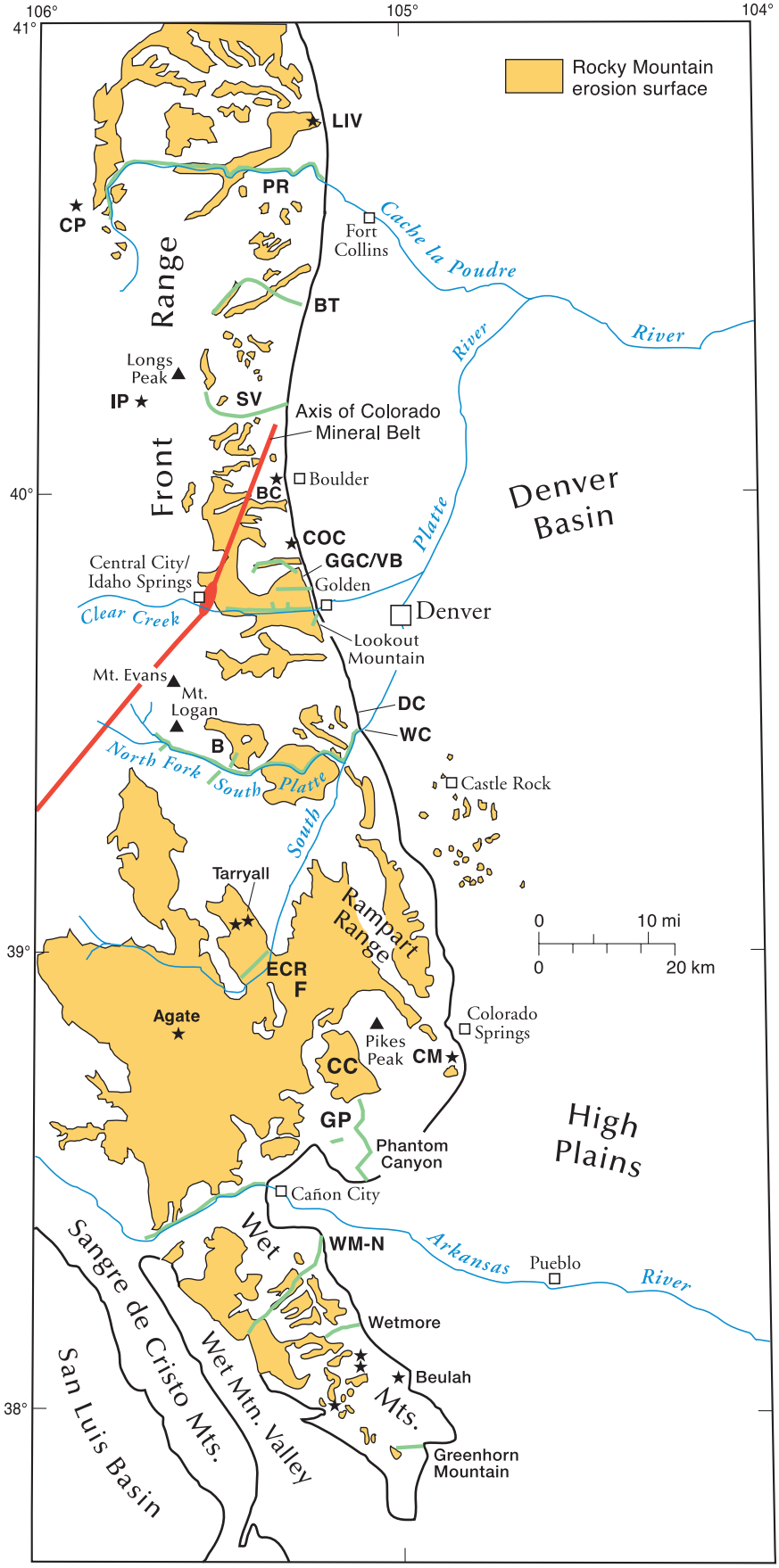

FIGURE 1—Index map of Front Range and Wet Mountains showing fission-track sample traverses (green lines), isolated sample localities (stars), geographic areas mentioned in the text, and distribution of the Rocky Mountain erosion surface (shaded). Traverses from north to south are Livermore (**LIV**); Poudre River (**PR**); Big Thompson (**BT**); St. Vrain (**SV**); Indian Peaks (**IP**); Boulder Canyon (**BC**); Coal Creek Canyon (**COC**); Golden Gate Canyon/Von Bibber Creek (**GGC/VB**); Lookout Mountain/Clear Creek, Deer Creek (**DC**); North Fork of the South Platte River; Tarryall Reservoir/Elevenmile Canyon Reservoir/Agate Creek (**ECR**); Cheyenne Mtn. (**CM**); Phantom Canyon; Garden Park (**GP**); Arkansas River; Wet Mountains-north (**WM-N**); Wetmore, and Greenhorn Mountain. Other key localities shown include: **CP** = Clark Peak; **B**= Bailey, **WC** = Waterton Canyon; **F** = Florissant fossil beds; and **CC** = Cripple Creek volcanic field. Distribution of the Rocky Mountain erosion surface is from Coleman (1985); note remnants of the Rocky Mountain surface on the High Plains near Castle Rock. Location of Idaho Springs/Central City mining district from Sims (1963) and approximate trend of Colorado Mineral Belt from Bryant et al. (1981).

when used in conjunction with temperature histories derived from track-length data, can be used to estimate total rock uplift and total denudation of this area since Laramide deformation (Pazzaglia and Kelley 1998). The Rocky Mountain erosion surface further allows us to constrain Laramide denudation. Evaluation of regional late Cenozoic epeirogenic uplift (McMillan et al. 2002; Leonard 2002) is outside the scope of this study.

The structural style and mechanics of Laramide (Late Cretaceous–middle Eocene) deformation of the Front Range and Wet Mountains have been subjects of debate for many decades and remain so today. Recent papers by Weimer (1996), Weimer and Ray (1997), Kelley and Chapin (1997), and Erslev et al. (1999) furnish good reviews of the topic, as well as useful new insights. An impediment to structural analysis of the interior of these ranges has been the lack of a structural datum in the Proterozoic rocks that form the cores of the mountains. In this study we provide a structural datum, namely the base of the fossil PAZ for fission tracks in apatite that developed during Mesozoic burial of the area and was deformed primarily during the Laramide orogeny. This datum was at a depth of 2.5–4 km at the beginning of Maastrichtian time (~ 71 Ma; Weimer 1996). The PAZ was approximately horizontal, but had some relief on it

due to differences in Phanerozoic sediment thickness and facies changes across the area, variations in the fluorine/chlorine ratio in the apatite in different Proterozoic lithologies, and elevated geothermal gradients in the vicinity of Laramide intrusives. However, abrupt changes in the elevation of the PAZ over short lateral distances observed today are likely the result of Laramide or post-Laramide faulting.

A second significant controversy concerns the timing and magnitude of Cenozoic uplift and erosion of the Front Range and Wet Mountains. Much of the debate centers on the interpretation of paleoELEVATION information extracted from studying the morphology of fossil leaves. During middle to late Eocene time, a regional erosion surface of relatively low relief developed on Proterozoic rocks exposed in the Front Range and Wet Mountains and extended eastward onto Laramide synorogenic deposits on the High Plains (Epis and Chapin 1975). This surface, the Rocky Mountain erosion surface (Evanoff and Chapin 1994), was subsequently covered in some areas by volcanic and volcaniclastic units including the 36.7 Ma Wall Mountain Tuff (Epis and Chapin 1974; McIntosh and Chapin 1994; 2004 this volume) and the upper Eocene Castle Rock Conglomerate (Welch 1969; Morse 1985). MacGinitie (1953) concluded from his study of the Florissant leaves that the flora grew at elevations ranging from 300 to 900 m during late Eocene time. The plants are preserved in 34.1 Ma (McIntosh and Chapin 2004 this volume) sediments that overlie the Wall Mountain Tuff in a paleovalley on the Rocky Mountain erosion surface (Fig. 1). The present elevation of Florissant is ~ 2.5 km. Epis and Chapin (1975) proposed, on the basis of MacGinitie's interpretation, that the Southern Rocky Mountains developed moderate relief during Laramide deformation, that the mountains were eroded to a surface of low relief with an elevation of 300–900 m by approximately 35 Ma, and that the erosion surface was subsequently uplifted 1.5–2.0 km during late Cenozoic time. Epis and Chapin (1975) constructed a schematic cross section from the Sawatch Range northeastward across the Front Range that emphasized late Cenozoic block faulting of the late Eocene surface, including high-angle normal faulting on the east side of the Front Range. However, re-evaluation of the Florissant flora using new techniques developed by Wolfe (1992) and Wolfe et al. (1998) led Meyer (1986; 1992), Gregory (1992), and Gregory and Chase (1992) to infer that the Florissant area was at an elevation of 2.2–3.3 km during late Eocene time. These findings led Gregory and Chase (1994) and Chapin and Cather (1994) to suggest that the Southern Rocky Mountains attained their current elevation during Laramide crustal thickening. An essential piece to the puzzle was added by Leonard and Langford (1994), who demonstrated that the remnants of the upper Eocene Wall Mountain Tuff overlying the synorogenic sedimentary package on the High Plains can be projected upslope to near the crest of the Front Range, leaving little room for late Cenozoic fault offset between the High Plains and the Front Range. Thus, during late Eocene time, the eastern front of the Southern Rocky Mountains was buried under approximately 1 km of sediment derived from the mountains. The present-day 500–1,000-m east-facing escarpment along the eastern Front Range is therefore the result of differential erosion and removal of these sediments during late Cenozoic time (Leonard and Langford 1994; Chapin and Cather 1994). More recently, the methods of Wolfe (1992) have been called into question by Meyer (2003) and the mean annual temperatures that form the basis of the paleoelevation analysis of Gregory (1992) may be 5 °C too low. Much of the discussion concerning the topographic evolution of the Southern Rocky Mountains is focused on the area around the southern Front Range (Fig. 1), where late Eocene volcanic and sedimentary rocks are preserved on the High Plains and where the erosion surface can be dated both in the mountains and on the High Plains. Epis and Chapin (1975), Leonard and Langford (1994), and Gregory and Chase (1992, 1994) have all made the tacit assumption that other portions of the Southern Rocky Mountains with well-developed erosion surfaces share a similar history. In this study, we use AFT ages and preservation of the Late Cretaceous PAZ to evaluate this assumption.

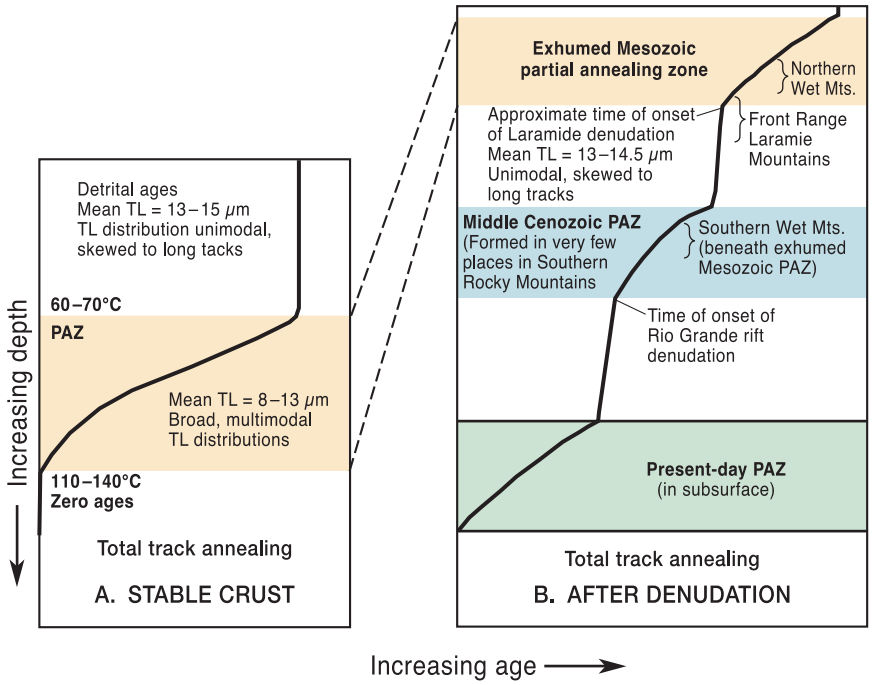

FIGURE 2—Diagram showing the relationship of fission-track age and length as a function of depth during maximum burial in Late Cretaceous time (**A**), and after denudation (**B**). Diagram described in the text. **TL** = track length. **PAZ** = partial annealing zone. **SRM** = Southern Rocky Mountains. Representative portions of the AFT age-depth curve that are preserved in the Front Range and Wet Mountains are shown for reference. Modified from Naeser (1979b) and Pazzaglia and Kelley (1998).

The interpretations presented in this paper are based on data derived from nearly 200 samples collected from the Colorado–Wyoming state line in the northern Front Range to Greenhorn Mountain at the south end of the Wet Mountains (Fig. 1). Published AFT data from Naeser (1979b), Bryant and Naeser (1980), Cervany (1990), Cunningham et al. (1994), McCallum and Naeser (1977), Sharp and Naeser (1986), and Naeser et al. (2002) were also incorporated into the analysis. Detailed descriptions of the data are presented as a series of maps, age-elevation plots, and track-length histograms for seven areas in the Front Range and Wet Mountains. The data are then integrated into a series of east-west schematic cross sections and one north-south cross section that illustrate our biases in resolving the controversies mentioned above. The data are also used to assess the amount of denudation asso-

ciated with early versus late Laramide deformation and subsequent middle Cenozoic erosion that led to development of the Rocky Mountain erosion surface on the Front Range and Wet Mountains. These results include the previously overlooked influence of the low-thermal conductivity Pierre Shale on rock uplift and denudation calculations. The thermal effects of the Colorado Mineral Belt and significant latest Eocene to Oligocene volcanism in central Colorado on the AFT data are also evaluated.

Fission-track analysis

Chemical composition and temperature are the primary factors controlling fission-track annealing in the mineral apatite. Green et al. (1986) noted that tracks in chlorapatite are more resistant to annealing than those in fluorapatite. Carlson et al. (1999) demonstrated that the composition of apatite can affect the annealing temperature of tracks by as much as 30 °C. In a relatively stable geological environment where temperatures vary uniformly as a function of depth, AFT age and track lengths decrease systematically with depth (Fig. 2a; Naeser 1979a; Fitzgerald et al. 1995). At temperatures less than 60– 70 °C, tracks that are produced by the spontaneous fission of ^{238}U are retained and annealing is relatively minor (Fig. 2a). The AFT ages of detrital grains in sedimentary rocks at shallow depths (temperatures < 70 °C) are equivalent to or greater than the stratigraphic age of the rock unit and the mean track lengths range from 13 to 15 μm. In the temperature range known as the partial annealing zone (PAZ), which is between 60–70 °C and 110–140 °C, depending on the composition of the apatite and the duration of heating, the AFT ages and track lengths are reduced compared to the original AFT ages and lengths. Mean track lengths in the PAZ are typically 8–13 μm. Finally, at temperatures above 110–140 °C, tracks that are formed are quickly destroyed and the fission-track age is zero. If after a period of relative stability, the crust is rapidly cooled during denudation related to a tectonic event, the fossil PAZ may be exhumed and the time of cooling and the paleodepth of the top or bottom of the PAZ can be estimated (Fig. 2b; Gleadow and Fitzgerald 1987). If the tectonically disturbed area cools rapidly (> 5° C/m.y.), the mean track lengths in rocks that are at the base of the fossil PAZ (below the break-in-slope on the age-depth profile) are generally > 14 μm, and the AFT ages from below the base of the exhumed PAZ can be used to estimate the timing of the onset of denudation. If the rock column cools more slowly during uplift and/or erosion, the mean track length at the base of the fossil PAZ is typically < 14 μm, and the apparent AFT age more loosely constrains timing of the initiation of cooling (Foster and Gleadow 1992).

Recently, Kamp and Tippett (1993) and Fitzgerald et al. (1995) demonstrated that AFT analysis is a powerful tool in evaluating the tectonic and denudational history of mountain systems in convergent settings. Using the elevation of the base of the PAZ, the timing of denudation recorded below the PAZ, estimates of mean surface elevation before and after a tectonic event, and estimates of paleogeothermal gradients and surface temperatures, these authors were able to constrain surface uplift, rock uplift, and denudation. Surface uplift and rock uplift are both tied to the same frame of reference, mean sea level. Surface uplift is vertical motion of the earth's surface with respect to mean sea level, whereas rock uplift is the displacement of rock from the subsurface toward the surface with respect to mean sea level. In contrast, denudation is tied to a different frame of reference, the earth's surface, and it is a measure of displacement of rock with respect to the surface. The three types are motion are related:

$$\text{surface uplift} = \text{rock uplift} - \text{denudation}$$

The isostatic and tectonic components of denudation can be estimated from:

$$\text{Isostatic} = [\text{crustal density } (2.7\ \text{gm/cm}^3)/\text{mantle density } (3.3\ \text{gm/cm}^3)] \times \text{denudation}$$

$$\text{Tectonic} = \text{rock uplift} - \text{isostatic component}$$

Methods

More than 200 samples were collected from Proterozoic rocks exposed in the Front Range and the Wet Mountains (Fig. 1). A three-part sampling strategy was adopted in this study. First, we collected samples along age-elevation traverses in areas with significant vertical relief along the margins of the ranges (Lookout Mountain, Colorado Springs area, Pikes Peak, and Wet Mountains). Elevations of the samples were determined from U.S. Geological Survey 1:24,000 scale topographic maps to an estimated accuracy of ± 6 m. Next we sampled in the major drainages of the range and we found that the cooling history in the center of the Front Range was different from that on the margins. We then sampled on either side of mapped faults intersecting major valleys within the range in an effort to locate structures that accommodated the transition between areas with contrasting cooling histories. Additional areas with significant vertical relief within the range (e.g., Mt. Logan and Longs Peak) were examined in this stage of the study.

The fission–track analysis methods used in this study are fully described in Kelley et al. (1992) and are briefly summarized here. Apatite was separated from the samples using standard heavy-liquid and magnetic separation techniques. Apatite grains were mounted in epoxy, polished to expose the grains, and etched for 25 seconds in a 5 M solution of nitric acid to reveal the fission tracks. The grain mounts were then covered with muscovite detectors and sent to the Texas A&M Nuclear Science Center for irradiation. The neutron flux was calibrated with Durango apatite age standards and Corning Glass CN-6. A zeta value of 5,516 ± 300 was determined using the CN-6 glass and the accepted age of 31.4 ± 0.5 Ma for Durango apatite (Green 1985). Individual grain ages were calculated using the methods of Hurford and Green (1983), and the χ^2 statistic (Galbraith 1981) was applied to determine whether the individual ages belong to a single population. Mixed ages caused by partial annealing of apatite with variable chemical composition and/or sedimentary provenance are indicated when the ages do not pass the χ^2 statistic at the 5% probability level. If the individual-grain ages pass the χ^2 test, the pooled age is computed using the methods of Galbraith and Laslett (1985). If the sample fails the χ^2 test, the central age, a weighted mean age estimate that eliminates a bias toward grains with higher mean track densities, is calculated as outlined by Galbraith and Laslett (1993). The pooled age and central age are identical for χ^2 probabilities > 85%. Several samples of gneiss and schist that are interpreted to have been within the partial annealing zone during Mesozoic burial of the region fail the χ^2 test. Failure of the test is likely due to differences in chemical composition among the apatite grains in these metasedimentary rocks. Rounded apatite grains and the presence of grains with large etch pits, which is indicative of higher chlorine concentrations (Donelick 1991), were observed in the gneiss and schist samples failing the statistical tests.

Confined track-length distributions in the apatite-grain mounts were determined using a microscope fitted with a 100-x dry lens, a drawing tube, and a digitizing tablet. Horizontal, well-etched, confined tracks (tracks completely enclosed within the crystal) in grains with prismatic faces were measured. The orientation of the tracks with respect to the c-axis was also determined.

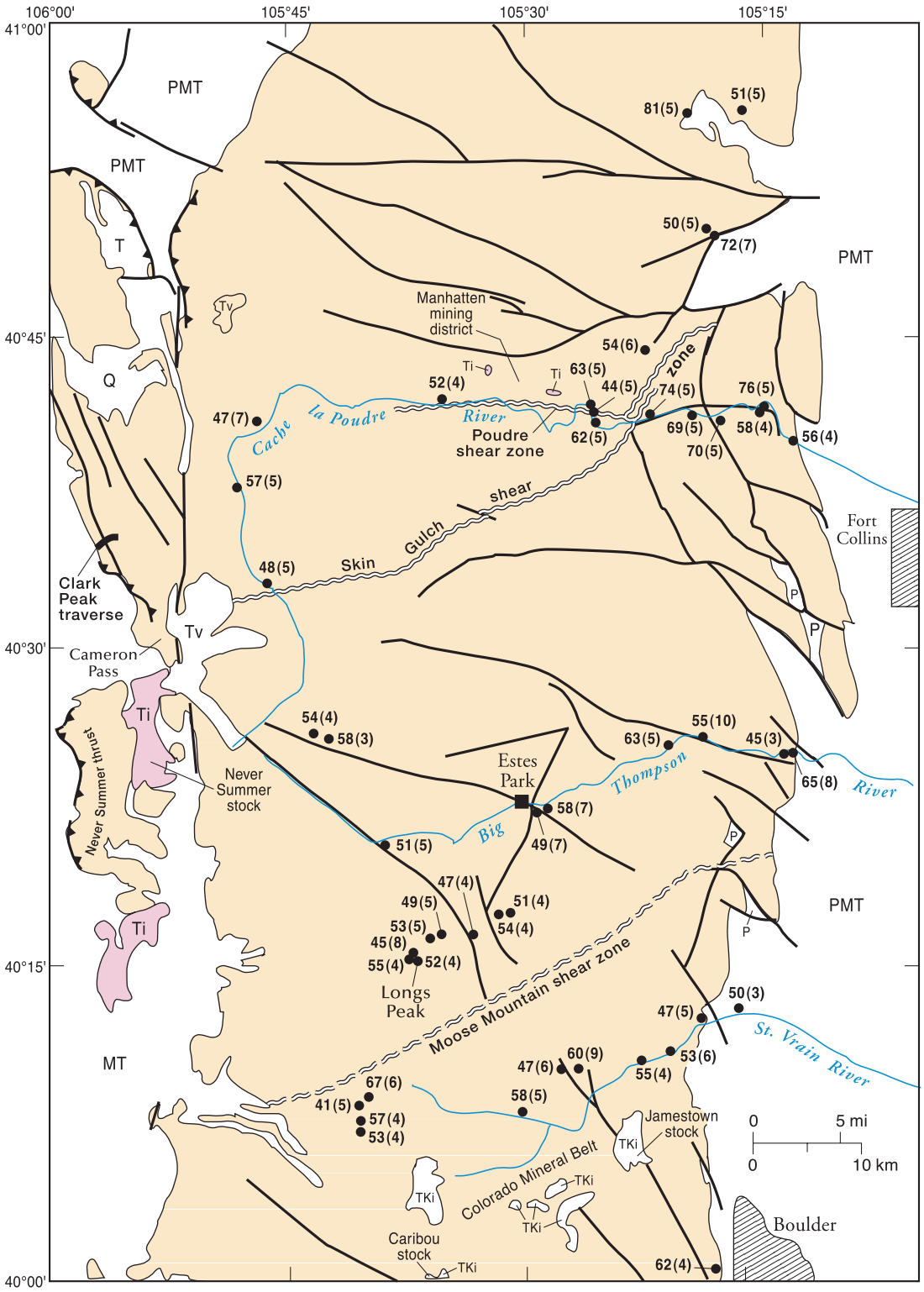

FIGURE 3—Simplified geologic map of the northern Front Range (after Braddock and Cole 1978, 1990). AFT ages, with standard error of the age enclosed in parentheses, are shown adjacent to the sample localities (filled circles). See Table 1 for sample numbers, elevations, and analytical data. **Pale orange** = undivided Proterozoic metasedimentary and igneous rocks; **PMT** = undivided Paleozoic, Mesozoic, and Tertiary sedimentary rocks; **MT** = undivided Mesozoic and Tertiary sedimentary rocks; **P** = undivided Paleozoic sedimentary rocks; **TKi** = Cretaceous to Tertiary intrusives; **Ti** = Tertiary intrusives (33–60 Ma in Manhattan district, McCallum and Naeser 1977; 29.5 ± 1.5 Ma near Cameron Pass, Corbett 1968); **Tv** = Tertiary volcanics. Faults shown as bold lines, dashed where buried or uncertain, teeth on upper plate of thrust faults.

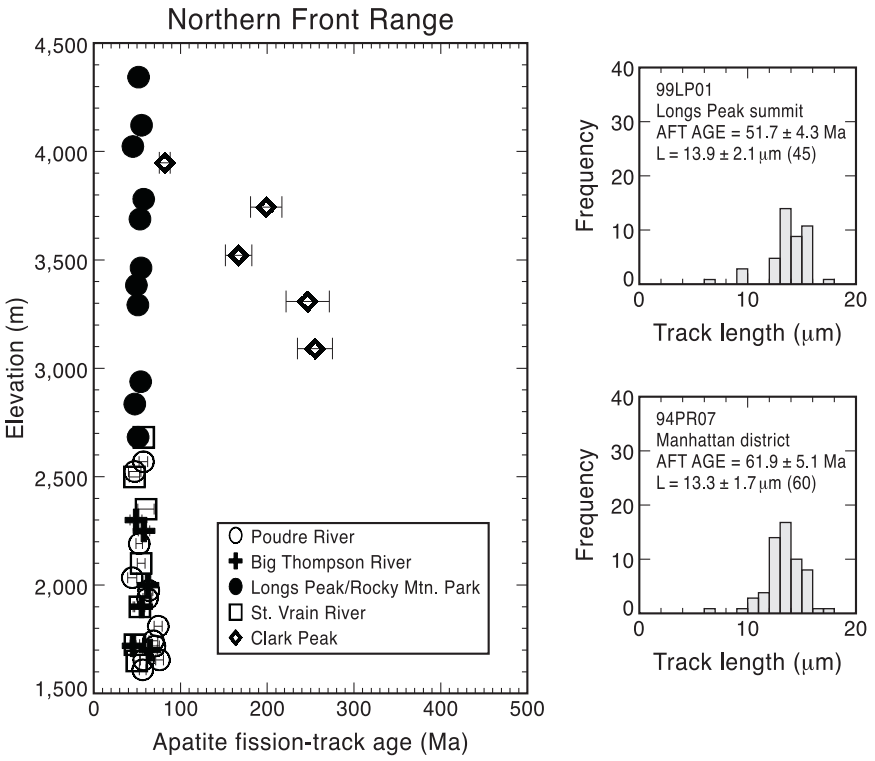

FIGURE 4—AFT ages for northern Front Range plotted as a function of elevation. Age error bars are 2 σ. Track-length distributions for the summit of Longs Peak (99LP01) and a sample near the Manhattan mining district (94PR07) are shown to the right. AFT age, standard error of age, mean track length, standard deviation of length, and number of confined tracks measured (in parentheses) shown on track-length histogram for each sample. See Table 1 for analytical data.

Time-temperature estimates were derived from the age and track length data using the AFTsolve computer program of Ketcham et al. (1999). The program is based on a model that considers differences in annealing kinetics among apatites of variable composition (Carlson et al. 1999). Other annealing algorithms available in the literature (e.g., Laslett et al. 1987; Crowley et al. 1991; Corrigan 1991, 1993) consider apatites of a single composition, usually that of Durango apatite (0.41 wt.% Cl). The AFTsolve model was used to estimate the cooling curves for samples with more than 50 confined track-length measurements and with ages passing the χ^2 test.

The chemical compositions of six representative apatite samples from gneissic and granitic samples along the Lookout Mountain, Pikes Peak, and Wet Mountain traverses (92GO01, 92GO02, 92PP05, 92PP06, 92WM12, and 92WM13) were determined using an electron microprobe with an electron-beam accelerating voltage of 15 kV and a beam current of 15nA. Five grains were analyzed in each sample and each grain was probed twice. All six samples contained < 0.10 wt.% Cl. The apatites from gneiss samples on Lookout Mountain consistently yielded weight percent totals < 100%, suggesting that these apatites may contain OH^- or abundant rare-earth elements. Additional microprobe analyses are needed for the apatites from the 1.7 Ga metasediments.

Apatite fission-track results

Northern Front Range

Forty-six samples were collected between the Colorado–Wyoming border and the St.Vrain River in the northern Front Range (Fig. 3). Most of the samples are from the Proterozoic basement, which is composed of metasedimentary and metavolcanic rocks intruded by 1.7 Ga foliated, calcalkaline plutonic rocks and 1.4 Ga granites, such as the Longs Peak-St. Vrain batholith and the Sherman granite (Selverstone et al. 1997). Two major shear zones are present in the northern Front Range, the Skin Gulch and the Moose Mountain. Abbot (1972) used Rb-Sr dating of ductile features within the Skin Gulch shear zone to demonstrate that this fault has a Proterozoic ancestry at ~ 1.4 Ga. Abbott (1976) noted that this shear zone has been reactivated in the brittle regime at least twice. The latter phase of brittle deformation, presumably related to the Laramide orogeny, is associated with the development of iron-stained breccia and gouge zones. The sense of Laramide displacement along this fault is poorly known. The Moose Mountain shear zone shows predominantly 1.4 Ga deformation with an earlier 1.7 Ga history. This zone appears to be a profound boundary, separating rocks of different metamorphic grade and supracrustal type (Selverstone et al. 1997). It too has been reactivated in the brittle regime because cataclastic features are superimposed on the mylonitic fabric and the Pennsylvanian Fountain Formation is offset (Selverstone et al. 1997).

The Laramide-age faults on the eastern margin of the northern Front Range are dominantly east-northeast-dipping reverse faults that are most likely backthusts that may sole into a blind west-dipping detachment beneath the Denver Basin (Erslev 1993; Erslev and Selvig 1997). A lower crustal wedge beneath the northern Front Range is needed to balance the cross sections and account for the uplift of the range (Erslev and Holdaway 1999). The west side of the range is bounded by the east-dipping Never Summer thrust fault with large (~ 10 km; Erslev et al. 1999) lateral displacement.

The eastern end of a discontinuous, northeast-trending line of intrusives that roughly parallels the Colorado Mineral Belt to the south (Fig. 1) crosses the western portion of the Cache la Poudre traverse (Fig. 3). The Never Summer stock, which is located about 12 km southwest of the westernmost sample on the Poudre River traverse (Ti, west edge of Fig. 3), is composed of 28.2 ± 0.7 Ma rhyolite and 28.8 ± 1.5 Ma granite (zircon fission-track ages; Gamble 1979) at the south end and 29.5 ± 1.5 Ma granodiorite and monzonite (K-Ar age; Corbett 1968) at the north end. The volcanic rocks at Cameron Pass include 24–29 Ma rhyolites, tuffs, breccias, and andesitic flows derived from the Never Summer stock and volcanic centers to the south (Izett 1974; Corbett 1968; Gamble 1979). Zircon fission-track ages for intermediate composition, porphyritic dikes and small intrusives associated with the Manhattan mining district (Fig. 3), which is the northeasternmost intrusive center in the northern Colorado intrusive belt, are 54–60 Ma (McCallum and Naeser 1977). The zircon fission-track age of a small (1 km by 0.3 km) rhyolite body within the district is 33.3 ± 6.7 Ma (McCallum and Naeser 1977; Shaver et al. 1988).

The northeastern end of the Colorado Mineral Belt, a northeast-trending zone of late Mesozoic through late

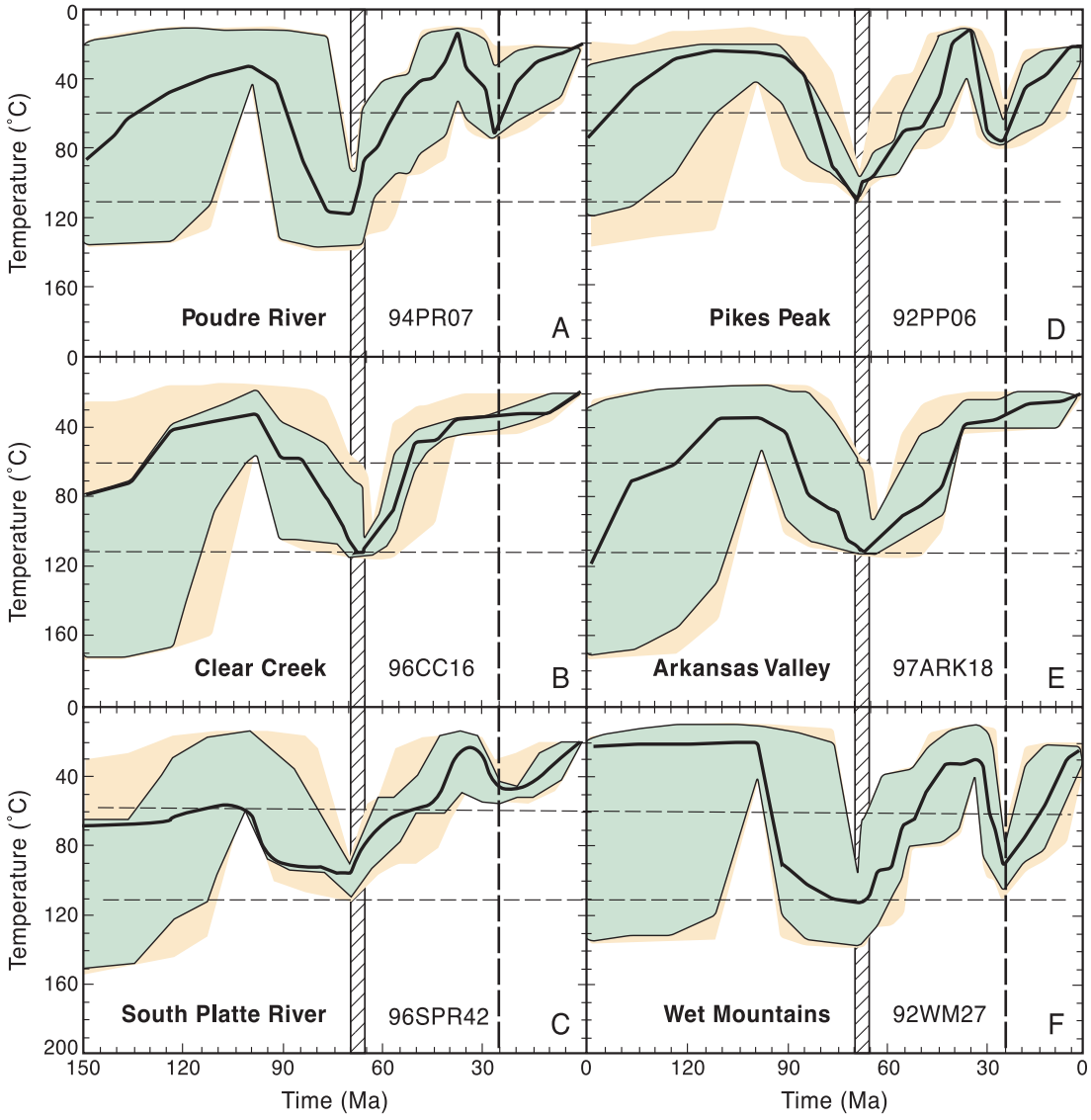

FIGURE 5—Representative thermal histories from the Front Range and Wet Mountains that fit the age and track-length data. The following geologic constraints were imposed on each model. The area now occupied by the Front Range was near the surface during the deposition of the near-shore facies of the Dakota Group at 100 Ma (Weimer 1996). The unconformity beneath the Dakota Group formed at 110–112 Ma. The area reached maximum burial in Late Cretaceous time during deposition of the upper Pierre Shale at ~ 70–71 Ma (Weimer 1996). Minor Laramide deformation began at 71 Ma, but significant deformation began 67–63 Ma (Tweto 1975; Hoblitt and Larson 1975). A period of quiescence indicated by the development of a 54 Ma paleosol in the southern Denver Basin and the formation of the Rocky Mountain erosion surface by 37 Ma before eruption of the Wall Mountain Tuff were also considered in the modeling. Some of the AFT data require an Oligocene to early Miocene thermal event to fit the data; the ages of local volcanism were included in those models (e.g., Poudre River, Pikes Peak, and Wet Mountains). The orange and green areas show the range of thermal histories satisfying the AFT data and the black line is the thermal history providing the best fit to the data. The range of estimates for the onset of Laramide deformation is shown as the vertical box with the stripped pattern, and the waning of Oligocene volcanism in Colorado (McIntosh and Chapin 2004 this volume) is shown as a vertical dashed line. Horizontal lines mark the apatite partial annealing zone (110–60 °C).

Cenozoic intrusives and associated mineral deposits that extends from the Four Corners area to Jamestown, Colorado (approximately 50 km northwest of Denver), is located near the St. Vrain traverse. The Jamestown stock (Fig. 3) contains two phases, a 45 Ma syenite and a 72 Ma granodiorite. Zircon fission-track ages of 45–48 Ma and an AFT age of 47 ± 6 Ma are reported for the Jamestown stock by Cunningham et al. (1994). The K-Ar age of the nearby Caribou stock (Fig. 3) is 63 ± 6 Ma (Marvin et al. 1974).

AFT ages plotted as a function of elevation in the northern Front Range, as well as representative track-length histograms, are shown in Figure 4. Sample numbers, elevations, and analytical data are listed in Table 1 (found on pages 61–69) with the AFT ages printed in bold type. The AFT ages in the Poudre River valley and along the northeastern edge of the Front Range just south of the state line are slightly older (44–81 Ma) than those to the south in the Big Thompson and St. Vrain drainages (45–65 Ma); the oldest ages are located along the northeastern margin of the area. The mean track lengths for the Poudre river traverse are from 13.3 to 13.8 μm, and the slightly broad unimodal shape of the track-length distributions are similar for all

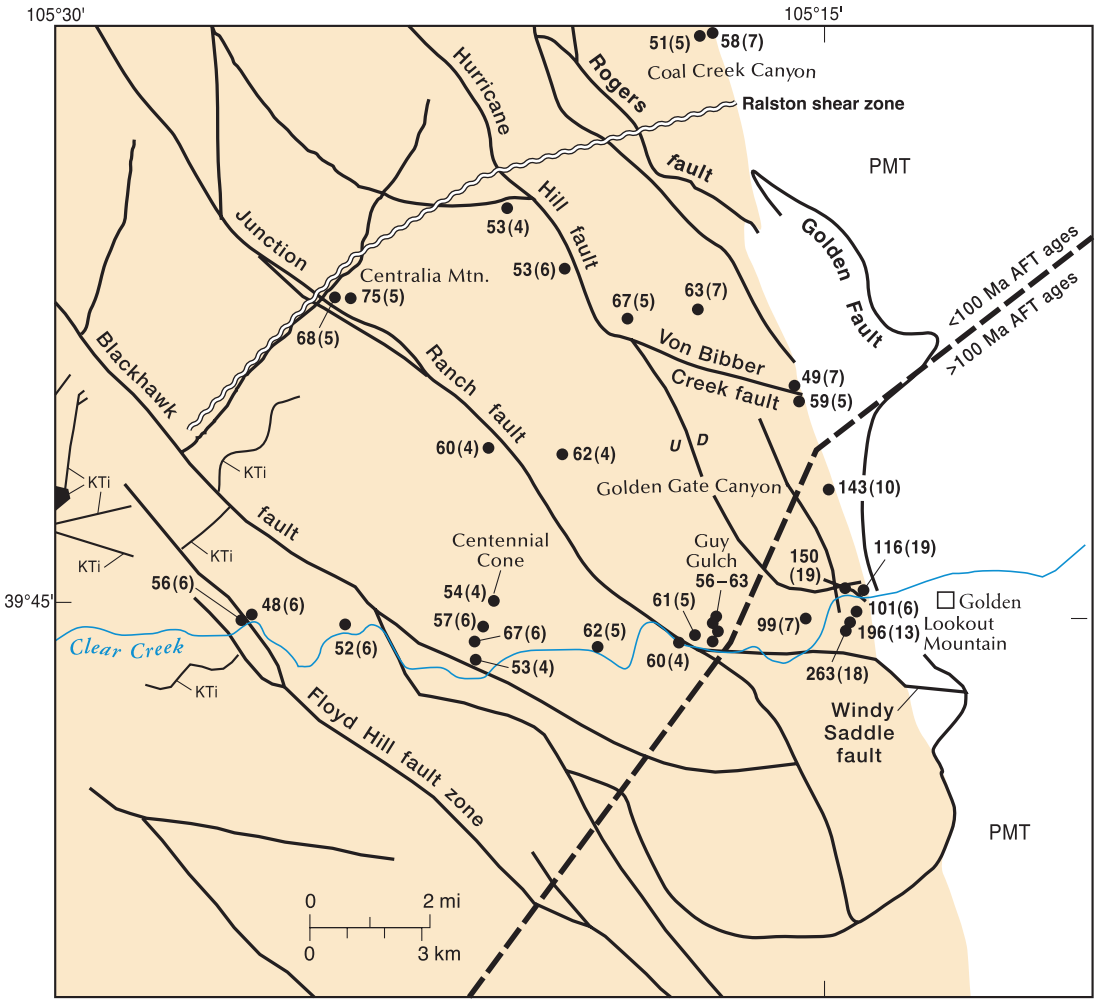

FIGURE 6—Simplified geologic map of the Clear Creek valley (after Bryant et al. 1981). AFT ages, with standard error of the age enclosed in parentheses, are shown adjacent to the sample localities (filled circles). See Table 1 for sample numbers, elevations, and analytical data. Shaded area = undivided Proterozoic gneisses, **PMT** = undivided Paleozoic, Mesozoic, and Tertiary sedimentary rocks, **KTi** = dikes and intrusives in Colorado Mineral Belt. Faults shown as bold lines; relative motions determined from AFT data shown as **U**=up and **D**=down.

samples along this traverse (Table 1, Fig. 3, 94PR07). The AFT ages to the south and to the north of the east-west trending Poudre shear zone are similar, suggesting relatively little Laramide-age vertical displacement across this fault. The AFT ages on the east side of the Skin Gulch shear zone tend to be somewhat older (56–75 Ma) than those to the west (44–63 Ma), although the age difference is not statistically significant. The relatively young AFT age of 44 ± 5 Ma determined for the breccia within the Poudre River shear zone may reflect annealing due to warm fluid that caused the iron staining; however, the small quantity of apatite recovered from this sample precludes the track-length analysis required to test this idea. A representative example of the modeled temperature histories of three samples (94PR02, 94PR07, and 94PR10) containing abundant confined tracks is shown in Figure 5a. Significant cooling occurred during Laramide deformation (70–50 Ma), followed by a period of stability coincident with the timing of erosion surface development in the southern Front Range. The mean track lengths in the 13 μm range are due to a reheating event in Oligocene to Miocene time, with maximum temperatures on the order of 80 °C.

The mean track lengths of samples with more than 50 measurements are generally 13.5–14.7 μm for samples in the Big Thompson, Longs Peak, and St. Vrain areas. The track-length data, coupled with the nearly constant cooling age of 45–65 Ma over a large elevation range (~3 km; Figure 4) is indicative of very rapid Laramide cooling. The middle Cenozoic heating event recorded in the Poudre River data is not found in the AFT data from the Longs Peak area. Although there are no samples from immediately adjacent to the Moose Mountain shear zone, the data from the Big Thompson and St. Vrain drainages do not indicate significantly different Cenozoic cooling histories across this boundary. In contrast to the southern Front Range, which will be discussed later, AFT ages > 100 Ma and the base of a fossil annealing zone, commonly preserved south of the mineral belt, have not yet been found in the northeastern Front Range. Cervany (1990) found a PAZ preserved on Clark Peak in the southernmost Medicine Bow Mountains of Colorado just north of Cameron Pass along the western marginal thrust fault of the range (Fig. 3). The AFT ages of Cervany (1990) are plotted as a function of elevation on Figure 4. Note that the ages increase with decreasing elevation on Clark Peak, opposite the expected trend shown in Figure 2b. The AFT ages > 100 Ma on this profile have short mean track lengths (~ 11 μm) characteristic of samples within the PAZ, and the youngest sample at high elevation has a

track length of ~ 13 μm. The unusual age-elevation pattern suggests that the fossil PAZ on Clark Peak is tilted to the west.

Transition zone—Boulder Canyon to Golden Gate Canyon

A dozen samples were obtained from the 1.7 Ga gneisses exposed at or near the eastern range front between Boulder (Fig. 3) and Golden (Fig. 6) in an effort to document the cooling histories associated with the marked change in Laramide structural style between the northern and southern Front Range that nearly coincides with the location of the Colorado Mineral Belt and the Ralston–Idaho Springs shear zone. As noted by Erslev and Selvig (1997), the eastern margin of the Front Range has a north-northwest trend between Colorado Springs and Golden (Fig. 1), but the margin has a more northerly trend north of Golden. The east-northeast-vergent Golden thrust fault is a prominent surface feature south of Golden, but the Golden thrust may swing far to the east and may become a blind thrust fault beneath the Denver Basin north of Golden (Erslev and Selvig 1997). Consequently west-southwest-vergent thrust and reverse faults dominate the eastern margin of the range north of Golden.

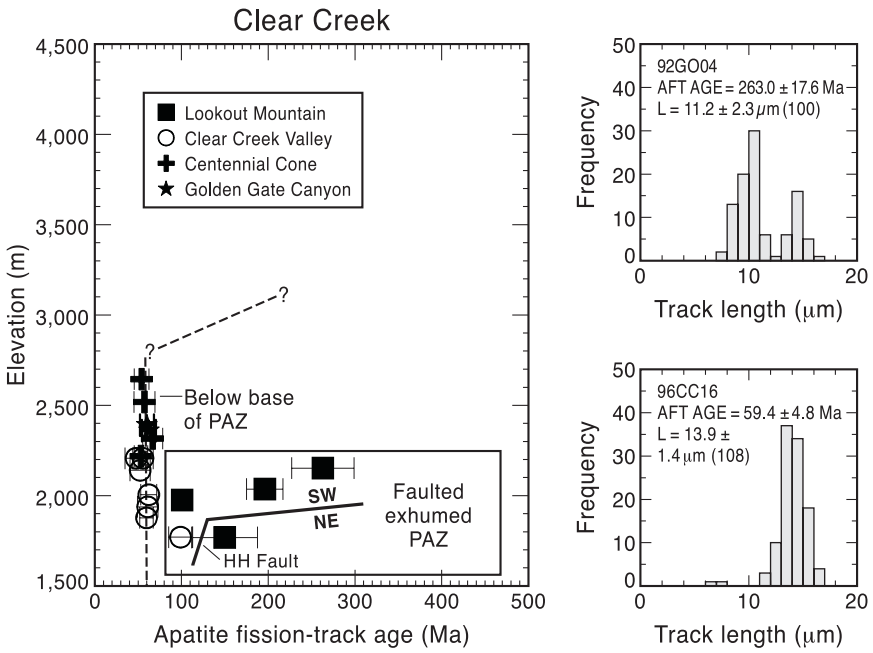

FIGURE 7—AFT ages for the Clear Creek area plotted as a function of elevation. Age error bars are 2 σ. Track-length distributions for the highest elevation sample on Lookout Mountain (92G004) and the lowest elevation sample from Centennial Cone (96CC16) are shown on the right side of the diagram. **HH fault** = Hurricane Hill fault zone. AFT age, standard error of age, mean track length, standard deviation of length, and number of confined tracks measured (in parentheses) are shown on track-length histogram for each sample. See Table 1 for analytical data.

The AFT age of the sample from the mouth of Boulder Creek (Fig. 3) is 62 ± 4 Ma with a relatively short mean track length of 12.8 μm. These data appear to reflect the complex, two-stage intrusive history of the nearby Jamestown stock (Fig. 3). The samples from the mouth of Coal Creek canyon and the mouth of Von Bibber Creek to the Centralia Mountain area (Fig. 6) yield Laramide (49–75 Ma) cooling ages and relatively long mean track lengths (13.2–14.2 μm). A different pattern is found at the mouth of Golden Gate Canyon, where an AFT age of 143 ± 10 Ma and a short mean length of 11.3 μm was measured at the range front, and Laramide cooling ages were determined 8 km to the west within the range. This is the northernmost exposure of a pattern that is quite characteristic of the southern Front Range. We interpret the >100 Ma AFT age associated with a short mean track length to have been within the apatite PAZ. The distance between the Laramide cooling age at Von Bibber Creek and the > 100 Ma age at the mouth of Golden Gate Canyon is ~ 3 km, and no mapped fault has been recognized crossing the range front between these two points.

Lookout Mountain–Clear Creek

In this section, new AFT data from age-elevation traverses on Lookout Mountain, Centennial Cone, and a ridge adjacent to Guy Gulch near Golden, Colorado, as well as from both sides of northwest-trending faults intersecting Clear Creek Canyon, are presented. All samples collected on Lookout Mountain and in the Clear Creek valley are from 1.7 Ga (Peterman et al. 1968) metasedimentary gneisses, the dominant rock type in this portion of the Front Range. The intrusives of the Colorado Mineral Belt, which lies to the northwest of the Clear Creek traverse (Figs. 1, 6), are 60–65 Ma (Cunningham et al. 1994) in this area.

Lookout Mountain—Samples in the Golden area were collected from gneisses exposed at the mouth of Clear Creek and along the Lookout Mountain Road. AFT ages from this traverse plotted as a function of elevation and a representative track-length histogram are shown in Figure 7. Significant differential annealing of the multiple apatite age populations in the metasedimentary rocks, the low slope of the age-elevation profile, the short mean lengths, and broad track-length distributions (Fig. 7) are all characteristic of an exhumed partial annealing zone, like that seen at the mouth of Golden Gate Canyon. Considering that the base of the PAZ is not exposed and because there are multiple age populations in these samples, the timing of exhumation is loosely constrained to be related to Laramide deformation and early Neogene erosional denudation. Evidence of significant late Neogene denudation is not found in the AFT data from low-elevation samples on this traverse (Fig. 7).

According to Van Horn (1957), a west-northwest–trending fault is present between the two lowest elevation samples (150 Ma [92GO01] and 101 Ma [92GO02]; Fig. 6), but a later geologic map of the area by Bryant et al. (1981) does not include this feature. The structure at the mouth of Clear Creek Canyon is complex, with east-west trending fault planes with nearly horizontal slickenlines that are similar in orientation to the fault mapped by Van Horn (1957) intersecting northwest-trending faults with poorly developed dip-slip slickenlines. The dips on the northwest-trending faults are 60° SW and 53° NE. Approximately 200–300 m of vertical displacement along the faults between the sample at the mouth of Clear Creek Canyon (92GO01) and the lowest elevation samples at Lookout Mountain has disrupted the PAZ (Fig. 7), bringing the southwest block up with respect to the northeast block. The AFT results indicate vertical motion across these faults, which are part of the Hurricane Hill fault zone, although it is not possible to determine for certain exactly which fault or faults are responsible for the offset. Thus, the AFT cooling ages can be quite useful in

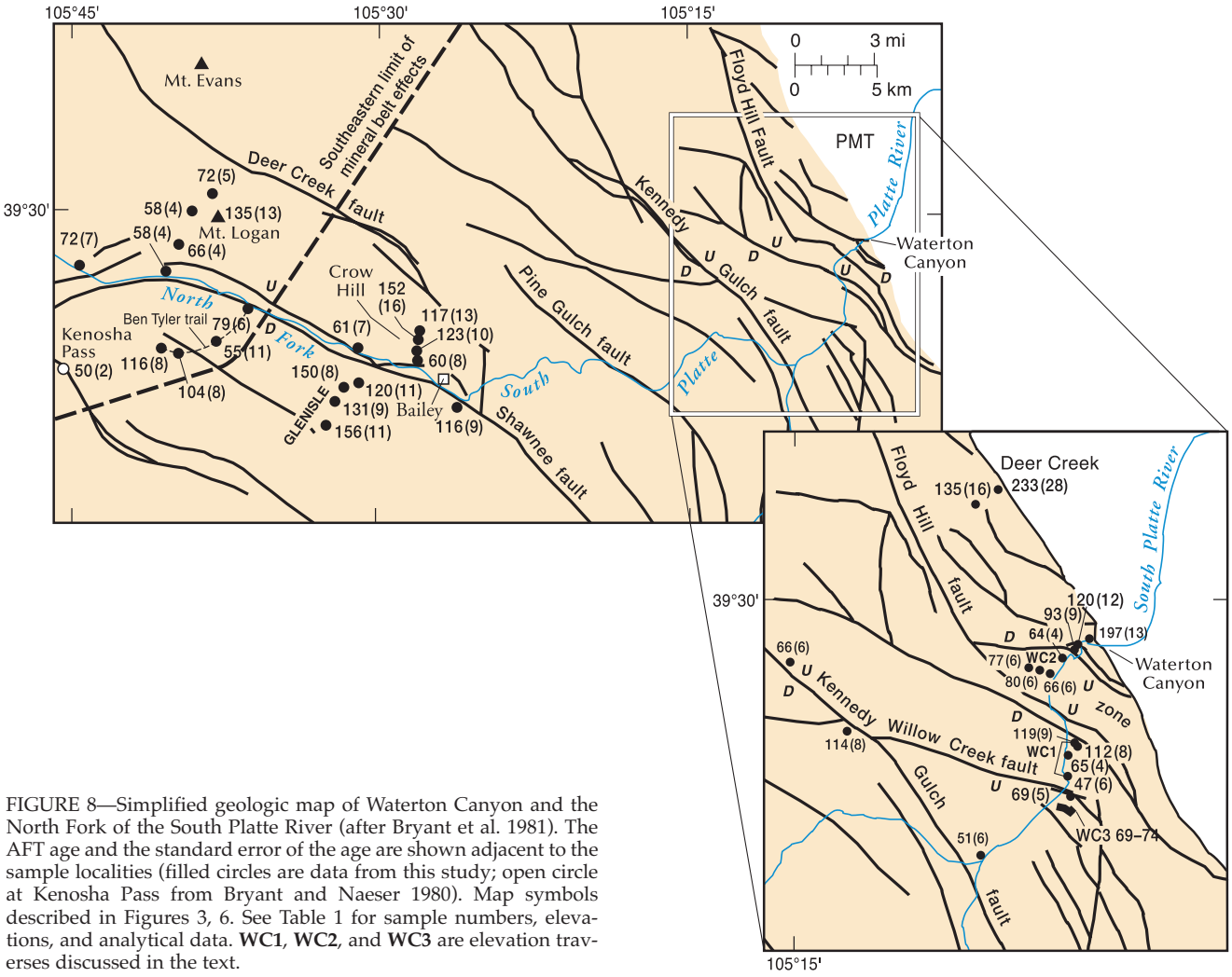

FIGURE 8—Simplified geologic map of Waterton Canyon and the North Fork of the South Platte River (after Bryant et al. 1981). The AFT age and the standard error of the age are shown adjacent to the sample localities (filled circles are data from this study; open circle at Kenosha Pass from Bryant and Naeser 1980). Map symbols described in Figures 3, 6. See Table 1 for sample numbers, elevations, and analytical data. **WC1**, **WC2**, and **WC3** are elevation traverses discussed in the text.

identifying vertical offset and determining the relative motion across fault zones. An inherent weakness in this type of analysis is that large amounts of displacement (at least 200 m) or fortuitous positioning of the AFT PAZ with respect to the modern topographic surface are required to effectively locate fault zones with significant vertical displacement.

Clear Creek Canyon—Steps were taken when collecting the samples along Clear Creek to try to avoid the complicating thermal effects of the Colorado Mineral Belt, which lies on the western edge of Figure 6. However, the thermal effects of the Colorado Mineral Belt, which will be discussed in detail in a later section, appear to be much broader than expected. The AFT data from Proterozoic gneisses in Clear Creek Canyon show a decrease in age at low elevation from east to west (Fig. 6). The AFT age at the eastern margin of the Front Range in Clear Creek canyon is 150 ± 19 Ma (sample 92GO01, as discussed above). West of the Hurricane Hill fault zone (Fig. 6), the AFT age decreases to 99 ± 7 Ma (94CC01); this sample is in the same fault block as the Lookout Mountain age-elevation traverse and is also within the PAZ (Figs. 6, 7). A short (200 m) age-elevation traverse on a ridge just east of the Junction Ranch fault (Guy Gulch) has AFT ages of 56–63 Ma and mean track lengths of ~ 14 μm. These data indicate that the base of the PAZ, which separates ages > 100 Ma from samples that cooled during Laramide time (Fig. 2b), is tilted toward the east. This abrupt transition in age can be connected to the transition observed between Golden Gate Canyon and Von Bibber Creek along a line that roughly parallels the Colorado Mineral Belt (Fig. 6, dashed line), suggestive of a causal relationship. West of sample 94CC01 (99 ± 7 Ma), the ages at low elevation range from 48 to 67 Ma and the mean track lengths range from 13.8 to 14.5 μm, registering rapid Laramide cooling of the area (96CC16, Figs. 5b, 6). Samples from an age-elevation traverse on Centennial Cone (Fig. 6) yielded only Laramide AFT ages (53–67 Ma; Fig. 7); the fossil PAZ appears to have been removed by denudation from this portion of the Clear Creek drainage. The elevation of the base of the PAZ in the vicinity of Centennial Cone is above 2,645 m (the elevation of the highest sample). These results can be used to provide a minimum estimate of about 880 m of relief on the base of the PAZ between the eastern edge of the range and Centennial Cone (Fig. 7).

South Platte River

Waterton Canyon to Bailey

The tectonic significance of the decrease in AFT age from the eastern margin to the core of the Front Range along Clear Creek is equivocal due to the thermal effects of Neogene to Cretaceous intrusive activity in the Front Range. However, AFT sample traverses from the mouth of the South Platte River, which are located far from obvious Phanerozoic igneous activity (> 30 km), provide unique insight into the internal structure of the Front Range. In Waterton Canyon, where the South Platte River exits the Front Range southwest of Denver, the AFT age at low elevation on the eastern

margin of the range is 197 ± 13 Ma (Fig. 8), comparable to the AFT results at Lookout Mountain (Figs. 6, 7). AFT ages from Deer Creek to the north also are >100 Ma (Fig. 8). The AFT age in Waterton Canyon drops to 64 ± 4 Ma within 1.5 km of the mountain front across a series of northwest-trending faults (Fig. 8). Rocks on the west side of this fault zone, which contains both dip-slip and oblique-slip slickensides, clearly have moved up with respect to the east side.

Samples were collected along three age-elevation traverses in Waterton Canyon. The first profile, WC1 (Figs. 8,9), consists of two samples from the river valley and two samples from a ridge southwest of a splay of the Floyd Hill fault zone in Mill Gulch. A fossil PAZ with AFT ages > 100 Ma and broad track-length distributions (95SPR29 and 95SPR30) is preserved on the ridge, while Laramide AFT ages (94SPR19 and 94SPR20) are present below the break-in-slope at about 1,900 m on the age-elevation profile. In contrast, the WC2 profile (Figs. 8, 9), which includes three samples (95SPR31 through 95SPR33) from a ridge on the northeast side of the Floyd Hill fault, yields only Laramide AFT ages. The base of the PAZ must be at elevations above 2,100 m,s the elevation of the highest sample on the traverse). These results can be used to estimate that at least 200 m of down-to-the-west motion has occurred across this branch of the Floyd Hill fault zone. The fault that separates WC1 from WC2 has oblique-slip slickenlines with rakes of 31–49° SE on planes dipping 65–80° NE. Riedel shear fractures on the fault surface indicate left-lateral, reverse movement; the sense of vertical displacement is consistent with the AFT results. Elevation traverse WC3, on a ridge south of Strontia Reservoir, includes samples 96SPR38 (highest elevation 2,073 m) through 96SPR42 (Fig. 9) and lies south of a fault in Willow Creek. The ages of 69–74 Ma are indicative of Laramide cooling and up to the southwest offset on the fault in Willow Creek.

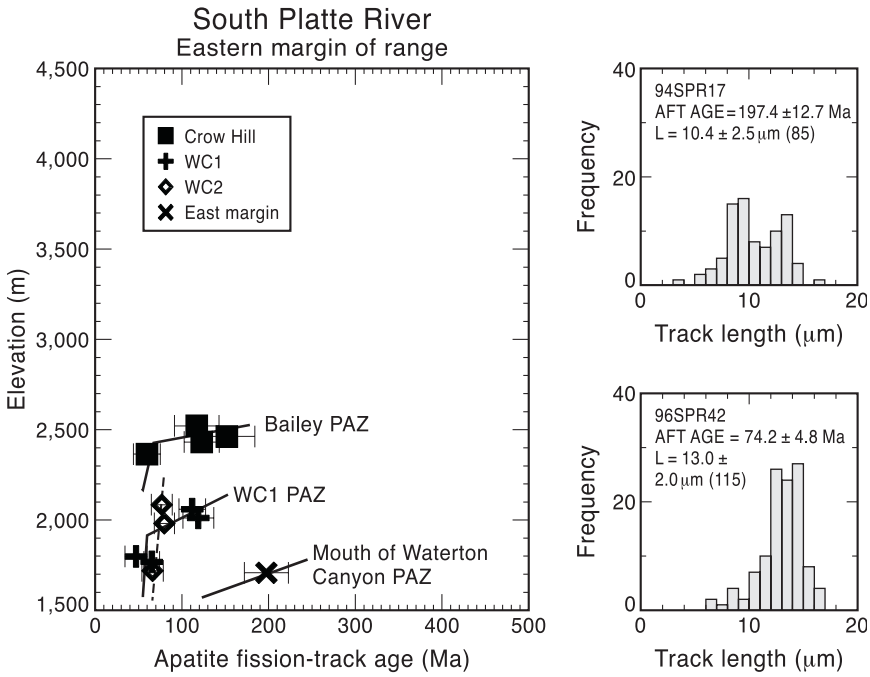

FIGURE 9—Age-elevation profiles for Waterton Canyon and Crow Hill traverses adjacent to the South Platte River valley along the eastern margin of the range. Age error bars are 2 σ. Track-length distributions for the easternmost sample in Waterton Canyon (94SPR17) and the sample just west of the Willow Creek fault zone (96SPR42) are shown to the right. AFT age, standard error of age, mean track length, standard deviation of length, and number of confined tracks measured (in parentheses) shown on track-length histogram for each sample. See Table 1 for analytical data. **WC1** and **WC2** are elevation traverses in Waterton Canyon discussed in the text.

Northwest of Waterton Canyon two samples were collected on either side of the Kennedy Gulch fault zone, which, based on its map pattern with respect to topography, is an east-dipping, high-angle fault. The sample on the east side of the fault, which lies on the same block as the WC2 profile in Waterton Canyon (Fig. 8), has an age of 66 ± 6 Ma (94SPR14). In contrast, the age on the west side is 114 ± 8 Ma (94SPR15) indicating that the east side is the upthrown block. Consequently both the Kennedy Gulch and the Floyd Hill fault zones are east-dipping reverse faults.

Figure 5c shows a typical cooling history for samples with Laramide AFT ages from the Waterton Canyon area. In contrast to the Clear Creek samples, the Waterton Canyon samples typically have slightly shorter mean track lengths in the 13.0 μm range. The data seem to indicate that a mild reheating (20–50 °C) event affected the area in the Neogene. Because local Neogene volcanism is not evident, heating by burial, as indicated by locally preserved gravels (Bryant et al. 1981) or by regional volcanism, to be discussed later, are possible mechanisms. Although Scott (1963) maps some andesite dikes in the Waterton Canyon area, subsequent mappers did not include these features on their maps (Trimble and Machette 1979; Bryant et al. 1981). Attempts to locate and examine the dikes in the Kassler quadrangle (Scott 1963) were unsuccessful, although unfoliated basalt float was found in Mill Canyon.

Farther west, towards the center of the range, samples were collected along age-elevation traverses on both sides of the northwest-trending Shawnee fault zone (Fig. 8). Age and track-length data from an age-elevation traverse on Crow Hill along U.S. Highway 285 north of Bailey (Figs. 8, 9) suggest the presence of the base of a fossil PAZ at an elevation of 2,400 m in this area. Southwest of the fault, near Glenisle, the AFT ages range from 116 to 156 Ma, and the mean track lengths are short, characteristic of rocks within the PAZ. The slight break-in-slope on this vertical traverse (Fig. 10) may be related to a previously unmapped fault in this hillside where exposures are poor, or it may be due to differences in apatite composition between the granodiorite and the gneisses exposed in this area. In contrast to the rocks within the PAZ found on the southwest side of the Shawnee fault zone, the base of a PAZ is exposed on the northeast side of the fault at Bailey. Two AFT ages from the Platte River valley north of the fault zone are 61 ± 7 and 60 ± 8 Ma, indicating that the northeast side has moved up with respect to the southwest side.

Mt. Logan and Mt. Evans

A sample traverse on Mt. Logan (Fig. 8; 96SPR44 through 96SPR48) reveals the presence of the base of a PAZ at an elevation of ~ 3,500 m on the north side of the peak. These data indicate that between Crow Hill and Mt. Logan, the base of the PAZ steps up ~ 1 km over a distance of approximately 17 km (Figs. 8, 10). There are no mapped faults between the two areas that would accommodate this rather sharp change in elevation in the base of the PAZ. Similarly, the base of the PAZ rises about a kilometer over a distance of 9 km between

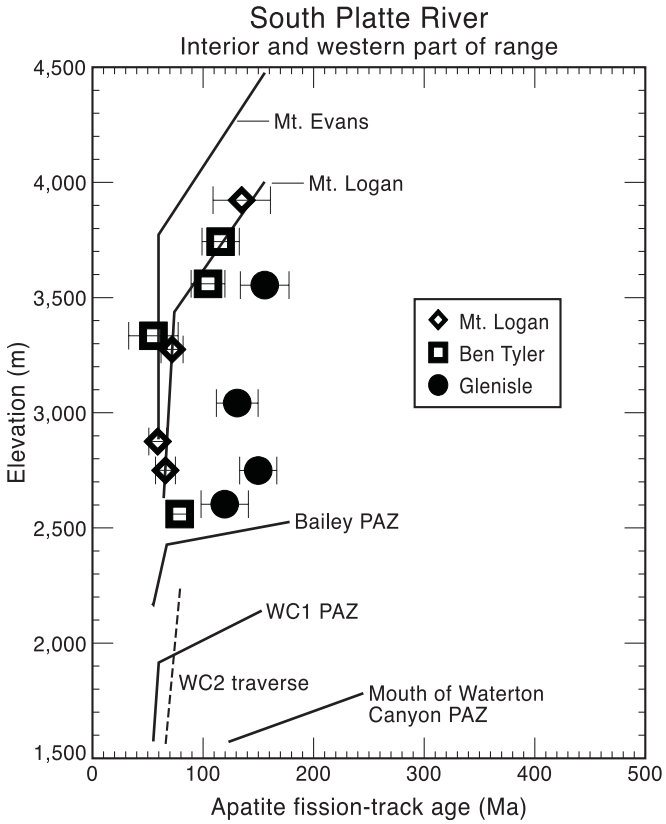

FIGURE 10—Age-elevation profiles from the North Fork of the South Platte River in the interior and near the western edge of the range. The data from the Glenisle, Ben Tyler trail, and Mt. Logan traverses are shown. The general trends on the eastern margin data from Figure 9 (Bailey, WC1, WC2 and the mouth of Waterton Canyon) are shown for reference. The general trend of the Bryant and Naeser (1980) data on Mt. Evans is also shown for reference; these data are plotted in detail on Figure 13.

Glenisle and the Ben Tyler trail (Figs. 8, 10).

Bryant and Naeser (1980) determined AFT ages for the Proterozoic Mount Evans batholith, just north of Mt. Logan, within the core of the Front Range (Figs. 1, 8). Ages at elevations greater than 3,500 m range from 90 to 134 Ma and are interpreted to represent a fossil PAZ that developed during burial of the area in Mesozoic time; this interpretation is consistent with our results. At elevations between 2,400 m and 3,500 m, the ages range from 58 to 68 Ma and mean track lengths are ~ 14 μm (Naeser et al. 2000), indicating rapid cooling during Laramide deformation. The AFT ages on Mt. Evans are significantly older than the nearby (11 km) 35 Ma Montezuma stock (Cunningham et al. 1994), so Neogene magmatism along the Colorado Mineral Belt has not affected this area. Bryant and Naeser (1980) also found a 50 ± 2 Ma AFT age at Kenosha Pass (Fig. 8; elevation 3,048 m) and > 100 Ma AFT ages 4 km to the south (just off the west edge of Fig. 8, elevation 2,822 m). The combination of the Kenosha Pass, Glenisle/Ben Tyler, Mt. Logan/Crow Hill, and Mt. Evans results suggests that faulting does not control the elevation of the apatite PAZ in this part of the Front Range, as it does further to the east. Instead, it appears that the base of the PAZ has been warped upward by elevated heat flow associated with Laramide magmatism along the Colorado Mineral Belt. The approximate position of the upwarp is well constrained by the Bryant and Naeser (1980) data at and south of Kenosha Pass (4 km), and is loosely constrained by the Ben Tyler trail/Glenisle and Mt. Logan/Crow Hill results (~ 9 and 17 km, respectively; see dashed line on Fig. 8), and can be tied to the abrupt upwarp of the PAZ recorded in the Lookout Mtn./Clear Creek data.

AFT ages on the west side of the Front Range adjacent to the range-bounding Elkhorn thrust south of Kenosha Pass range from 130 to 473 Ma; these ages were used by Bryant and Naeser (1980) to suggest that most of the Laramide displacement on the Elkhorn fault is lateral, not vertical. These AFT results mirror those found on the east side of the range south of Von Bibber Creek. Taken together, the Lookout Mountain and Waterton Canyon AFT data and the Elkhorn thrust results of Bryant and Naeser (1980) suggest that denudation during Laramide deformation was greatest in the core of the Front Range and less on the eastern and western margins. Lateral displacement dominated on the margins, while vertical motion was more important in the center of the range.

Southwestern South Platte River

Nine samples were collected near Tarryall Reservoir and Elevenmile Canyon Reservoir (Fig. 11) in order to build on the data set of Bryant and Naeser (1980) for the west side of the Front Range. Two AFT ages from the Tarryall Reservoir area record Laramide denudation (75–78 Ma) and are significantly younger than the 352 Ma AFT age determined by Bryant and Naeser (1980) along the Elkhorn thrust fault. This age pattern mirrors that seen on the eastern margin of the Front Range. However, near Elevenmile Canyon Reservoir, the age pattern is complex with ages generally becoming younger toward the southwest (Fig. 11). A block southwest of the Elkhorn thrust appears to show steep tilting toward the south to southwest. The younger ages in the Elevenmile Canyon Reservoir area may be due to burial of this region by tuffs and lavas from the Thirtynine Mile volcanic field, which is located immediately to the south (Fig. 11). Alternatively, the Elkhorn thrust is paralleled by several faults in the vicinity of Elevenmile Canyon Reservoir, and the AFT age pattern may reflect jostling of fault blocks in a manner analogous to that seen in Waterton Canyon.

Pikes Peak

The Proterozoic Pikes Peak Granite, which underlies much of the Pikes Peak area, contains abundant fluorite and little apatite, except at the very highest elevations (Naeser et al. 2000). Consequently, the Pikes Peak Granite was avoided in this study, and samples (Table 1) were collected from Proterozoic granodiorite and migmatitic gneisses exposed southeast and south of Pikes Peak from two age-elevation traverses (Figs. 12, 13). The first traverse is along the Phantom Canyon Road, which roughly coincides with the axis of the Cripple Creek arch, a south-plunging, basement-involved anticline on the south side of Pikes Peak (Chase et al. 1993). The lowest elevation sample is in a small fault block known as the Gnat Hollow structure (Chase et al. 1993) that is bounded on the north by a thrust fault with < 500 m of displacement. The second traverse crosses two down-to-the-west normal faults of probable late Cenozoic age located on the western limb of the Cripple Creek arch in the Garden Park area of the Oil Creek graben.

Although most of the samples were chosen to avoid the complicating thermal effects of the Oligocene intrusions associated with the Cripple Creek volcanic center one sample, located approximately 1 km from the nearest phonolite intrusion (92PP04; Fig. 12), was collected to gauge the lateral extent of the thermal disturbance related to this volcanism. $^{40}Ar/^{39}Ar$ dates on the phonolites at Cripple Creek are 30.9–32.5 Ma, and the hydrothermal alteration associated with mineralization in the district has been determined to be 28.2–31.3 Ma (K.D. Kelley et al. 1998). The AFT age of 27 ± 2 Ma and the mean track length of 14.4 ± 1.6 μm for 92PP04

indicates that the tracks in this apatite were completely annealed by hydrothermal activity at the Cripple Creek volcanic center.

The denudation history of the Pikes Peak area derived from samples away from the most direct effects of the Cripple Creek volcanic center is similar to that found in the Waterton Canyon area, except that the magnitude of the Neogene thermal event, here linked to the volcanism at Cripple Creek, is more pronounced. At low elevation on the east side of the Front Range near Colorado Springs (Fig. 12), an AFT age of 171 ± 20 Ma was obtained for sample 92PP01; the mean track length is short (11.1 ± 2.5 μm), indicating a fossil PAZ like that seen at Lookout Mountain. The broad, bimodal histogram for this sample is analogous to the distributions from the Lookout Mountain profile. However, along the southeastern and southern margin of Pikes Peak, younger ages are found. A sample from a small fault block on the southeast edge of the Front Range (Fig. 12) yielded an age of 44.5 ± 4.3 Ma and a mean track length of 13.4 ± 1.6 μm. Modeling of the age and length data for this sample implies rapid cooling of this block in the last 10–20 Ma. The cause for this rapid cooling is not clear, although it may be related to normal faulting in this corner of the Front Range (Scott et al. 1978). On the south side of Pikes Peak, the base of a fossil PAZ is preserved in the Phantom Canyon age-elevation profile (Fig. 13). The AFT age of a sample of Pikes Peak Granite from the summit of Pikes Peak is 449 ± 57 Ma, with a mean track length of 12.1 ± 2.1 μm (Naeser et al. 2000). Our highest elevation sample (92PP05) has an age of 212 ± 21 Ma and a track length of 11.2 ± 1.9 μm, indicative of a rock from within the fossil PAZ. Sample 92PP03, which is separated from 92PP05 by a fault, is also in the fossil PAZ, with an age of 124 ± 11 Ma and a mean track length of 12.4 μm. A break-in-slope on the age-elevation profile occurs at a modern elevation of approximately 2,600 m (Fig. 13).

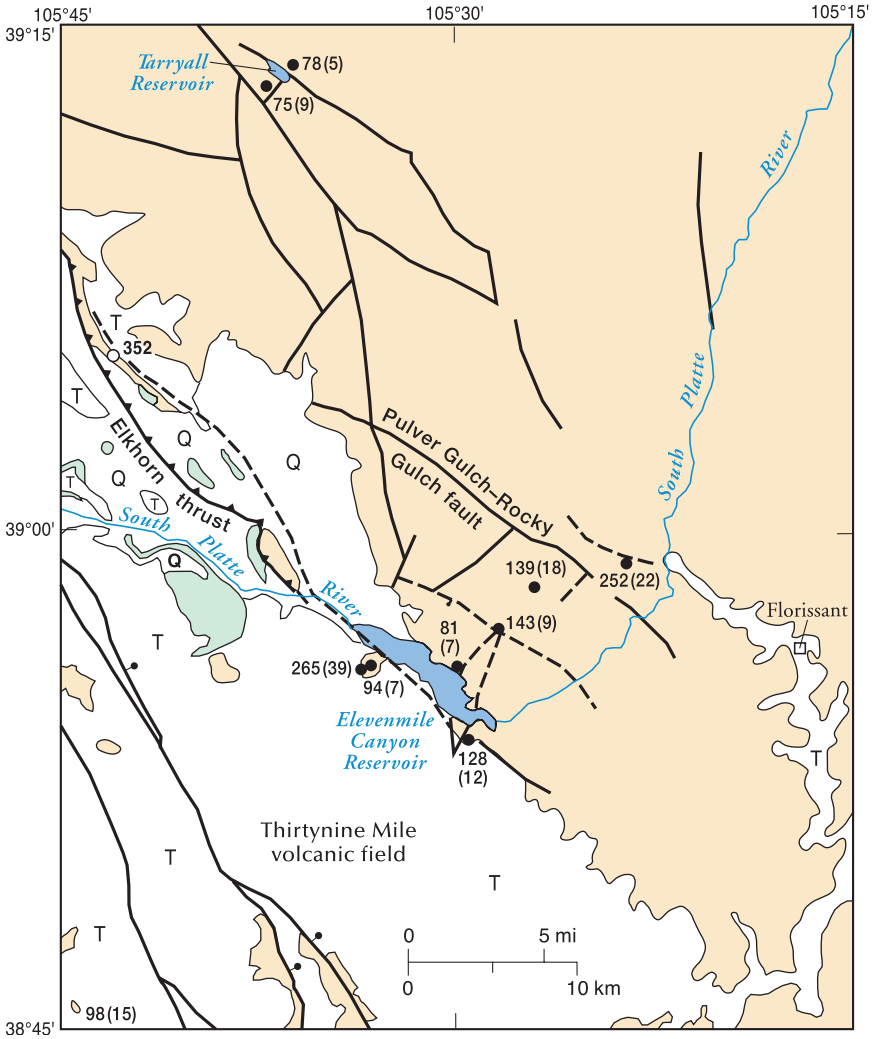

FIGURE 11—Simplified geologic map of the southwestern South Platte River valley (after Bryant et al. 1981; Scott et al. 1978). Elevenmile Canyon Reservoir and Tarryall Reservoir are shown for reference. The AFT age and the standard error of the age are shown adjacent to the sample localities (solid circles are data from this study; open circle from Bryant and Naeser 1980). **Pale orange** = undivided Proterozoic metasedimentary and igneous rocks, **green** = Mesozoic sedimentary rocks, **T** = Tertiary gravels and volcanics, **Q** = Quaternary alluvium. Faults shown as bold lines, dashed where buried or uncertain, ball on the downthrown side of normal faults, teeth on upper plate of thrust faults. See Table 1 for sample numbers, elevations, and analytical data.

An uplifted fossil PAZ is also present in the Garden Park area (Oil Creek graben) to the west of Phantom Canyon (Fig. 12), but the break-in-slope occurs at a significantly lower modern elevation of about 2,000 m. The ages in the fossil PAZ range from 195 to 111 Ma (Table 1) and the mean track lengths are generally less than 12 μm, whereas the ages below the PAZ range from 64 to 67 Ma with mean track lengths that are similar to those seen in the Phantom Canyon profile. The difference in elevation of the base of the fossil PAZ between the Garden Park and Phantom Canyon areas is likely related to the fact that Phantom Canyon lies on the axis and the Garden Park traverse is on the limb of a Laramide-age, basement-involved fold. Down-to-the-west normal faults along the Oil Creek graben, as shown on Figure 12, may also be a factor.

The data from the lower portion of the Phantom Canyon Road clearly show substantial cooling (denudation) due to Laramide deformation (Fig. 13); however, the mean track lengths of 12.1–12.8 μm and the broad unimodal track-length distributions for these samples suggest that they did not cool rapidly through the PAZ. The time-temperature history that best fits the AFT data for 92PP06 (below the PAZ at an elevation of 2,482 m) is presented in Figure 5d. The results can be used to infer that the Phantom Canyon area started cooling during the early phase of Laramide deformation. The Rocky Mountain erosion surface under the 36.7 Ma Wall Mountain Tuff and the 30.9–32.5 Ma flows from the Cripple Creek volcanic field is currently at an elevation of about 2,900 m, only about 300 m above the inflection point on the age-elevation profile. Consequently, the fact that 92PP06 had to be near the surface in late Eocene time is included as a constraint in the model. Superimposed on the Laramide cooling history is an Oligocene heating event that attained maximum temperatures of ~ 80°C. This event is the primary cause of the short mean track lengths on the Pikes Peak and Garden Park profiles. The timing of the event is coincident with the activity at Cripple Creek, although this

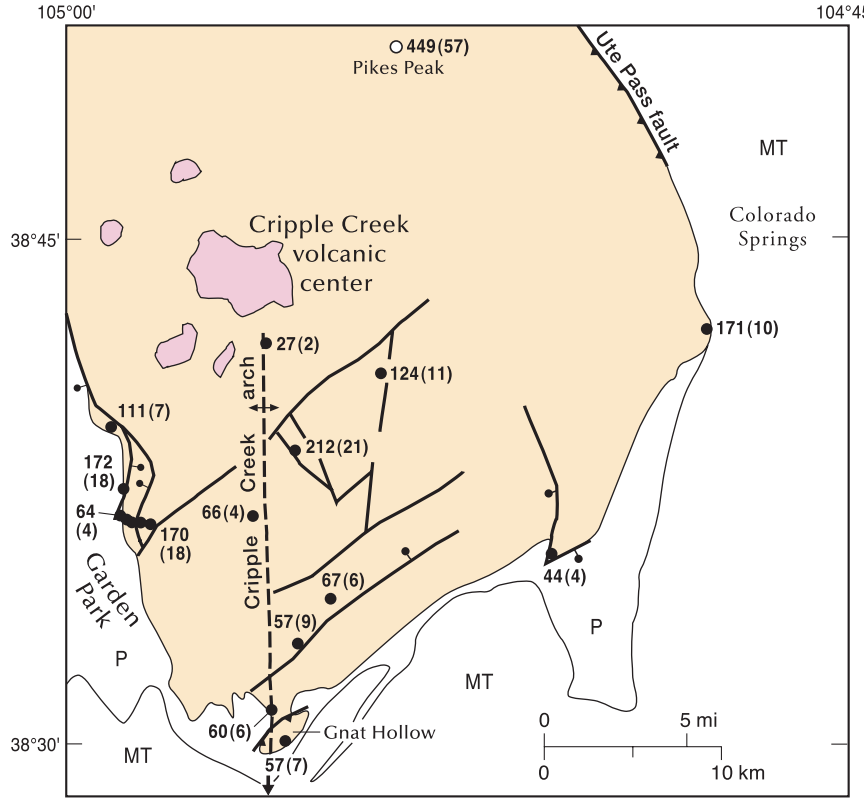

FIGURE 12—Simplified geologic map of the southeastern Front Range in the vicinity of Pikes Peak (after Scott et al. 1978). The AFT age and the standard error of the age are shown adjacent to the sample localities (solid circles are data from this study; open circle from Naeser et al. 2000). **Pale orange** = undivided Proterozoic metasedimentary and igneous rocks, **P** = undivided Paleozoic sedimentary rocks, **MT** = undivided Mesozoic and Tertiary sedimentary rocks, **pink** = Cripple Creek volcanic rocks. Faults shown as bold lines, ball on the downthrown side of normal faults, teeth on upper plate of thrust faults. See Table 1 for sample numbers, elevations, and analytical data.

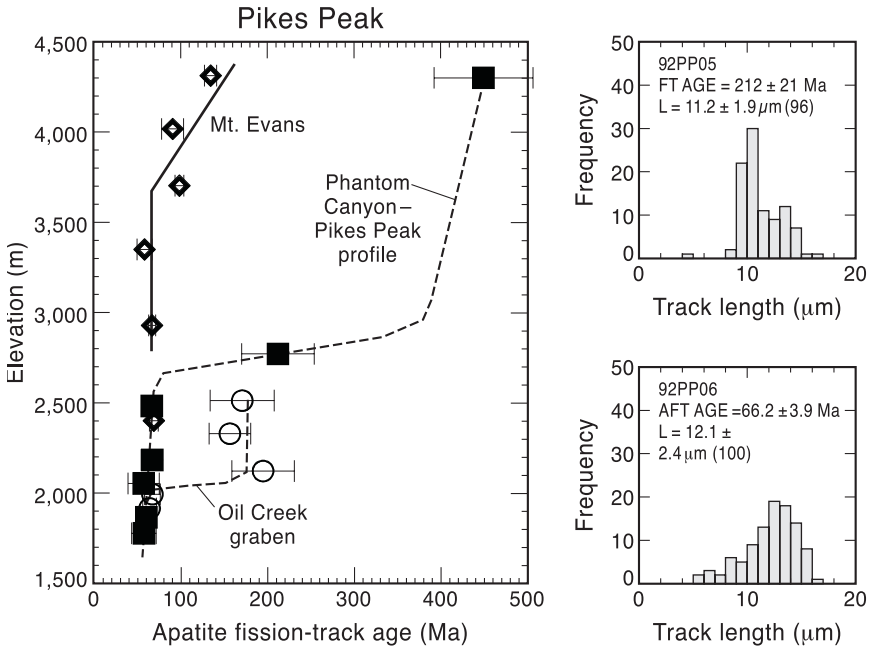

FIGURE 13—AFT ages plotted as a function of elevation for the Phantom Canyon–Pikes Peak profile (solid squares) and Garden Park–Oil Creek graben traverses (open circles). AFT data from Mt. Evans (Bryant and Naeser 1980) are shown for comparison (diamonds). Age error bars are 2 σ. Track-length distributions for samples within the fossil PAZ (92PP05) and at base of the fossil PAZ (92PP06) on the Phantom Canyon traverse are presented at right.

event covers a much larger aerial extent than one would expect from the mapped size of the intrusions.

Arkansas River valley

Proterozoic migmatitic gneiss and granitic rocks exposed in the Arkansas River valley lie in the transition between the Front Range to the north and the Wet Mountains to the south. The area is cut by a number of north- to northwest-trending faults, including the Cotopaxi, Texas Creek, Echo Park, and Ilse–Currant Creek fault zones, which are characterized by wide breccia and gouge zones. Samples were collected in three areas. First, 13 samples were collected on both sides of the major fault zones that intersect the valley (Fig. 14) along the highway that follows the Arkansas River. Second, samples were obtained from both sides of the Currant Creek fault zone, north of the Arkansas Valley. Finally, samples were taken along elevation traverses in the block west of the Cotopaxi fault (South Burno Mountain), in the block between the Cotopaxi and Texas Creek faults (Garell Peak), and to the east of the Texas Creek fault.

The AFT ages from the Arkansas River profile range from 55 to 78 Ma with mean track lengths of 13–13.5 μm (Fig. 15, 94ARK01), along the western one-third of the traverse. To the east of Echo Park AFT ages range from 92 to 174 Ma with mean track lengths of 10–12 μm, indicative of samples within the PAZ (Fig. 15, 94ARK09). The ages on both sides of large faults that cross the Arkansas River are similar except across the Echo Park and Cotopaxi faults, where the older age on the west side is compatible with mapped down-to-the west offsets (Scott et al. 1978). The largest gradient in age along this profile occurs in the block between the Texas Creek and Echo Park faults; this gradient is consistent with the eastward tilt of Echo Park half-graben. The ages along the Currant Creek fault zone to the north of the Arkansas River are from both within and below the fossil PAZ and lack a constant pattern with respect to the fault (Fig. 14). One block between the two strands of the fault zone seems to be strongly tilted toward the west. The age distribution here is reminiscent of the complex pattern in the Elevenmile Canyon Reservoir area to the north. The offset of the Rocky Mountain erosion surface across the Currant Creek fault is down-to-the west; the younger ages on the northeast side of the zone are consistent with the observed offset.

The age-elevation traverses in the western part of the Arkansas Valley

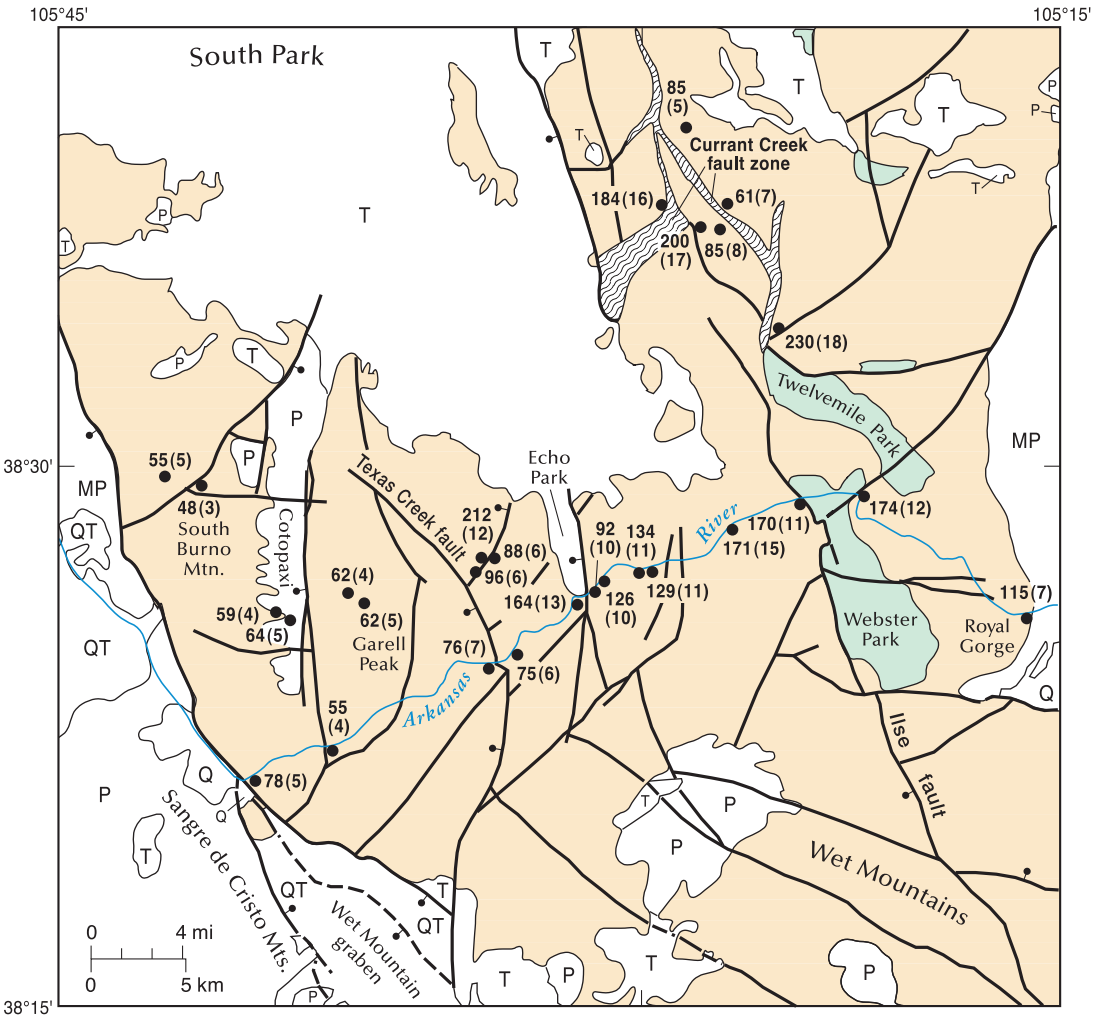

FIGURE 14—Simplified geologic map of the Arkansas Valley (after Scott et al. 1978). The AFT age and the standard error of the age are shown adjacent to the sample localities (solid circles). Map symbols as described in Figures 3 and 11. Shear zone shown as wavy lines. See Table 1 for sample numbers, elevations, and analytical data.

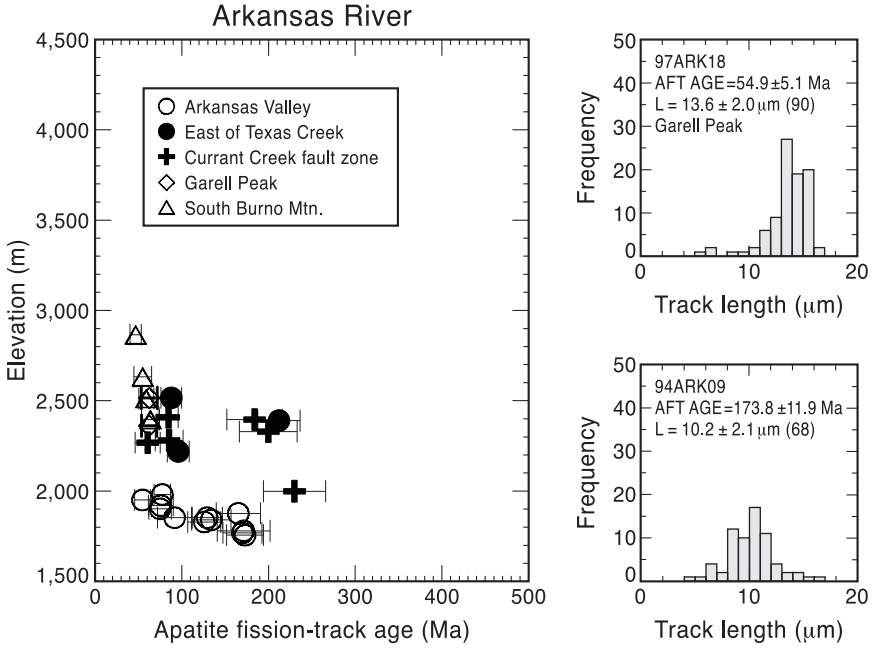

FIGURE 15—Age-elevation profiles for Arkansas River traverse. Age error bars are 2 σ. Track-length distributions for Garell Peak (97ARK18) and the sample immediately east of Webster Park (94ARK09) are shown to the right. AFT age, standard error of age, mean track length, standard deviation of length, and number of confined tracks measured (in parentheses) shown on track-length histogram for each sample. See Table 1 for analytical data.

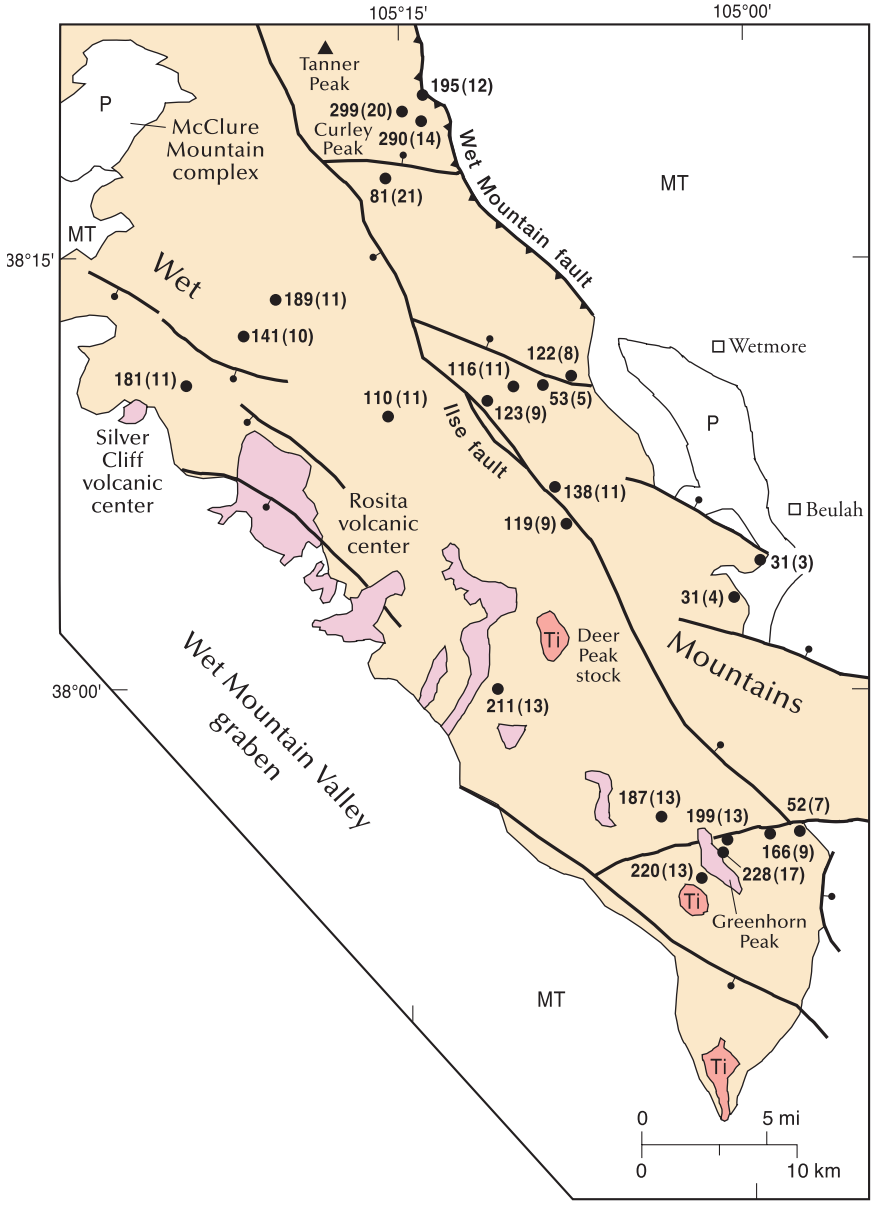

FIGURE 16—Simplified geologic map of the Wet Mountains. Symbols as described in Figures 3 and 11. **Pink** = late Eocene to Miocene volcanic rocks, **Ti (red)** = Oligocene (?) intrusives. After Scott et al. (1978). See Table 1 for sample numbers, elevations, and analytical data.

show that the base of the PAZ is preserved at a moderate elevation in a fault block just east of Texas Creek, but it has been removed by erosion from the high points on Garell Peak and South Burno Mountain (Fig. 15). The exposure of a fossil PAZ to the east and Laramide AFT ages at higher elevation to the west (Figs. 14, 15) mimics the pattern seen in the Front Range (e.g., Figs. 6, 8), although the width of the zone of older AFT ages is much wider along the Arkansas River (20 km here compared to 1.5–5 km). This zone of older AFT ages at low elevation may be part of a complex ramp-like transition zone between the Front Range and Wet Mountains. No thrust fault has been mapped along the east side of the area and the Garden Park (Chandler) syncline separates this block from the Pikes Peak block to the east. The AFT age pattern seen here is most likely a continuation of the folding of the PAZ seen along the south side of Pikes Peak, with the base of the PAZ in the Arkansas River valley tilted toward the east, forming the western limb of a syncline. Rio Grande rift normal faulting on the west side of the block (Fig. 14) probably enhanced the tilt to the east. The thermal history recorded by the track-length data for samples below the PAZ (e.g., 97ARK18, Fig. 5e) shows relatively rapid Laramide cooling, followed by slower cooling likely related to the development of the Rocky Mountain erosion surface. The Neogene thermal event found in the Waterton Canyon and Pikes Peak data is not found here.

The Pikes Peak and Arkansas Valley areas, characterized by basement folding and a large westward step in the trend of the Southern Rocky Mountains, roughly corresponds to the projection of a broad northeast-trending Proterozoic boundary (Karlstrom and Bowring 1993), suggesting a possible link between this major crustal feature and the change in style of Laramide deformation. This boundary, at its inception, was a low-angle, north-dipping subduction zone that separated the arc terranes of the 1.8–1.7 Ga Yavapai and the 1.7–1.6 Ga Mazatzal provinces that have been identified by geochemical and geochronologic data (Shaw and Karlstrom 1999). The boundary does not consist of a discrete shear zone, but instead appears to have been folded during arc accretion during the Proterozoic (Shaw and Karlstrom 1999). This enigmatic boundary may have set the stage for the complex transition between the Front Range to the north and the Wet Mountains to the south.

Fryer (1996) completed a detailed structural analysis of minor faults cutting Cretaceous sandstones in the Webster Park area. He concluded that the Ilse fault, a major longitudinal fault in the Wet Mountains to the south (see next section), is a thrust fault. However, the similarity of the AFT ages on both sides of this structure argues against a strong dip-slip component of motion across the fault. The stress orientations observed by Fryer (1996), which are similar to those seen along the San Andreas fault (Zoback et al. 1987), cannot be used to rule out strike-slip movement. Although minor vertical motion during Laramide deformation did occur, as indicated by structures in the Cretaceous sedimentary rocks in Webster Park, the Ilse fault likely had a significant component of right-lateral slip, based on the presence of a wide zone of crushing and shearing associated with the fault, on a predominance of right-slip kinematic indicators, and on the orientation of the Twelvemile Park and Webster Park folds adjacent to the fault (Chapin 1983).

Wet Mountains

The Wet Mountains, which partly coincide with the location of the Apishapa uplift of Pennsylvanian–Permian age, are a north-northwest-trending mountain block that merges with the Front Range near Royal Gorge on the north and terminates to the south as a south-plunging anticline (Fig. 16).

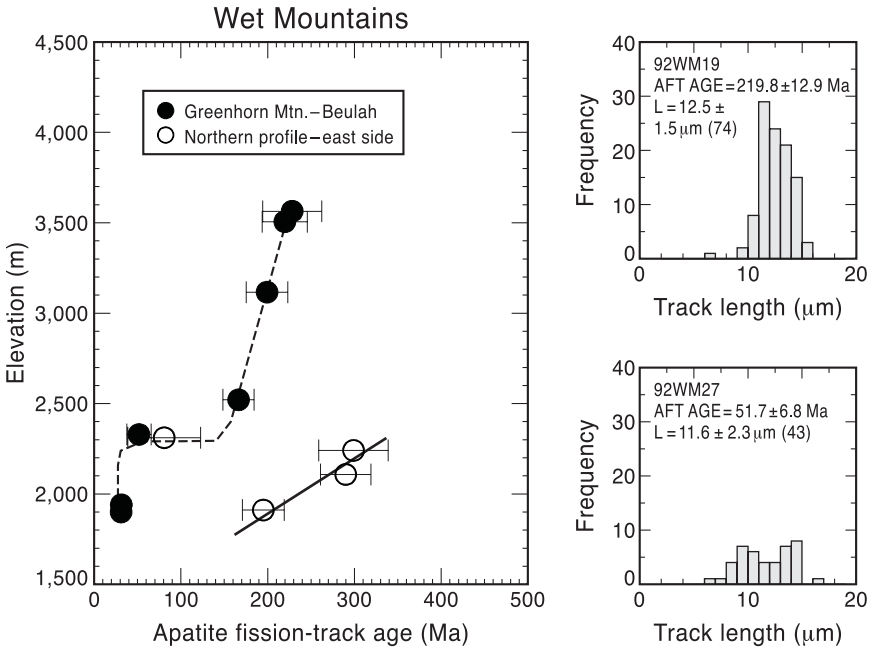

FIGURE 17—Age-elevation plots for the northeastern Wet Mountains and Greenhorn Mountain profiles. Track-length distributions for highest sample (92WM19) and lowest sample (92WM27) on Greenhorn Mountain shown at right.

The Wet Mountain thrust forms the northeastern margin of the block, and late Cenozoic normal faults are present on the southeastern side of the Wet Mountains. The geometry of the Wet Mountain thrust fault on the northeast side of the range is the subject of some debate. Jacob (1983) proposed that this thrust fault dips at a low angle to the west while Noblett et al. (1987) suggest that the fault shows high angle, east–vergent reverse motion with some evidence of later normal motion. Taylor (1975) depicted the Wet Mountain fault as a normal fault. The Wet Mountains are bounded on the west by the west–tilted Wet Mountain half-graben. Proterozoic migmatites, granodiorites, and granites are the dominant rock types exposed in the core of the range. The Wet Mountains are capped by the Rocky Mountain erosion surface (Fig. 1), with 27–38 Ma volcanic rocks from the Silver Cliff–Rosita Hills–Deer Peak volcanic centers locally covering the surface on the western margin of the block (Siems 1968; Scott and Taylor 1974; Sharp 1978; Taylor 1974). The Rocky Mountain erosion surface is also preserved under the 33.4 Ma (McIntosh and Chapin 2004 this volume) andesitic flows on Greenhorn Mountain at the south end of the range.

The northwest-trending Ilse fault (Fig. 16) divides the Wet Mountains into two distinctive segments characterized by different metamorphic protoliths and structural trends (Singewald 1966; Brock and Singewald 1968; Taylor 1975; Noblett et al. 1987). Two phases of Cenozoic movement have occurred along this fault. Sixteen km of right-lateral strike-slip motion during Laramide deformation has been inferred from the offset of Proterozoic features (Noblett et al. 1987). Late Cenozoic normal movement on the Ilse fault has offset the Rocky Mountain surface, dropping the west side down to form a 300-m-high, 20-km-long west-facing scarp in the northern part of the range (Taylor 1975). The down-to-the-west offset of the Rocky Mountain surface decreases to the north and is not evident in the Webster Park area.

AFT samples were collected from Proterozoic migmatitic gneisses and granodiorite along three traverses through the Wet Mountains (Fig. 16). Where possible, samples were collected away from the middle Cenozoic Silver Cliff–Rosita–Deer Peak volcanic centers on the west side of the mountains and away from the Oligocene intrusive centers in the southern part of the range to avoid complicating interpretation of the AFT data. Sharp and Naeser (1986) found that a mineralized pipe containing Proterozoic and Cambrian boulders within the Proterozoic terrane about 5 km from Silver Cliff yield AFT ages of 28 ± 3 and 33 ± 2 Ma, establishing that AFT ages are totally reset locally by the volcanism.

AFT ages from the northern profile are typically 140–300 Ma (Fig. 16; Table 1), except for one sample (92WM05) with an age of approximately 81 Ma that was collected near an east-trending cross-fault in the range. The three eastern samples along the northern traverse are from an elevation profile near Curley Peak in the more rugged eastern portion of the range. The ages decrease from about 300 Ma at high elevation to 195 Ma at the lowest elevation (Fig. 17; Table 1). The age of the sample from high elevation is indistinguishable from the 293 Ma AFT age determined by Olson et al. (1977) for the McClure Mountain alkaline intrusive complex. Vertical Laramide displacement is minor along this profile; lateral displacement along the range-bounding, low angle thrust fault is significant (Jacob 1983). Sample 92WM05, collected to the south of Curley Peak, is also on the east side of the Ilse Fault at a higher elevation than the Curley Peak samples, but it has a younger AFT age (81 ± 21 Ma). The error estimate for 92WM05 is high because only 7 datable grains were found; although the error is high, the age is significantly younger than the ages determined north of the fault. This younger age can be used to infer a minimum estimate of up-to-the-south displacement on the east-trending normal fault separating the two areas (open circles, Fig. 17). If we assume that the base of the Laramide PAZ is just below the lowest elevation sample on the Curley Mountain traverse (92WM01), then the minimum offset on the fault is 400 m.

Taylor (1975) presents geologic evidence for significant late Cenozoic displacement across north-trending faults in the northern Wet Mountains. Near the northernmost summit of the Wet Mountains (Tanner Peak), gravels containing clasts from the McClure Mountain complex and the 32.9 Ma Gribbles Park Tuff (McIntosh and Chapin 1994) are at an elevation 500 m higher than they are upstream (to the west). Taylor (1975) also notes that volcanic material containing Gribbles Park Tuff is present in an isolated outcrop southwest of Cañon City. This outcrop is 1,130 m below the base of the gravels capping Tanner Peak, which is just north of the Curley Mountain profile. However, the outcrop southwest of Cañon City is a debris flow whose time of emplacement is not known, and it should not be used to estimate the amount of Neogene offset on the mountain-front fault.

The three western samples on the northern traverse, with ages ranging from 141 to 189 Ma (Fig. 16), are from the Rocky Mountain erosion surface west of the Ilse fault. These samples are located about 30 km southeast of samples with similar ages in the Arkansas River valley. Note that the three western samples are higher in elevation and are younger than the Curley Peak samples (Table 1). The age contrast

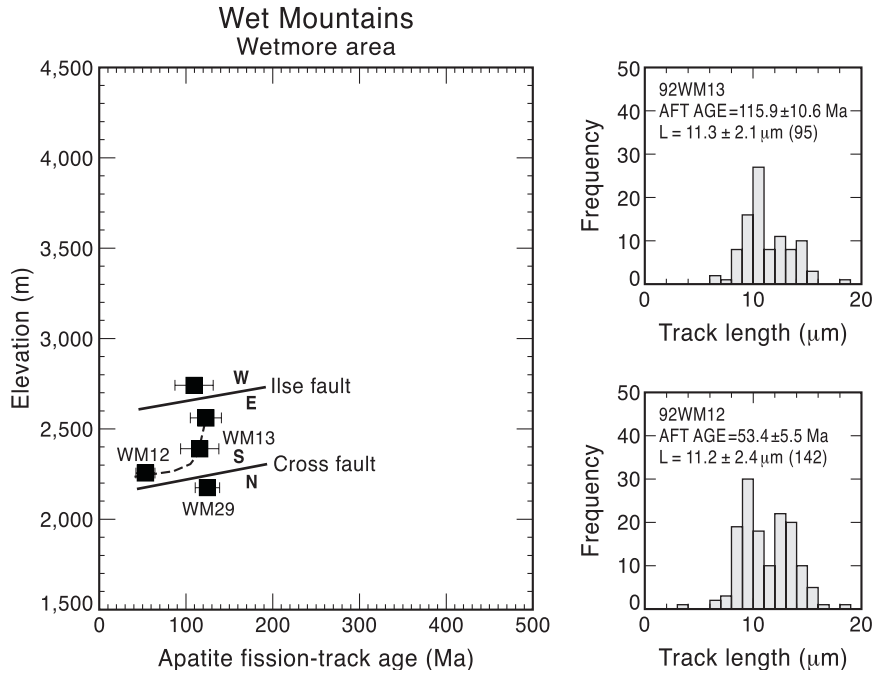

FIGURE 18—Age-elevation profile for Wetmore area showing relationship of AFT age data to Ilse fault and northwest-trending cross fault (Fig. 16). Representative track-length distributions from this profile are presented at right.

may be due to burial by tuffs and lava flows during volcanism on the west side of the range. Alternatively, the age difference may indicate that the east side of the northern Wet Mountains moved down with respect to the west side during Laramide deformation, as indicated by the structural relations in Webster Park to the north. The down-to-the-west offset observed on this segment of the Ilse fault today occurred during late Cenozoic rifting.

The five samples from the Wetmore area (Fig. 16) collectively yield the youngest AFT ages in the Wet Mountains (53–123 Ma). Sample 92WM11 (AFT age of ~ 110 Ma), which is located to the west of the Ilse fault, is the youngest of the west-side samples. The three highest elevation samples (92WM10, 92WM13, 92WM12) from the east side of the Ilse fault display an interesting age-elevation relationship (Fig. 18). The ages decrease from approximately 123 Ma at high elevation (92WM10) to 53 ± 6 Ma at lower elevation (92WM12). The shape of this portion of the age-elevation profile (Fig. 18) may represent the exposure of the top of a fossil middle Cenozoic PAZ in the Wetmore area (compare to Fig. 2). The lowest elevation sample, 93WM29, which is separated from 92WM12 (53 Ma) by a fault, has an age of 122 ± 8 Ma. If we assume that the lowest elevation sample (93WM29) is in about the same position in the uplifted PAZ as the middle elevation sample (92WM13; see Fig. 18), we estimate a minimum of 215 m of down-to-the-north offset across the southeast-trending fault.

The AFT data from the Wetmore area also record a middle Cenozoic thermal event. The Wetmore samples did not cool significantly during Laramide deformation and reached a minimum temperature of ~ 60 °C at approximately 40 Ma. The young age and bimodal histograms of the Wetmore samples are best explained by having a heating event with a maximum temperature of ~ 80° C at 30 Ma superimposed on an otherwise relatively simple cooling history. The area cooled substantially during the last 15 Ma. The similarity of the timing of the heating event with the age of volcanism in the Silver Cliff–Rosita–Deer Peak volcanic field suggests a causal relationship. One possible way of explaining the ~ 20 °C rise in temperature is to invoke burial of this portion of the Wet Mountains by a < 1-km-thick middle Cenozoic volcanic section (perhaps in a paleovalley) that has since been stripped away; remnants of lava and debris flows are preserved on the Rocky Mountain erosion surface in the southern and western parts of the range. Alternatively, although the area is about 15 km from the nearest volcanic center, it is possible that the higher temperatures are simply related to elevated geothermal gradients during volcanism.

South of Wetmore, two samples were collected on either side of the Ilse fault in an attempt to determine whether significant vertical offset had occurred across the fault (Fig. 16). Within error, the ages and track length distributions are the same across the fault and are comparable to those found on opposite sides of the Ilse fault on the Wetmore profile. Consequently, at least along this particular section of the Ilse fault, the vertical offset since late Paleozoic time is less than the resolution of the AFT method. Similar results were also found on either side of the Ilse fault to the north in the Webster Park area.

The data from the Greenhorn Mountain profile show that the southern Wet Mountains have experienced a thermal history that is different from those reconstructed for the Front Range and northern Wet Mountains. The AFT ages vary from 228 ± 17 Ma for Proterozoic rocks collected a short distance below the Oligocene andesitic flows (33.4 Ma; McIntosh and Chapin 2004 this volume) that form the summit of Greenhorn Mountain to 31 ± 4 Ma at the lowest elevations near the town of Beulah (Fig. 16). Broad track-length distributions with mean track lengths of 11–12.5 μm characterize all samples from this traverse. Based on the shape of the age-elevation profile and on short mean track-length data from the lowest-elevation samples, the top of an uplifted middle Cenozoic PAZ is exposed in the southern Wet Mountains. Modeling of the low-elevation AFT data in the Beulah and Greenhorn Mountain areas (Fig. 5f) indicates that the south end of the Wet Mountains was strongly heated to temperatures of 95–110 °C at 25–30 Ma, which overlaps the timing of emplacement of several volcanic centers near the southern Wet Mountains (Spanish Peaks, Mt. Maestas, and Rosita–Silver Cliff). Assuming that the top of Greenhorn Mountain was at the surface at 33 Ma, as indicated by the presence of the andesitic lava flows, and that the Beulah age and track-length data constrain the temperatures of the rocks at low elevation to be ~ 95 °C, we can estimate the paleogeothermal gradient during Oligocene time at the south end of the Wet Mountains. Assuming a surface temperature of 15 °C, the temperature difference of (95 °C–15 °C) divided by 1,700 m, the difference in elevation between the two points, yields a gradient estimate of ~ 47 °C/km.

In summary, based on the aerial and vertical distribution of >100 Ma ages in the Wet Mountains (Figs. 16, 17), the amount of Laramide denudation in the Wet Mountains is comparable to that along the eastern margin of the Front Range. Because Laramide AFT cooling ages are not present below the fossil PAZ, vertical uplift of the center of the Wet

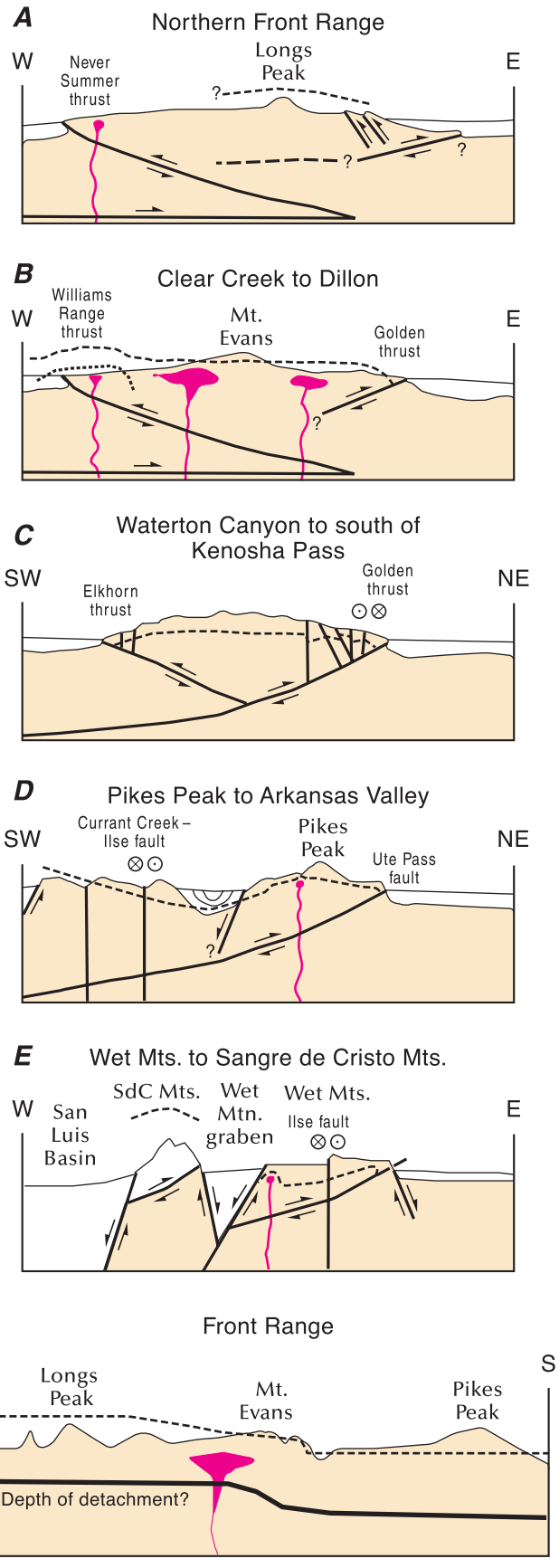

FIGURE 19—Schematic cross sections showing the geometry of the faults and the disruption of the base of the PAZ by Laramide and subsequent extensional deformation in the Front Range and Wet Mountains. Top panel (**A**) after Erslev and Holdaway (1999). **Brown** = Proterozoic basement and unshaded areas are undivided sedimentary cover of Phanerozoic age. The **red shaded areas** are Mesozoic to Cenozoic plutons. The base of the PAZ is shown as a dashed line, and the Tertiary disturbance of the AFT ages on the west side of the Front Range is shown as a heavy dashed line on **B**. **Strike-slip symbols**: circle with dot indicates the block moving out of the page, whereas the circle with x signifies the block moving into the page. The vertical exaggeration of each cartoon varies to accommodate emphasis of certain details in each section.

Mountains during Laramide deformation was apparently significantly less than that in the interior of the Front Range. Lateral displacement along the thrust faults on the east side of the range apparently dominated the style of Laramide deformation in the Wet Mountains.

The amount of middle Cenozoic heating and late Cenozoic denudation increases from north to south. The low elevation sample in the northern part of the range has an AFT age of 195 Ma, whereas the low elevation ages near the south end range from 31 to 52 Ma. Down-to-the-north cross faults within the Wet Mountains, such as the faults south of Curley Peak and in the Wetmore area, have accommodated some of the differential uplift between the northern and southern parts of the mountain block. A northward tilting of the Wet Mountains is also supported by the fact that the Rocky Mountain erosion surface at the south end of the range is at a higher elevation (~ 3,500m) than it is in the northern part of the mountain block (2,300–2,500 m). The middle Cenozoic temperature increase in the Wetmore area in the east central part of the range is only about 20 °C, but it is > 90 °C just 15 km to the south in the Beulah area. The cause for this sudden rise in temperature is not likely due to the local volcanism because > 200 Ma AFT ages are preserved near intrusives in the southern Wet Mountains (Fig. 16). Instead, these data may record the northern edge of a regional heat flow anomaly associated with Oligocene volcanism and late Oligocene to early Miocene regional denudation along the High Plains-Southern Rocky Mountains boundary that extends southward into New Mexico (Kelley and Chapin 1995; Chapin et al. 2004 this volume).

Discussion

A summary of the geometry of the partial annealing zone

Figure 19 summarizes the Laramide and post-Laramide disruption of the apatite fission-track PAZ in the Front Range and Wet Mountains. The PAZ likely had gentle topography at subsurface depths of 2.5–4 km at the end of Late Cretaceous marine sedimentation in the Southern Rocky Mountain region. In the northern Front Range, the fossil PAZ has been removed by erosion from the highest peaks (Fig. 19a). The east side of the northern Front Range was broken by a series of northwest-trending, northeast-dipping back thrusts above a postulated blind thrust at depth, with arching of the range possibly aided by eastward insertion of a lower crustal wedge (Erslev and Holdaway 1999; Erslev et al. 1999). The west side of the northern Front Range is bordered by the low-angle, east-dipping Never Summer Thrust, which displaces Proterozoic basement as much as 10 km westward over sedimentary strata of the North Park syncline. A west-tilted fossil PAZ is preserved on the west side of the range on Clark Peak just north of the line of cross section (Cervany 1990).

Mt. Evans, in the central Front Range (Fig. 19b), is located just inside of a northeast-trending line that marks the southeastern edge of the area affected by the plutons of the Colorado Mineral Belt (Fig. 8). The base of the PAZ occurs at an elevation of 3,500 m on Mt. Evans, which is approximate-

ly 1 km higher than the base of the PAZ on Crow Hill (2,400 m) near Bailey, approximately 20 km to the southeast. The change in the elevation of the PAZ is sharp and is not controlled by faulting. The pattern is similar between Von Bibber and Golden Gate Canyons, where the northeast-trending line intersects the western edge of the Denver Basin (Fig. 6). At the latitude of Mt. Evans, the Front Range is bounded on the west by the east-dipping, low-angle Williams Range thrust, which displaces Proterozoic rocks westward at least 9 km over Cretaceous Pierre Shale (Erslev et al. 1999). Middle Cenozoic intrusive activity along the Colorado Mineral Belt and Rio Grande rift extension on the west side of the range have reset the AFT ages in the vicinity of Dillon to 7–40 Ma (dashed line on left side of Fig. 19b; Naeser et al. 2002). The east side of the Front Range is bounded by the Golden thrust. The Golden fault has been variously interpreted to be high-angle reverse, moderate-angle reverse, low-angle thrust, and even a normal fault (Berg 1962a,b; Jacob 1983; Kelley and Chapin 1997). The preservation of old (> 100 Ma) AFT ages at low elevation along the margin of the range indicates that the Front Range moved laterally over the adjacent Denver Basin above a low- to moderate-angle thrust during Laramide deformation.

Figure 19c represents the area between Waterton Canyon and the Elkhorn thrust south of Kenosha Pass that is outside the thermal affects of the Colorado Mineral Belt. Here, the base of the PAZ, which is exposed in several places within the range, is higher in the center of the range than it is at the margins, but the amount of upwarp is much less than it is to the north. As in Figure 19b, > 100 Ma AFT ages are preserved along the eastern edge of the range at Waterton Canyon and at Deer Creek. The Elkhorn thrust is the dominant structural feature on the west side. This cross section shows that the southern Front Range is basically a basement arch with both the eastern and western margins thrust laterally over the adjacent basins. The center of the Front Range has moved up with respect to the margins across northwest-trending faults in the basement. A few back-thrusts with left-slip displacement (e.g., Kennedy Gulch, Floyd Hill) have been documented in Waterton Canyon.

Figure 19d is a northeast-southwest schematic cross section extending from Pikes Peak along the north side of the Arkansas River canyon west through Burnt Mountain (Fig. 14). At this latitude the Front Range is bound on the east by the Ute Pass–Cheyenne Mountain thrust fault (Scott et al. 1978; Jacob 1983; Jacob and Albertus 1985). Pikes Peak is a monadanock that towers above the remnants of the Rocky Mountain erosion surface with late Eocene to early Oligocene volcanic rocks locally preserved on the surface. The western margin of the Front Range is marked by a Laramide syncline in the Garden Park area (Fig. 12) and by down-to-the west, late Cenozoic normal faulting along the Oil Creek–Fourmile Creek drainage. The west-directed Elkhorn thrust, which forms the western margin of the Front Range to the north, is not exposed south of Elevenmile Canyon Reservoir (Figs. 1, 10). The elevation of the base of the PAZ is downwarped from 2,600 m on Pikes Peak to < 1,650 m at Royal Gorge. The elevation of the base of the PAZ is between 1,800 m and 2,900 m in the Arkansas River valley, and this marker generally dips to the east. The AFT ages are basically the same across the Ilse fault, which argues against significant vertical Laramide offset across this structure.

The Laramide fault geometry on the eastern margin of the Wet Mountains block (Fig. 19e) is similar to that in the Front Range. Most of the AFT ages are greater than 100 Ma and the mean track lengths are generally short, features characteristic of residence in the pre-Laramide PAZ. Exceptions are the lowest sample on Greenhorn Mountain (52 Ma; Fig. 16), the lowest sample near Wetmore (53 Ma), and the two low-elevation samples near Beulah. All of these younger AFT ages have short mean lengths and multimodal length distributions (Fig. 16). Modeling of the AFT data (Fig. 5f) indicates an Oligocene thermal event ranging from 80 to 110°C. Preservation of the late Mesozoic PAZ (as much as 1.3 km thick) throughout the Wet Mountains indicates that Laramide denudation was less than that in the Front Range. The existence of Eocene and Oligocene AFT cooling ages at the base of the PAZ indicates that the cooling history here is dominated by middle Cenozoic events.

Figure 19f is a north-south schematic section of the Front Range portraying the kilometer-scale warping of the base of the late Mesozoic PAZ. The possible geometry of the middle crustal detachment zone of Erslev et al. (1999) is also shown. The relatively sharp upwarp of the PAZ south of Mt. Evans is constrained by the AFT data in the North Fork of the South Platte River. We will explore potential explanations for the north-south geometry of the PAZ in the next section.

North-south change in elevation of the PAZ in the Front Range

Three possible factors affecting the south to north geometry of the fossil PAZ in the Front Range (Fig. 19f) are examined. These factors include (1) elevated geothermal gradients in the vicinity of the Colorado Mineral Belt; (2) structural tilting due to pluton inflation; and (3) changes in the thickness of the low-thermal conductivity Pierre Shale.

Thermal modeling of the Colorado Mineral Belt—A large gravity low on the west side of the Front Range centered on Leadville, Colorado, has been attributed to composite Laramide and Neogene granitic plutons that are on the order of 50 km in diameter (Case 1965; Tweto and Case 1972; Steven 1975; Isaacson and Smithson 1976). The gravity low associated with the Colorado Mineral Belt becomes much less prominent to the northeast, and the gravity trough is approximately 15–20 km wide in the Boulder–Central City segment of the Colorado Mineral Belt. Here we will investigate the thermal effects Laramide plutons on the geometry of the PAZ in two key places. First, we will determine if the abrupt change in the elevation of the PAZ (1 km over a distance of 4 km) in the Clear Creek area can be explained by simple thermal effects. Second, we will see if it is possible to raise the temperatures on the summit of Longs Peak to > 110 °C using only heat from Laramide plutons.

The westernmost sample on the Clear Creek traverse is approximately 1 km from a dike associated with the mineral belt and is about 4 km from the outer margin of mineralization near Idaho Springs and Central City (Figs. 1, 6). Sims (1963) used sphalerite to estimate that temperatures within the zone of most intense mineralization in the Idaho Springs–Central City district were 400–600 °C, whereas temperatures on the margins of the mineralized area ranged from 150 to 300 °C. Similarly, the fluid inclusion data of Rice et al. (1985) provide temperatures estimates of 200–420 °C for the Central City district. The maximum half-width of the Idaho Springs intensely-mineralized zone is about 3 km (Sims 1963), and the half-width of the Colorado Mineral Belt at this latitude based on surface exposures of the plutons is approximately 8.5 km (Bryant et al. 1981).

A conductive thermal model was run to investigate the possible thermal effects from the Colorado Mineral Belt on the Clear Creek AFT data. Oxygen isotope data from Proterozoic rocks in the Central City district show that the mineralizing fluids were confined to fractures in the mineral belt and did not flow pervasively through the Proterozoic gneisses (Rice et al. 1985), so the assumption of conductive heat flow outside the mineral belt is appropriate. The intru-

sive activity and mineralization most likely occurred at depths of approximately 1–2 km, based on the porphyritic nature of the intrusives in the mineral belt and pressure information derived from the study of fluid inclusions (Rice et al. 1985). We used a two-dimensional, finite-difference model (Jaluria and Torrance 1986). We assumed that the entire 17-km-wide mineral belt was underlain by a granitic magma chamber (800 °C plus latent heat) that was emplaced at a depth of 2–4 km. This model is conservative because, in light of the gravity data, the plutons may be wider at depth. The thermal conductivity of the Proterozoic country rock is estimated to be 2.9 W/m°K. Instantaneous emplacement was assumed because many of the K-Ar and apatite and zircon fission-track ages from the intrusions are concordant (Cunningham et al., 1994). An average basal heat flow of 63 mW/m² was used in the model.

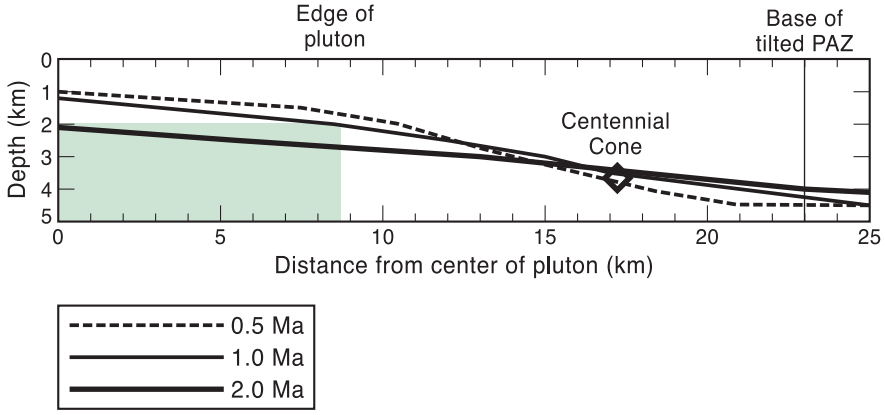

FIGURE 20—Plot of the position of the 110 °C isotherm as a function of time and distance from pluton center in the Clear Creek area. The green region marks the half-width of the pluton. The position of Centennial Cone with respect to the Colorado Mineral Belt is shown for reference. The lines show the evolution of the 110° C isotherm 0.5 Ma (dashed line), 1.0 Ma (solid line), and 2.0 Ma (heavy solid line) after pluton emplacement.

Figure 20 shows the position of the 110 °C isotherm as a function of time for a pluton emplaced at a depth of 2 km below the surface; the results are similar for a pluton at a 4 km depth, but the effects are more subdued. Under these conditions, the base of the PAZ in the vicinity of Centennial Cone located 9 km from the edge of the mineralized zone, would be elevated ~1 km above its background level of 4.5 km below the surface at 1 Ma. The slope on the PAZ is gentle at 1 Ma. Note that by 2 Ma, heat from the pluton diffuses out to the area of the age transition (dashed line, Fig. 20; Fig. 6), reducing slope on the isotherm. Although the relative relief on the isotherm between the mouth of Clear Creek canyon and Centennial Cone appears to be related to elevated temperatures in the vicinity of plutons along the Colorado Mineral Belt, the abrupt nature of the transition cannot be explained by thermal diffusion alone.

Thus the 1 km upwarp of the base of the Mesozoic PAZ is in part due to the thermal effects of Laramide-age plutonic activity along the Colorado Mineral Belt. Note that the transition is found only along the southern edge of the Colorado Mineral Belt and is not recorded to the north (Fig. 3). A strictly thermal effect due to plutonism should be somewhat symmetrical. On Mt. Evans, which lies within the influence of the southern edge of the Colorado Mineral Belt, the base of the PAZ is preserved, but the base of the PAZ is not preserved on Longs Peak. This observation indicates that either more exhumation has occurred on Longs Peak compared to Mt. Evans or the thermal affects of the Colorado Mineral Belt pushed the 110 °C isotherm to a position that is 850 m higher on Longs Peak. Both Mt. Evans and Longs Peak are in comparable positions with respect to the Colorado Mineral Belt.

Using geologic and geophysical constraints, a simple conductive thermal model was designed to determine whether the extrapolated position of the 110 °C isotherm (PAZ; Fig. 21) on Longs Peak is caused by elevated heat flow in the vicinity of plutons. The width of the prominent gravity low across the Front Range was used to estimate the width of the pluton, which is about 40 km. For simplicity, the modeled pluton is centered on the exposure of stocks located southeast of Longs Peak, which may not be strictly true because the gravity anomaly is skewed to the south of the stock exposures. However, we are trying to reasonably maximize the heat input into the Longs Peak area by magmatism. In this model, we are constrained to put the top of the pluton at a minimum of 4 km below the surface because, based on the modern topography, the top of the stock is 1.7 km below the summit of Longs Peak (Fig. 20) and at least 2.5–3.5 km of Phanerozoic section sat on the basement in this area prior to Laramide deformation (Bryant et al.,1981).

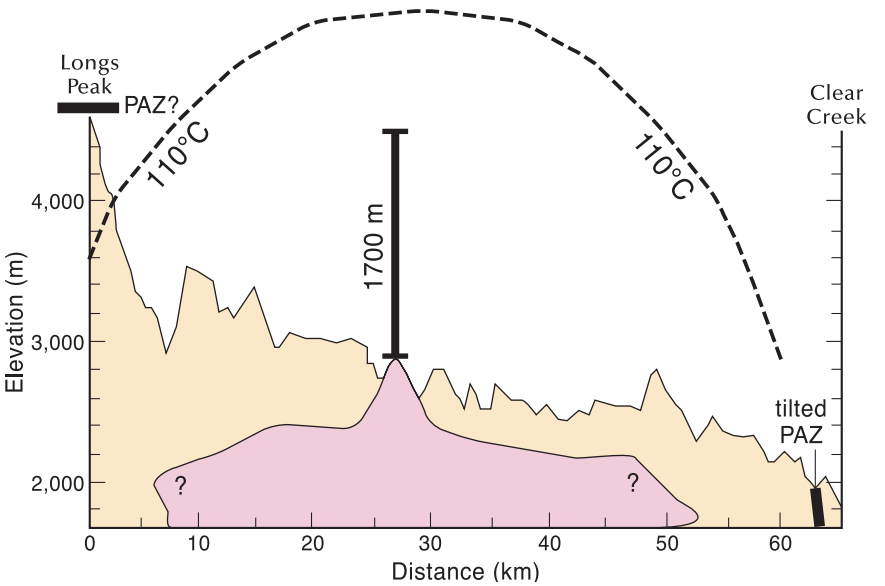

FIGURE 21—Illustration of the modern topography between Longs Peak and Clear Creek plotted from 30 m digital elevation data. Vertical exaggeration is 12.5. The approximate geometry of the magma body in this area (pink) is based on surface exposures of the plutons (Bryant et al. 1981; Braddock and Cole 1978) and gravity data. The estimated position of the 110 °C isotherm based on the thermal model discussed in the text is shown as a dashed lines, and the heavy line above Longs Peak is the estimated observed position of the base of the PAZ. The modern elevation difference between the top of the pluton and the summit of Longs Peak is 1,700 m.

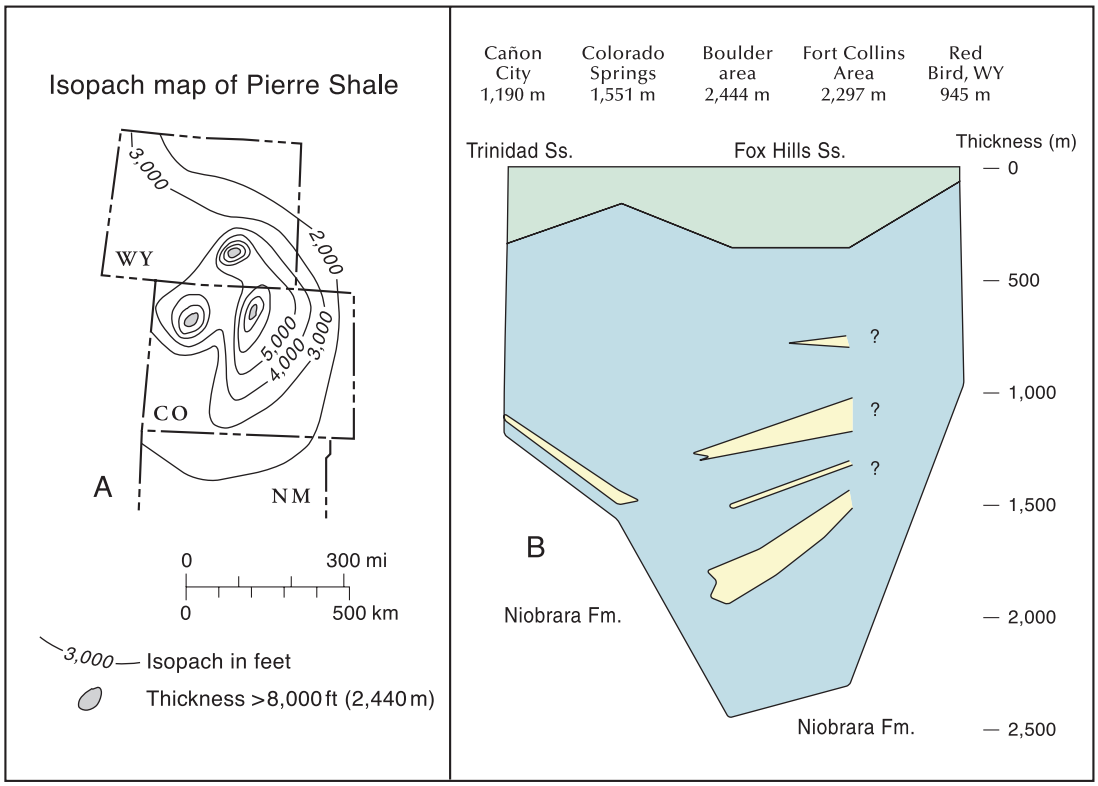

FIGURE 22—(**A**) Isopach map of Pierre Shale from Tourtelot (1962). (**B**) Stratigraphic sections from Scott and Cobban (1965, 1975, 1986a,b). **Green** = sandy shale; **blue** = shale; **yellow** = sandstone.

An average basal heat flow of 63 mW/m^2 was used in the model.

The relative temperature increase on the Longs Peak summit due to heating by magmatism, assuming the pluton geometry in Figure 21, is only about 20 °C above background temperatures. Based on the calculated position of the 110 °C isotherm at 1 Ma after pluton emplacement, which is the time of maximum heating of the country rock, the base of a PAZ should be preserved on Longs Peak (Fig. 21). The AFT ages on the summit of Longs Peak could be reset during Laramide plutonism only if the magma chamber is directly under the peak. No geologic or geophysical evidence support the presence of a pluton under Longs Peak. Consequently, the thermal effects of the Colorado Mineral Belt do not fully explain the prevalence of Laramide cooling ages on Longs Peak and in the northern Front Range.

Pluton inflation—The transition in the elevation of the base of the PAZ shown in Figure 6 in Clear Creek canyon is more abrupt than that predicted from thermal effects alone. Inflation (Brown and McClelland 2000; Petford et al. 2000) during the emplacement of Laramide plutons, which are often modeled as tabular bodies 8–25 km thick (Issacson and Smithson 1976) may have structurally enhanced the doming of the base of the PAZ.

Thermal consequences of thick Cretaceous marine shale—Another possible explanation for the apparently higher temperatures in the northern Front Range compared to the southern Front Range is related to variations in the thickness of the Late Cretaceous Pierre Shale. Figure 22a is an isopach map of the Pierre Shale in the Southern Rocky Mountain area and Figure 22b is a compilation of measured sections through this unit along the eastern margin of the Front Range, as well as a section in Black Hills in Wyoming. Both of these diagrams show that the Pierre Shale is significantly thicker in the northern Front Range compared to surrounding areas. Scott and Cobban (1965) note that the thickness of the Pierre increases rather abruptly between Kassler just south of Denver (1,585 m) and Boulder (2,440 m; this hingeline roughly coincides with the Colorado Mineral Belt. Sass and Galanis (1983), Blackwell and Steele (1989), and Forster and Merriam (1997) have measured or estimated the thermal conductivity of the Pierre Shale in the mid-continent and found it to be quite low (1.2 W/m°K). These authors have determined that modern geothermal gradients are 50–60 °C/km through this unit in South Dakota and Kansas. This thick shale package should have a profound effect on the temperatures of rock units beneath it.

To test this idea, two hypothetical temperature-depth curves were constructed for conditions at the end of Cretaceous time before the Laramide Orogeny (Fig. 23) using the thermal resistance method of Bullard (1939). The thickness of the Pierre Shale in the Cañon City area and in the Fort Collins area (Fig. 22b) is used. The thickness of the section between the Proterozoic basement and the top of the Cretaceous Niobrara Formation is from Weimer (1996) and Scott et al. (1978). Scott and Cobban (1965, 1975, 1986a,b) and Izett et al. (1971) point out that the Pierre Shale contains very little sandstone in the southern Front Range but that the amount of sandstone increases toward the north. Consequently, a typical Pierre thermal conductivity of 1.2 W/m°K is assumed for the southern profile and a higher thermal conductivity of 1.5 W/m°K is used to account for the facies changes documented by Scott and Cobban (1965, 1975, 1986a,b) to the north. Average thermal conductivity values (e.g., Carter et al. 1998) are assigned to sandstones, limestones, basement rocks, and units of mixed lithology in the section. An average basal heat flow value of 63 mW/m^2 is used in these calculations. An atmospheric mean annual surface temperature of 20° C is assumed for the end of

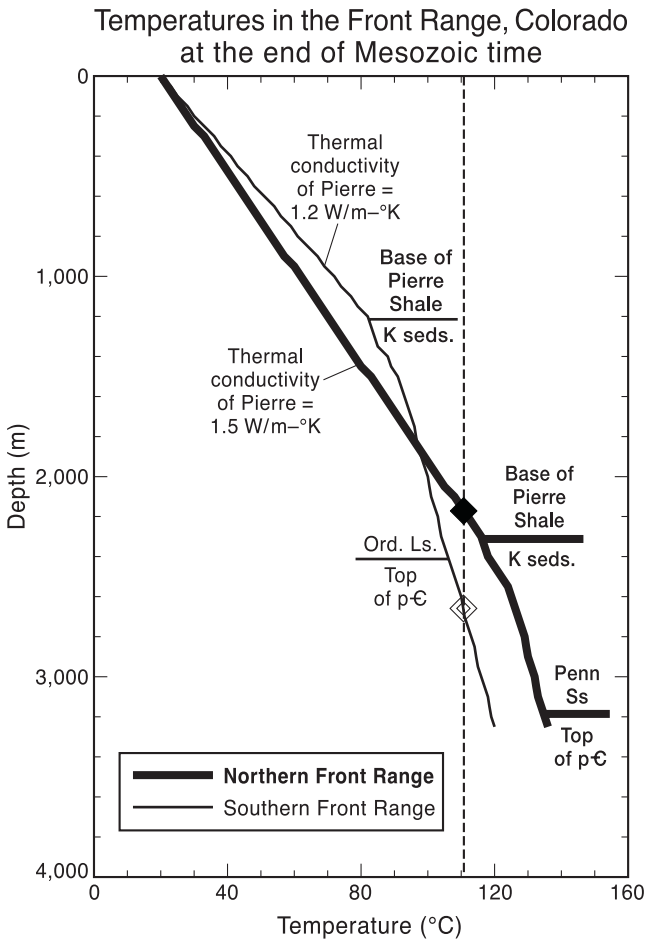

FIGURE 23—Estimated temperature as a function of depth before Laramide deformation for the Pikes Peak area and the Longs Peak area using the methods and assumptions outlined in the text. **K seds.** = Cretaceous sedimentary rocks; **Ord. Ls.** = Ordovician Limestone; **Penn Ss** = Pennsylvanian sandstone; and **p€** = Proterozoic basement.

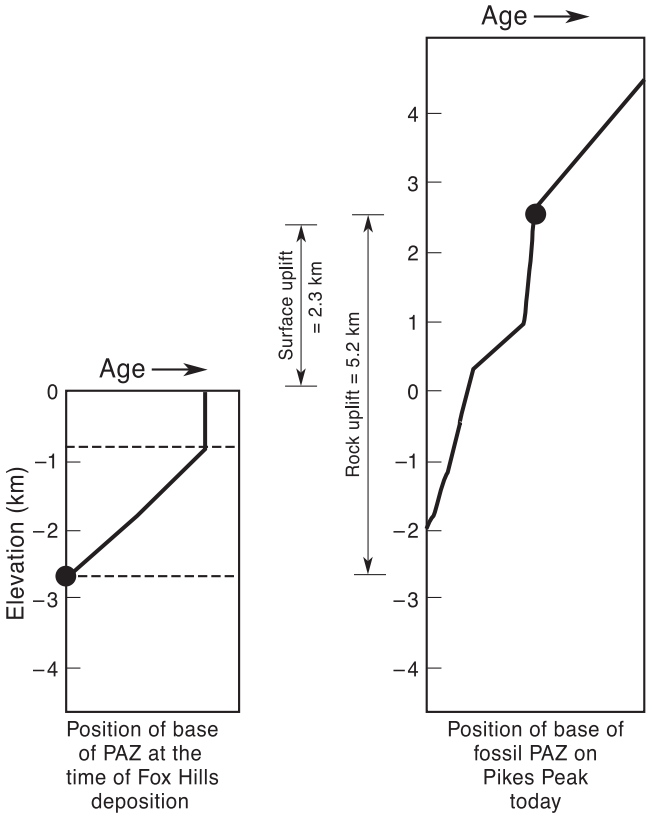

FIGURE 24—An illustration of the rock uplift calculation that considers the influence of the Pierre Shale on the pre-Laramide thermal structure of the southern Front Range. The depth of the PAZ at the end of the Cretaceous shown in Figure 23 in the Pikes Peak area is used in the calculation.

Mesozoic time. Total annealing occurs at ~ 110 °C in most fluorapatites.

The calculated temperature profiles show that the 110 °C isotherm was in the Proterozoic basement in the southern Front Range in Late Cretaceous time (open diamond, Fig. 23), as recorded by the preservation of a fossil PAZ on Pikes Peak (Fig. 13). In contrast, the base of the PAZ was in the Pierre Shale in the northern Front Range prior to Laramide deformation (solid diamond, Fig. 23). The temperature at the top of the basement was ~ 100 °C in the southern Front Range and ~ 135 °C in the north. Thus, an increase in the thickness of Cretaceous sedimentary units in the northeastern Front Range, and the resultant increase in basement temperature could be in part responsible for the fact that the Mesozoic PAZ is not preserved in the basement here. The Mesozoic PAZ formed in the overlying sedimentary units, which have since been stripped away.

What is controlling the north-south geometry of the PAZ?—Although none of the three thermal or structural phenomena discussed above completely explain the observed AFT age distributions across the Colorado Mineral Belt and in the northern Front Range, a combination of heating and tilting due to plutonic activity in the Colorado Mineral Belt and the south to north increase in the thickness of the Pierre Shale appear to have led to the pattern that we see today. The emplacement of plutons along the Colorado Mineral Belt certainly raised the elevation of the 110 °C isotherm by > 1 km, but thermal diffusion predicts that the transition between > 100 Ma AFT ages and Laramide cooling ages would occur over several tens of kilometers (Fig. 20) rather than over the 3–4 km observed in Clear Creek and at Kenosha Pass. One possibility is pluton inflation and buoyancy of the crust in the Colorado Mineral Belt enhanced the tilt of the PAZ. The distribution of Pierre Shale helps explain the large area of the northern Front Range that lacks a preserved PAZ, but Late Cretaceous sedimentation patterns do not account for the abrupt upwarp of the Mesozoic PAZ southeast of the Colorado Mineral Belt.

Denudation estimates

Constraints on the total amount of surface uplift, rock uplift, and denudation in the Front Range since the end of Cretaceous time can be determined from the AFT data in areas not influenced by the Colorado Mineral Belt, namely the Pikes Peak and Waterton Canyon areas. The present mean elevation of the Front Range is approximately 2.5 km (Gregory and Chase 1994). The paleomean surface elevation in the Southern Rocky Mountains at the end of Mesozoic time was sea level because the Fox Hills Sandstone was deposited in a beach environment. Sea level was approximately 150–200 m higher compared to today, so the total mean surface uplift in the Front Range is approximately 2.3 km (Fig. 24). The depth of the base of the PAZ with respect to sea level at the end of Mesozoic time was calculated to be at ~ 2.6 km below sea level, as described above (open diamond, Fig. 23) and is shown as a solid circle on Figure 24a. The present elevation of the base of the fossil PAZ on Pikes Peak is 2.6 km (solid circle, Fig. 24b). Thus, the total amount

of rock uplift is 5.2 km (Fig. 24b) and denudation is 2.9 km in this area. Using a similar analysis for the North Fork of the South Platte River, rock uplift varies from 3.9 to 4.9 km between the mouth of Waterton Canyon and Bailey. Denudation in this area is 1.4–2.4 km. The thickness of the sedimentary section used to determine the position of the 110 °C isotherm in Figure 23 indicates that rock uplift in the Longs Peak area is > 6.4 km. The amount of rock uplift, primarily driven by Laramide deformation, appears to increase from south to north in the Front Range. For comparison, the modern elevation of the base of the PAZ on Laramie Peak in the Laramie Mountains of Wyoming is ~ 3 km above sea level (Cervany 1990) and the rock uplift is 6.8 km (Kelley 2004). The modern average surface elevation in the northern Laramie Mountains is ~ 2.4 km; consequently, the amount of denudation is ~ 3.8 km. In Sybille Canyon in the central Laramie Mountains, the rock uplift is only 5.7 km, the surface uplift is 1.85 m and the amount of denudation is 3.85 m, similar to the value for the northern Laramie Mountains (Kelley 2002). AFT data from the Laramie Mountains are consistent with long-wavelength folding of the basement, with highs in the vicinity of U.S. Interstate 80 in the south and Laramie Peak in the north, with an intervening low along the Cheyenne belt, mirroring the modern topographic profile of the range (Kelley 2004).

Summary

The distribution of the base of the AFT PAZ provides meaningful structural information that can be used to document previously unsuspected relationships in the interior of the Front Range due to Laramide deformation and plutonism. The model that the Front Range is basically a basement arch thrust over basins on either side (e.g., Kelley and Chapin 1997) is confirmed by the AFT data. The AFT data further demonstrate that offset across northwest-trending faults in the basement (Waterton Canyon), as well as basement folding (Pikes Peak), were important in bringing the center of the range up with respect to the margins. The preservation of the late Mesozoic PAZ and the lack of Laramide cooling ages in the Wet Mountains leads to the interpretation that this mountain chain was thrust laterally during Laramide deformation; Laramide arching in the Wet Mountains was minimal. The thermal and possible inflationary influences of the Colorado Mineral Belt are clearly defined by the AFT data on the southeastern margin of the Colorado Mineral Belt trend. The AFT data in the northern part of the range likely reflect the combined affects of increased thickness in the Pierre Shale to the north and greater amounts of rock uplift during Laramide deformation toward the north.

The question of substantial late Cenozoic differential uplift of the Front Range and northern Wet Mountains relative to the High Plains seems to be resolved by the preservation of old (> 100 Ma) AFT ages at low elevation along the mountain front, although the results do not preclude young epeirogenic uplift (McMillan et al. 2002; Leonard 2002). The 500–1,000 m east-facing escarpment that forms the Southern Rocky Mountains–High Plains margin is not a fault scarp (Leonard and Lansford 1994). We have previously postulated (Chapin and Kelley 1997) that an increase in precipitation, beginning in latest Miocene–early Pliocene time, led to exhumation of the Laramide arches bordering the High Plains. Wyoming geologists have long argued that the Laramide ranges in that state stand in bold relief because of Cenozoic removal of large volumes of orogenic sediments that filled the basins (e.g., Knight 1953; Moore 1960).

The Rocky Mountain erosion surface rises in elevation and becomes increasingly dissected southward along the crest of the Wet Mountains. On Greenhorn Peak the Rocky Mountain surface is at an elevation of 3,564 m, approximately the same elevation as the base of the PAZ on Mount Evans; however, there are approximately 1,000 m of Proterozoic rocks within the pre-Laramide PAZ beneath the Rocky Mountain erosion surface on Greenhorn Peak. Approximately 200 m of latest Eocene (33.4 Ma; McIntosh and Chapin 2004 this volume) andesitic lava flows rest on the Rocky Mountain surface and make up the summit of Greenhorn Peak at a elevation of 3,764 m. The southern Wet Mountains contain several small intrusions and remnants of late Eocene to early Oligocene volcanic rocks (Fig. 15) that may be related to the early Oligocene thermal event recorded by the AFT ages and track lengths mentioned previously. The south end of the Wet Mountains is the only place along the entire length of the Front Range and Wet Mountains, where normal faults and the AFT data indicate differential uplift of the mountains with respect to the High Plains. The south end of the Wet Mountains also marks a major boundary in the volcanic and thermal history of the Southern Rocky Mountains. AFT ages greater than 80 Ma have not been found along the High Plains–Rocky Mountain front south of the Wet Mountains (Kelley and Chapin 1995; Kelley et al. 1992). Oligocene and early Miocene AFT ages in the Sangre de Cristo Mountains (Lindsey et al. 1986; Kelley et al. 1992) likely reflect elevated heat flow and related rift flank uplift and erosion. Extensive basaltic volcanism in the Rio Grande rift and late Oligocene to early Miocene intrusive activity along the High Plains margin ends at the latitude of the Wet Mountains.

The AFT data from areas in and south of the South Platte River record a latest Eocene to Oligocene heating event that becomes more prominent to the south, reaching a maximum in the southern Wet Mountains (Fig. 5). The AFT data from the Poudre River area also show this event, but the area between the Poudre and the Platte valleys, and in the Arkansas Valley, do not record this event. In places like the Poudre River, Pikes Peak, and the Wetmore area in the Wet Mountains, this event can be directly tied to known volcanic centers (e.g., Manhattan mining district, Cripple Creek, Silver Cliff–Rosita–Deer Peak). In other areas like Waterton Canyon and the south end of the Wet Mountains, the link is nebulous. Steven (1975) suggested that most of south central Colorado, including the Front Range and the Wet Mountains, was covered by a composite volcanic field during middle Cenozoic time. McIntosh and Chapin (2004 this volume) document a large amount of volcanism in central Colorado between 32 and 38 Ma, whereas volcanism in the Spanish Peaks/Mt. Maestas area southwest of the Wet Mountains is 21–35 Ma, with most ages ranging from 21 to 26 Ma (Miggins et al. 1999; Penn et al. 1994). This regional volcanism and Rio Grande rift development become more pronounced to the south and may be the source of the heating that is recorded by the AFT data. Chapin et al. (2004 this volume) show that the maximum lateral extent of Cenozoic volcanism in New Mexico (and by inference the maximum heat flow anomaly) occurred in Oligocene time and was followed by an early Miocene 21–16 Ma lull in volcanism.

Acknowledgments

The field work for this study was supported by the New Mexico Bureau of Geology and Mineral Resources. The samples were irradiated under the DOE Reactor Share Program at Texas A&M University. We thank Chuck Naeser, Kate Gregory, Steve Cather, Eric Erslev, Dave Blackwell, Frank Pazzaglia, and Robert Weimer for helpful discussions during the interpretation of this data. Eric Erslev, Chuck Naeser, and Robert Weimer provided thorough, constructive reviews of the paper. We would especially like to thank Laurel Goodwin for her guidance on the structural aspects of the project. Reviews by Alan Lester and two anonymous

GSA reviewers helped improve an earlier version of the manuscript.

References

Abbott, J. T., 1972, Rb-Sr study of isotopic redistribution in a Precambrian mylonite-bearing shear zone, northern Front Range, Colorado: Geological Society of America, Bulletin, v. 63, pp. 487–494.

Abbott, J. T., 1976, Geologic map of the Big Narrows quadrangle, Larimer County, Colorado: U.S. Geological Survey, Geologic Quadrangle Map GQ-1323, 1:24,000.

Berg, R. R., 1962a, Subsurface interpretation of the Golden fault at Soda Lakes, Jefferson County, Colorado: American Association of Petroleum Geologists, Bulletin, v. 41, pp. 704–707.

Berg, R. R., 1962b, Mountain flank thrusting in Rocky Mountain foreland, Wyoming and Colorado: American Association of Petroleum Geologists, Bulletin, v. 46, pp. 2019-2032.

Blackwell, D. D. and Steele, J. L., 1989, Heat flow and geothermal potential of Kansas: Kansas Geological Survey, v. 226, pp. 267–291.

Braddock, W. A., and Cole, J. C., 1978, Preliminary geologic map of the Greeley 1° x 2° quadrangle, Colorado and Wyoming: U.S. Geological Survey, Open-file Report 78-532, scale 1:250,000.

Braddock, W. A., and Cole, J. C., 1990, Geologic map of Rocky Mountain National Park and vicinity, Colorado: U.S. Geological Survey, Miscellaneous Investigations Map I-1973, scale 1:50,000.

Brock, M. R., and Singewald, Q. D., 1968, geologic map of the Mount Tyndall quadrangle, Custer county, Colorado: U.S. Geological Survey, Geologic Quadrangle Map GQ-596, scale 1:24,000.

Brown, E. H., and McClelland, W. C., 2000, Pluton emplacement by sheeting and vertical ballooning in part of the southeast Coast Plutonic Complex, British Columbia: Geological Society of America, Bulletin, v. 112, pp. 708–719.

Bryant, B., and Naeser, C. W, 1980, The significance of fission-track ages of apatite in relation to the tectonic history of the Front Range and Sawatch Range, Colorado, Part I: Geological Society of America, Bulletin, v. 91, pp. 156–164.

Bryant, B., McGrew, L. W., and Wobus, R. A., 1981, Geologic map of the Denver 1° x 2° quadrangle, north-central Colorado: U.S. Geological Survey, Miscellaneous Geologic Investigations Map I-1163, scale 1:250,000.

Bullard, E. C., 1939, Heat flow in South Africa: Proceedings Royal Society London, Series A, v. 173, pp. 474–502.

Carlson, W. D., Donelick, R. A., and Ketcham, R. A., 1999, Variability of apatite fission-track annealing kinetics—I. Experimental results: American Mineralogist, v. 84, pp. 1213–1223.

Carter, L. S., Kelley, S. A., Blackwell, D. D., and Naeser, N. D., 1998, Heat flow and thermal history of the Anadarko Basin, Oklahoma: American Association of Petroleum Geologists, Bulletin, v. 82, pp. 291–316.

Case, J. E., 1965, Gravitational evidence for a batholithic mass of low density along a segment of the Colorado Mineral Belt: Geological Society of America, Special Paper 82, p. 26.

Cervany, P. F., 1990, Fission-track thermochronology of the Wind River Range and other basement cored uplifts in the Rocky Mountain foreland: Unpublished Ph.D. dissertation, University of Wyoming, 189 pp.

Chapin, C. E., 1983, An overview of Laramide wrench faulting in the Southern Rocky Mountains with emphasis on Petroleum exploration; *in* Lowell, J. D. (ed.), Rocky Mountain foreland basins and uplifts: Rocky Mountain Association of Geologists, pp. 169–180.

Chapin, C. E., and Cather, S. M., 1994, Tectonic setting of the axial basins of the northern and central Rio Grande rift; *in* Keller, G. R., and Cather, S. M. (eds.), Basins of the Rio Grande rift—structure, stratigraphy, and tectonic setting: Geological Society of America, Special Paper 291, pp. 5–23.

Chapin, C.E ., and Kelley, S. A., 1997, The Rocky Mountain erosion surface in the Front Range of Colorado; *in* Boyland, D. W., and Sonnenberg, S. A. (eds.), Geologic history of the Colorado Front Range, Denver, Colorado: Rocky Mountain Association of Geologists, pp. 101–114.

Chapin, C. E., Wilks, M. E., and McIntosh, W. C., 2004 this volume, Space-time patterns of volcanism in New Mexico; *in* Cather, S. M., McIntosh, W. C., and Kelley, S. A. (eds.), Tectonics, geochronology, and volcanism in the Southern Rocky Mountains and Rio Grande rift: New Mexico Bureau of Geology and Mineral Resources, Bulletin 160, pp. 13–40.

Chase, R. B., Schmidt, C. J., and Genovese, P. W., 1993, Influence of Precambrian rock compositions and fabrics on the development of Rocky Mountain foreland folds; *in* Schmidt, C. J., Chase, R. B., and Erslev, E. A. (eds.), Laramide basement deformation in the Rocky Mountain foreland of the western United States: Geological Society of America, Special Paper 280, pp. 45–72.

Coleman, S. M., 1985, Map showing tectonic features of late Cenozoic origin in Colorado: U.S. Geological Survey, Miscellaneous Investigations Series Map I-1566, scale 1:1,000,000.

Corbett, M. K., 1968, Tertiary volcanism of the Specimen–Lulu–Iron Mountain area, north-central Colorado; *in* Epis, R. C. (ed.), Cenozoic volcanism in the southern Rocky Mountains: Colorado School of Mines, Quarterly, v. 63, pp. 1–37.

Corrigan, J. D., 1991, Deriving thermal history information from apatite fission-track data: Journal of Geophysical Research, v. 96, pp. 10,347–10,360.

Corrigan, J. D., 1993, Apatite fission-track analysis of Oligocene strata in south Texas, U.S.A.—testing annealing models: Chemical Geology (Isotope Geoscience Section), v. 104, pp. 227–249.

Crowley, K. D., Cameron, M, and Schaefer, R. L., 1991, Experimental studies of annealing of etched fission tracks in fluorapatite: Geochemica et Cosmochemica Acta, v. 55, pp. 1449–1465.

Cunningham, C. G., Naeser, S. W., Marvin, R. F., Luedke, R. G., and Wallace, A. R., 1994, Ages of selected intrusive rocks and associated ore deposits in the Colorado Mineral Belt: U.S. Geological Survey, Bulletin 2109, 31 pp.

Donelick, R. A., 1991, Crystallographic orientation dependence of mean etchable fission track length in apatite: a physical model and experimental observations: American Mineralogist, v. 76, pp. 83–91.

Epis, R. C., and Chapin, C. E., 1974, Stratigraphic nomenclature of the Thirtynine Mile volcanic field, central Colorado: U.S. Geological Survey, Bulletin, 1395-C, 23 pp.

Epis, R. C., and Chapin, C. E., 1975, Geomorphic and tectonic implications of the post-Laramide late Eocene erosion surface in the Southern Rocky Mountains; *in* Curtis, B. F. (ed.), Cenozoic history of the Southern Rocky Mountains: Geological Society of America, Memoir 144, pp. 45–74.

Erslev, E. A., 1993, Thrusts, back-thrusts, and detachment of Rocky Mountain foreland arches; *in* Schmidt, C. J., Chase, R. B., and Erslev, E. A. (eds.), Laramide basement deformation in the Rocky Mountain foreland of the western United States:Geological Society of America Special Paper 280, pp. 339–358.

Erslev, E. A., and Holdaway, S .M., 1999, Laramide faulting and tectonics of the northeastern Front Range of Colorado; *in* Lageson, D. R., Lester, A. P., and Trudgill, B. D. (eds.), Colorado and Adjacent Areas: Geological Society of America, Field Guide 1, pp. 41–49.

Erslev, E. A., and Selvig, B., 1997, Thrust, backthrusts and triangle zones—Laramide deformation in the northeastern margin of the Colorado Front Range; *in* Bolyard, D. W., and Sonnenberg, S. A. (eds.), Geologic history of the Colorado Front Range: Rocky Mountain Association of Geologists, pp. 65–76.

Erslev, E. A., Kellogg, K. S., Bryant, B., Ehrlich, T. K., Holdaway, S. M., and Naeser, C. W., 1999, Laramide to Holocene structural development of the northern Colorado Front Range; *in* Lageson, D. R., Lester, A. P., and Trudgill, B. D. (eds.), Colorado and adjacent areas: Geological Society of America, Field Guide 1, pp. 21–40.

Evanoff, E., and Chapin, C. E., 1994, Composite nature of the "Late Eocene surface" of the Front Range and adjacent regions, Colorado and Wyoming (abs.): Geological Society of America, Abstracts with Programs, v. 26, p. 12.

Fitzgerald, P. G., Sorkhabi, R. B., Redfield, T. F., and Stump, E., 1995, Uplift and denudation of the central Alaska Range—a case study in the use of apatite fission-track thermochronology to determine absolute uplift parameters: Journal of Geophysical Research, v. 100, pp. 20,175–20,191.

Fryer, S. L., 1996, Laramide faulting associated with the Ilse fault system, northern Wet Mountains, Colorado: Unpublished M.S. thesis, Colorado Sate University, Ft. Collins, 120 pp.

Förster, A. and Merriam, D. F., 1997, Heat flow in the Cretaceous of northwestern Kansas and implications for regional hydrology:

Kansas Geological Survey, Current Research in Earth Sciences Bulletin 240, http://www.kgs.ukans.edu/Current/1997/forster/forster1.html, accessed 01/19/2004.

Foster, D. A., and Gleadow, A. J. W., 1992, The morpho-tectonic evolution of rift-margin mountains in central Kenya—constraints from apatite fission-track thermochronology: Earth and Planetary Science Letters, v. 113, pp. 157–171.

Galbraith, R. F., 1981, On statistical models for fission track counts: Mathematical Geology, v. 13, pp. 471–478.

Galbraith, R. F., and Laslett, G. M., 1985, Some remarks on statistical estimation in fission-track dating: Nuclear Tracks and Radiation Measurement, v. 10, pp. 361–363.

Galbraith, R. F., and Laslett, G. M., 1993, Statistical models for mixed fission track ages: Nuclear Tracks and Radiation Measurement, v. 21, pp. 459–470.

Gamble, B. M., 1979, Petrography and petrology of the Mount Cumulus stock, Never Summer Mountains, Colorado: Unpublished M.S. thesis, University of Colorado Boulder, 75 pp.

Gleadow, A. J. W., and Fitzgerald, P. F., 1987, Uplift history and structure of the Transantarctic Mountains: new evidence from fission track dating of basement apatites in the Dry Valleys area, southern Victoria Land: Earth and Planetary Science Letters, v. 82, pp. 1–14.

Green, P. F., 1985, A comparison of zeta calibration baselines in zircon, sphene, and apatite: Chemical Geology (Isotope Geoscience Section), v. 58, pp. 1–22.

Green, P. F., Duddy, I. R., Gleadow, A. J. W., Tingate, P. R., and Laslett, G. M., 1986, Thermal annealing of fission tracks in apatite, 1. A qualitative description: Chemical Geology (Isotope Geoscience Section), v. 59, pp. 237–253.

Gregory, K. M., 1992, Late Eocene paleoaltitude, paleoclimate, and paleogeography of the Front Range region, Colorado: Unpublished Ph.D. dissertation, University of Arizona, Tucson, 246 pp.

Gregory, K. M., and C. G. Chase, 1992, Tectonic significance of paleobotanically estimated climate and altitude of the late Eocene erosion surface, Colorado: Geology, v. 20, pp. 582–585.

Gregory, K. M., and Chase, C. G., 1994, Tectonic and climatic significance of a late Eocene low-relief, high-level geomorphic surface, Colorado: Journal of Geophysical Research, v. 99, pp. 20,141–20,160.

Hoblitt, R., and Larson, E., 1975, Paleomagnetic and geochronologic data bearing on the structural evolution of the northeastern margin of the Front Range, Colorado: Geological Society of America, Bulletin, v. 86, pp. 237–242.

Hurford, A. J., and Green, P. F., 1983, The zeta age calibration of fission-track dating: Isotope Geoscience, v. 1, pp. 285–317.

Isaacson, L. B., and Smithson, S. B., 1976, Gravity anomalies and granite emplacement in west-central Colorado: Geological Society of America, Bulletin, v. 87, pp. 22–28.

Izett, G. A., 1974, Geologic map of the Trail Mountain quadrangle, Grand County, Colorado: U.S. Geological Survey, Geologic Quadrangle Map GQ-1156, scale 1:24,000.

Izett, G. A., Cobban, W. A., and Gill, J. R., 1971, The Pierre Shale near Kremmling, Colorado, and its correlation to the east and west: U.S. Geological Survey, Professional Paper 684-A, 19 pp.

Jacob, A. F., 1983, Mountain front thrust, southeastern Front Range and northeastern Wet Mountains, Colorado; *in* Lowell, J. D. (ed.), Rocky Mountain foreland basins and uplifts: Rocky Mountain Association of Geologists, pp. 229–244.

Jacob, A. F., and Albertus, R. G., 1985, Thrusting, petroleum seeps, and seismic exploration—Front Range south of Denver, Colorado; *in* Macke, D. L., and Maughan, E. K. (eds.), Rocky Mountain Field Trip Guide 1985: Society of Economic Paleontologists and Mineralogists, pp. 77–96.

Jaluria, Y., and Torrance, K. E., 1986, Computational heat transfer: Hemisphere Publishing Corporation, New York, 366 pp.

Kamp, P. J. J., and Tippett, J. M., 1993, Dynamics of Pacific plate crust in the South Island (New Zealand) zone of oblique continent-continent convergence: Journal of Geophysical Research, v. 98, pp. 16,105–16,118.

Karlstrom, K. E. and Bowring, S. A., 1993, Proterozoic orogenic history in Arizona; *in* Reed, J. L, Bickford, M. E., Houston, R. S., LInk, P. K., Rankin, D. W., Sims, P., and Van Schumus, W. R. (eds.), Precambrian—conterminous U.S.: Geological Society of America, The Geology of North America, v. C-2, pp. 188–211.

Ketcham, R. A., Donelick, R. A., and Carlson, W. D., 1999, Variability of apatite fission-track annealing kinetics—III. Extrapolation to geological time scales: American Mineralogist, v. 84, pp. 1235–1255.

Kelley, K. D., Romberger, S. B., Beaty, D. W., Pontius, J. A., Snee, L. W., Stein, H. J., and Thompson, T. B., 1998, Geochemical and geochronological constraints on the genesis of Au-Te deposits at Cripple Creek, Colorado: Economic Geology, v. 93, pp. 981–1012.

Kelley, S. A., 2004, Low-temperature cooling histories of the Cheyenne belt and the Laramie Peak shear zone, Wyoming, and the Soda Creek–Fish Creek shear zone, Colorado; *in* Keller, G. R., and Karlstrom, K. E (eds.), Lithospheric Evolution and Structure of the Rocky Mountain Region: American Geophysical Union Monograph.

Kelley, S. A., and Chapin, C. E., 1995, Apatite fission-track thermochronology of the Southern Rocky Mountains–Rio Grande rift–western High Plains provinces; *in* Bauer, P. W., Kues, B. S., Dunbar, N. W., Karlstrom, K. E., and Harrison, B. (eds.), Geology of the Santa Fe region: New Mexico Geological Society, Guidebook 46, pp. 87–96.

Kelley, S. A., and Chapin, C. E., 1997, Internal structure of the southern Front Range, Colorado, from an apatite fission-track thermochronology perspective; *in* Bolyard, D. W. and Sonnenberg, S. A. (eds.), Geologic history of the Colorado Front Range: Rocky Mountain Association of Geologists, pp. 43–48.

Kelley, S. A., Chapin, C. E., and Corrigan, J., 1992, Late Mesozoic to Cenozoic cooling histories of the flanks of the northern and central Rio Grande rift, Colorado and New Mexico: New Mexico Bureau of Mines and Mineral Resources, Bulletin 145, 39 pp.

Knight, S. H., 1953, Summary of the Cenozoic history of the Medicine Bow Mountains, Wyoming; *in* Laramie Basin, Wyoming and North Park, Colorado: Wyoming Geological Association, Guidebook 8, pp. 65–76.

Laslett, G. M., Kendall, W. S., Gleadow, A. J. W., and Duddy, I. R., 1982, Bias in measurement of fission-track length distribution: Nuclear Tracks, v. 6, pp. 79–85.

Laslett, G. M., Green, P. F., Duddy, I. R., and Gleadow, A.J. W., 1987, Thermal annealing of fission tracks in apatite, 2. A quantitative analysis: Chemical Geology (Isotope Geoscience Section), v. 65, pp. 1–13.

Leonard, E. M., 2002, Geomorphic and tectonic forcing of late Cenozoic warping of the Colorado piedmont: Geology, v. 30, pp. 545–578.

Leonard, E. M., and Langford, R. P., 1994, Post-Laramide deformation along the eastern margin of the Colorado Front Range—a case against significant faulting: Mountain Geologist, v. 31, pp. 45–52.

Lindsey, D. A., Andriessen, P. A. M., and Wardlaw, B. R., 1986, Heating, cooling, and uplift during Tertiary time, northern Sangre de Cristo Range, Colorado: Geological Society of America, v. 97, pp. 1133–1143.

MacGinitie, H. D., 1953, Fossil plants of the Florissant Beds, Colorado: Carnegie Institution of Washington, Publication, 198 pp.

Marvin, R. F., Young, E. J., Mehnert, H. H., and Naeser, C. W. (eds.), 1974, Summary of radiometric age determinations on Mesozoic and Cenozoic igneous rocks and uranium base metal deposits in Colorado: Isochron/West, no. 11, 41 pp.

McCallum, M. E., and Naeser, C. W., 1977, Fission track ages of Tertiary intrusive rocks in the Manhattan mining district, northern Front Range, Colorado: Isochron/West, no. 18, pp. 1–4.

McIntosh, W. C., and Chapin, C. E., 1994, $^{40}Ar/^{39}Ar$ geochronology of ignimbrites in the Thirtynine Mile volcanic field, Colorado; *in* Evanoff, E. (ed.), Late Paleogene geology and paleoenvironments of central Colorado: Geological Society of America, Field Trip Guidebook, pp. 23–26.

McIntosh, W. C., and Chapin, C. E., 2004 this volume, Geochronology of the central Colorado volcanic field; *in* Cather, S. M., McIntosh, W., and Kelley, S. A. (eds.), Tectonics, geochronology and volcanism in the Southern Rocky Mountains and Rio Grande rift: New Mexico Bureau of Mines and Mineral Resources, Bulletin 160, pp. 205–238.

McMillan, M. E., Angevine, C. L., and Heller, P. L., 2002, Postdepositional tilt of the Miocene–Pliocene Ogallala Group on the western Great Plains—evidence of late Cenozoic uplift of the Rocky Mountains: Geology, v. 30, pp. 63–66.

Meyer, H. W., 1986, An evaluation of the methods for estimating

paleoaltitude using Tertiary floras from the Rio Grande rift vicinity, New Mexico and Colorado: Unpublished Ph.D. thesis, University of California, Berkeley, 217 pp.

Meyer, H. W., 1992, Lapse rates and other variables applied to estimating paleoaltitudes from fossil flora: Paleogeography, Paleoclimitology, Paleoecology, v. 99, pp. 71–99.

Meyer, H. W., 2003, The fossils of Florissant: Smithsoniam Institution Press, 272 pp.

Miggins, D. P., Snee, L. W., Pillmore, C. L., Budahn, J. R., Kunk, M. J., and Stern, C. R., 1999, $^{40}Ar/^{39}Ar$ geochronology and geochemistry of sills within the Cretaceous Pierre Shale near the Spanish Peaks in south-central Colorado (abs.): Geological Society of America, Abstracts with Programs ,v. 31 p. A207

Moore, F., 1960, Summary of Cenozoic history, southern Laramie Range, Wyoming and Colorado; *in* Weimer, R. J., and Haun, J. D. (eds.), Guide to the Geology of Colorado: Geological Society of America, Rocky Mountain Association of Geologists, Colorado Scientific Society, Field Trip Guidebook, pp. 217–222.

Morse, D. G., 1985, Oligocene paleogeography in the southern Denver Basin; *in* Flores, R. M., and Kaplan, S .S. (eds.), Cenozoic paleogeography of west-central United States: Society of Economic Paleontologists and Mineralogists, Rocky Mountain Section, pp. 277–292.

Naeser, C. W., 1979a, Fission-track dating and geologic annealing of fission tracks; *in* Jager, E., and Hunziker, J. C. (eds.), Lectures in Isotope Geology: Springer-Verlag, pp. 154–169.

Naeser, C. W., 1979b, Thermal history of sedimentary basins—fission-track dating of subsurface rocks: Society of Economic Paleontologists and Mineralologists, Special Publication 26, pp. 109–112.

Naeser, C. W., Bryant, B., Kunk, M. J., Kellogg, K., Donelick, R. A., and Perry, W. J., Jr., 2002, Tertiary cooling and tectonic history of the White River Uplift, Gore Range, and western Front Range, central Colorado—evidence from fission-track and $^{40}Ar/^{39}Ar$ ages; *in* Kirkham, R. M., Scott, R. B., Judking, T. W. (eds.), Late Cenozoic evaporite tectonism and volcanism in west-central Colorado: Geological Society of America, Special Paper 366, pp. 31–53.

Noblett, J. B., Culler, R. L., and Bickford, M .E. 1987, Proterozoic crystalline rocks in the Wet Mountains and vicinity, Colorado; *in* Lucas, S. G., and Hunt, A. P. (eds.), Northeastern New Mexico: New Mexico Geological Society, Guidebook 38, pp. 73–82.

Olson, J. C., Marvin, R. F., Parker, R. L., and Mehnert, H. H., 1977, Age and tectonic setting of lower Paleozoic alkalic and mafic rocks, carbonatites, and thorium veins in south-central Colorado: U. S. Geological Survey, Journal of Research, v. 5, pp. 673–687.

Pazzaglia, F. J., and Kelley, S. A., 1998, Large-scale geomorphology and fission-track thermochronology in topographic and exhumation reconstructins of the Southern Rocky Mountains: Rocky Mountain Geology, v. 33, no. 2, pp. 229–257.

Penn, B. S., Wentlandt, R. F., Simmons, E. C., Snee, L. W., and Unruh, D. M., 1994, Geochemical evolution of the Spanish Peaks intrusive rocks of south-central Colorado (abs.): Geological Society of America, Abstracts with Programs, Rocky Mountain Section, v. 26, p. 58.

Peterman, Z. E., Hedge, C. E., and Braddock, W. A., 1968, Age of Precambrian events in the northeastern Front Range, Colorado: Journal of Geophysical Research, v. 73, pp. 2277–2296.

Petford, N., Cruden, A. R., MCCaffrey, K. J. W., and Vigneresse, J. -L., 2000, Granite magma formation, transport and emplacement in the Earth'' crust: Nature, v. 408, pp. 669–673.

Rice, C. M., Harmon, R. S., and Shepherd, T.J ., 1985, Central City, Colorado—the upper part of an alkaline porphyry molybdenum system: Economic Geology, v. 80, pp. 1769–1796.

Sass, J. H., and Galanis, S. P., Jr., 1983, Temperatures, thermal conductivity, and heat flow from a well in Pierre Shale near Hayes, South Dakota: U.S. Geological Survey, Open-file Report 83-25. 10 pp.

Scott, G. R., 1963, Quaternary geology and geomorphic history of the Kassler quadrangle, Colorado: U.S. Geological Survey, Professional Paper 421-A, 67 pp.

Scott, G. R., and Cobban, W. A., 1965, Geologic and biostratigraphic map of the Pierre Shale between Jarre Creek and Loveland, Colorado: U.S. Geological Survey, Miscellaneous Investigations Map I-439, scale 1:48,000.

Scott, G. R., and Cobban, W. A., 1975, Geologic and biostratigraphic map of the Pierre Shale in the Cañon City–Florence Basin and the Twelvemile Park area, south-central Colorado: U.S. Geological Survey, Miscellaneous Investigations Map I-937, scale 1:48,000.

Scott, G. R., and Cobban, W. A. 1986a, Geologic and biostratigraphic map of the Pierre Shale in the Colorado Springs–Pueblo area, Colorado: U.S. Geological Survey, Miscellaneous Investigations Map I-1627, scale 1:100,000.

Scott, G. R., and Cobban, W. A., 1986b, Geologic, biostratigraphic and structure map of the Pierre Shale between Loveland and Round Butte, Colorado: U.S. Geological Survey, Miscellaneous Investigations Map I-1700, scale 1:50,000.

Scott, G. R., and Taylor, R. B., 1974, Post-Paleocene Tertiary rocks and Quaternary volcanic ash of the Wet Mountain valley, Colorado: U.S. Geological Survey, Professional Paper 868, 15 pp.

Scott, G. R., Taylor, R. B., Epis, R. C., and Wobus, R. A., 1978, Geologic map of the Pueblo 1° x 2° quadrangle, south-central Colorado: U.S. Geological Survey, Miscellaneous Investigations Map I-1022, scale 1:250,000.

Selverstone, J., Hodgins, M., Shaw, C., Aleinikoff, J. N., and Fanning, C. M., 1997, Proterozoic tectonics of the northern Colorado Front Range; *in* Bolyard, D. W., and Sonnenberg, S.A. (eds.), Geologic history of the Colorado Front Range: Rocky Mountain Association of Geologists, pp. 9-18.

Sharp, W. N., 1978, Geologic map of the Silver Cliff and Rosita volcanic centers, Custer County, Colorado: U.S. Geological Survey, Miscellaneous Investigations Map I-1081, scale 1:24,000.

Sharp, W. N., and Naeser, C. W., 1986, Apatite fission-track age for the Bull Domingo boulder pipe, Custer County, Colorado: U.S. Geological Survey, Bulletin 1622, pp. 77–80.

Shaver, K. C., Neese, W. D., and Braddock, W. A., 1988, Geologic map of the Rustic Quadrangle, Larimer County, Colorado, U.S. Geological Survey, Geologic Quadrangle Geologic Quadrangle Map GQ-1619, scale 1:24,000.

Shaw, C. A., and Karlstrom, K. E., 1999, The Yavapai–Mazatzal crustal boundary in the Southern Rocky Mountains: Rocky Mountain Geology, v. 34, pp. 37–52.

Siems, P. L., 1968, Volcanic geology of the Rosita Hills and Silver Cliff district, Custer County, Colorado: Colorado School of Mines Quarterly, v. 63, pp. 89–124.

Sims, P. K., 1963, Geology of uranium and associated ore deposits, central part of the Front Range Mineral Belt, Colorado: U.S. Geological Survey, Professional Paper 371, 119 pp.

Singewald, Q. D., 1966, Description and relocation of part of the Ilse fault zone, Wet Mountains, Colorado: U.S. Geological Survey, Professional Paper 550-C, pp. 20–24.

Steven, T. A., 1975, Middle Tertiary volcanic field in the Southern Rocky Mountains: Geological Society of America, Memoir 144, pp. 75–94.

Taylor, R. B., 1974, Reconnaissance geologic map of the Deer Park quadrangle and southern part of the Hardscrabble Mountain quadrangle, Custer and Huerfano counties, Colorado: U.S. Geological Survey, Miscellaneous Investigations Map I-870, scale 1:24,000.

Taylor, R. B., 1975, Neogene tectonism in south-central Colorado; *in* Curtis, B. F. (ed.), Cenozoic history of the Southern Rocky Mountains: Geological Society of America, Memoir 144, pp. 211–226.

Tourtelot, H. E., 1962, Preliminary investigation of the geologic setting and chemical composition of the Pierre shale, Great Plains region: U.S. Geological Survey, Professional Paper 390, 74 pp.

Trimble, D. E. and Machette, M. N., 1979, Geologic map of the greater Denver area, Front Range urban corridor, Colorado: U.S. Geological Survey, Miscellaneous Investigations Map I-856-H, scale 1:100,000.

Tweto, O., 1975, Laramide (Late Cretaceous–early Tertiary) orogeny in the southern Rocky Mountains; *in* Curtis, B. F. (ed.), Cenozoic history of the Southern Rocky Mountains, Geological Society of America, Memoir 144, pp. 1–44.

Tweto, O., and Case, J. E., 1972, Gravity and magnetic features as related to the geology of the Leadville 30-minute quadrangle, Colorado: U.S. Geological Survey, Professional Paper 726-C, 31 pp.

Van Horn, R., 1957, Bedrock geology of the Golden quadrangle, Colorado: U.S. Geological Survey, Geologic Quadrangle Map GQ-103, scale 1:24,000.

Weimer, R. J., 1996, Guide to the petroleum geology and Laramide Orogeny, Denver Basin and Front Range, Colorado: Colorado Geological Survey, Bulletin 51, 127 pp.

Weimer, R. J., and Ray, R. R., 1997, Laramide mountain flank deformation and the Golden fault zone, Jefferson County, Colorado; *in* Bolyard, D. W., and Sonnenberg, S. A. (eds.), Geologic history of the Colorado Front Range: Rocky Mountain Association of Geologists, pp .43–48.

Welch, F. J., 1969, The geology of the Castle Rock area, Douglas County, Colorado: Unpublished M.S. thesis, Colorado School of Mines, T1154, 86 pp.

Wolfe, J. A., 1992, An analysis of present-day terrestrial lapse rates in the western conterminous United States and their significance to paleoaltitudinal estimates: U.S. Geological Survey, Bulletin 1964, 35 pp.

Wolfe, J. A., Forest, C. E., and Molnar, P., 1998, Paleobotanical evidence of Eocene and Oligocene paleoaltitiudes in midlatitude western North America: Geological Society of America, Bulletin, v. 110, pp. 665–678.

Zoback, M. D. and 12 others, 1987, New evidence on the state of stress of the San Andreas fault system: Science, v. 238, pp. 1105–1111.

TABLE 1—Apatite fission-track data for Front Range and Wet Mountians, Colorado. ρ_s = spontaneous track density; ρ_i = induced track density (reported induced track density is twice the measured density; ρ_d = track density in muscovite detector covering CN-6 (1.05 ppm); Reported value determined from interpolation of values for detectors covering standards at the top and bottom of the reactor packages (fluence gradient correction) number in parenthesis is the number of tracks counted for ages and fluence calibration or the number of track measured for lengths. **S.E.** = standard error; **P(χ)^2** = Chi-squared probability; **N.D.** = no data; $\lambda_f = 1.551 \times 10^{-10}yr^{-1}$, g = 0.5. zeta = 5516 ± 300 for apatite, 452 ± 56 for zircon. Mean track lengths not corrected for length bias (Laslett et al., 1982). Unless otherwise noted, the rock units are Proterozoic in age.

Traverse name	Sample number	Rock type	Latitude (N) Longitude (W)	Elevation (m)	Number of grains dated	ρ_s x 10^5 t/cm^2	ρ_i x 10^6 t/cm^2	ρ_d x 10^5 t/cm^2	Central age (Ma) (± 1 S.E.)	P(χ)^2 (%)	Uranium content (ppm)	Mean track length (µm) (± 1 S.E.)	Standard deviation track length
Northeast Front Range	00LIV02	granite	40°44.32 105°22.42	2150	20	1.19 (126)	1.23 (648)	1.011 (4600)	**54.0 ± 5.7**	99	13	14.0 ± 0.8 (26)	2.1
	00LIV03	granite	40°49.55′ 105°18.10′	1900	20	1.81 (156)	1.39 (600)	1.014 (4600)	**72.3 ± 7.1**	98	14	13.0 ± 0.9 (18)	2.0
	00LIV04	granitic gneiss	40°50.16 105°18.74	2000	20	1.51 (133)	1.65 (726)	0.993 (4600)	**50.0 ± 5.1**	99	17	13.6 ± 1.0 (11)	1.6
	00LIV05	granite	40°55.66′ 105°16.48′	2150	20	1.22 (129)	1.29 (681)	0.98 (4600)	**51.0 ± 5.3**	85	14	13.6 ± 2.8 (10)	2.9
	00LIV06	biotite schist	40°55.77′ 105°20.34′	2080	20	10.67 (956)	6.95 (3114)	0.965 (4600)	**81.2 ± 4.6**	30	75	13.9 ± 0.3 (112)	1.5
Cache la Poudre River	94PR01	schist	40°39.89′ 105°12.89′	1609	20	3.6 (421)	4.15 (2423)	1.18 (3756)	**56.4 ± 3.9**	75	36	N.D.	N.D.
	94PR02	schist	40°41.97′ 105°14.91′	1655	20	5.88 (630)	5.03 (2695)	1.18 (3756)	**75.8 ± 4.6**	96	44	13.4 ± 0.3 (100)	1.4
	94PR03	gneiss	40°41.51′ 105°15.32′	1655	20	4.35 (515)	4.87 (2884)	1.18 (3756)	**57.6 ± 3.9**	70	43	13.3 ± 0.6 (43)	2
	94PR04	schist/gneiss	40°41.30′ 105°17.70′	1719	17	4.28 (363)	3.94 (1670)	1.18 (3756)	**70.5 ± 5.0**	97	35	13.7 ± 0.7 (23)	1.7
	94PR05	gneiss	40°41.39′ 105°19.49′	1743	20	3.14 (322)	2.97 (1521)	1.18 (3756)	**68.7 ± 5.1**	>99	26	N.D.	N.D.
	94PR06	schist	40°41.50′ 105°22.23′	1810	20	4.73 (605)	4.16 (2659)	1.2 (3756)	**74.4 ± 4.6**	>99	36	N.D.	N.D
	94PR07	schist	40°40.61′ 105°25.74′	1938	11	3.56 (239)	3.76 (1264)	1.2 (3756)	**61.9 ± 5.1**	85	33	13.3 ± 0.4 (60)	1.8
	94PR08	gneiss	40°41.77′ 105°26.23′	1975	20	3.28 (289)	3.39 (1492)	1.2 (3756)	**63.4 ± 4.9**	99	30	13.8 ± 0.6 (24)	1.4
	94PR09	granite breccia	40°41.35′ 105°25.72′	2034	20	1.59 (94)	2.35 (695)	1.2 (3756)	**44.4 ± 5.2**	>99	20	N.D.	N.D
	94PR10	granodiorite	40°41.89′ 105°35.49′	2191	20	3.25 (354)	4.06 (2210)	1.2 (3756)	**52.5 ± 3.7**	98	36	13.7 ± 0.4 (46)	1.5
	94PR11	granodiorite	40°41.07′ 105°46.35′	2524	8	1.12 (54)	1.58 (379)	1.22 (3756)	**47.1 ± 7.1**	99	14	N.D.	N.D.
	94PR12	granodiorite	40°37.97′ 105°48.33′	2569	20	1.84 (212)	2.12 (1223)	1.23 (3756)	**57.3 ± 4.9**	85	18	13.6 ± 0.6 (34)	1.6
	94PR13	gniess	40°33.36′ 105°46.70′	2835	20	1.98 (143)	2.74 (990)	1.24 (3756)	**47.8 ± 4.7**	>99	24	13.4 ± 0.9 (19)	1.9
Big Thompson Canyon	96BT01	granitic gneiss	40°22.42′ 105°29.29′	2300	20	0.8 (64)	1.08 (431)	1.194 (3599)	**48.7 ± 6.8**	99	9	N.D.	N.D.
	96BT02	granitic gneiss	40°22.88′ 105°28.12′	2250	20	0.78 (100)	0.88 (566)	1.194 (3599)	**57.9 ± 6.7**	97	8	N.D.	N.D.
	96BT03	granite	40°25.79′ 105°19.12′	1900	20	0.63 (57)	0.17 (78)	0.276 (1011)	**55.3 ± 9.8**	>99	6	N.D.	N.D.
	96BT04	granite	40°25.35′ 105°13.93′	1720	20	3.14 (297)	4.54 (2145)	1.194 (3599)	**45.4 ± 3.4**	60	40	14.5 ± 0.5 (15)	1.0
	96BT05	granite porphyry	40°25.84′	1700	20	0.72	0.72	1.194	**64.8 ± 8.4**	99	6	N.D.	N.D.

TABLE 1—continued

Traverse name	Sample number	Rock type	Latitude (N) Longitude (W)	Elevation (m)	Number of grains dated	ρ_s x 10^5 t/cm^2	ρ_i x 10^6 t/cm^2	ρ_d x 10^5 t/cm^2	Central age (Ma) (± 1 S.E.)	P(χ)^2 (%)	Uranium content (ppm)	Mean track length (µm) (± 1 S.E.)	Standard deviation track length
			105°13.90′			(78)	(394)	(3599)					
	96BT06	granite (2 mica)	40°25.35′ 105°21.29′	2000	20	9.97 (296)	10.45 (1552)	1.194 (3599)	**62.5 ± 4.7**	85	91	14.7 ± 0.5 (55)	1.9
Longs Peak/ St. Vrain River	96SV01	Silver Plume granite porphyry	40°12.28′ 105°18.38′	1725	20	1.23 (158)	0.38 (237)	0.259 (1011)	**47.5 ± 5.2**	99	15	13.3 ± 0.7 (40)	2.2
	99SV02	Silver Plume Granite	40° 08.48′ 105° 30.13′	2682	20	2.27 (237)	2.53 (1323)	1.171 (4609)	**57.6 ± 4.7**	85	22	13.3 ± 1.2 (7)	1.6
	99SV03	Fountain Fm. sandstone	40° 12.91′ 105° 16.57′	1650	20	3.87 (384)	5.08 (2518)	1.181 (4609)	**49.5 ± 3.4**	75	45	13.6 ± 0.9 (20)	2
	99SV05	Silver Plume Granite	40° 10.932′ 105°20.497′	1900	20	0.96 (111)	1.19 (685)	1.193 (4609)	**53.1 ± 5.8**	85	10	13.8 ± 1.9 (6)	2.4
	99SV06	Silver Plume Granite	40° 10.279′ 105 °22.776′	2100	20	2.04 (229)	2.48 (1388)	1.205 (4609)	**54.6 ± 4.5**	97	21	13.2 ± 1.1 (24)	2.8
	99SV07	Silver Plume Granite (more mafic)	40°10.085′ 105° 26.866′	2350	20	0.48 (52)	0.49 (288)	1.214 (4609)	**60.2 ± 9.3**	>99	4	N.D.	N.D
	99SV08	Silver Plume Granite	40° 10.143′ 105° 27.786	2499	20	0.65 (79)	0.92 (562)	1.214 (4609)	**46.9 ± 5.9**	>99	8	12.5 ± 1.4 (11)	2.4
	99TS01	granitic gneiss	40° 17.564′ 105° 31.357′	3292	20	2.93 (230)	3.44 (1347)	1.085 (4609)	**50.9 ± 4.2**	98	33	13.9 ± 0.8 (0.8)	1.3
	99TS02	granitic gneiss	40° 17.710′ 105° 31.903′	2938	20	2.35 (274)	2.61 (1524)	1.096 (4609)	**54.1 ± 4.2**	91	25	13.9 ± 0.5 (47)	1.8
	99LP01	Silver Plume Granite	40° 15.310′ 105° 36.899′	4343	20	2.13 (221)	2.5 (1298)	1.105 (4609)	**51.7 ± 4.3**	79	24	13.9 ± 0.6 (45)	2.1
	99LP02	Silver Plume Granite	40° 15.297′ 105° 37.141′	4121	20	2.2 (282)	2.45 (1570)	1.117 (4609)	**55.1 ± 4.2**	70	23	13.3 ± 0.9 (27)	2.4
	99LP03	Silver Plume Granite	40° 15.616′ 105° 37.292′	4023	16	0.45 (33)	0.62 (227)	1.129 (4609)	**45.1 ± 8.5**	97	6	N.D.	N.D.
	99LP04	Silver Plume Granite	40° 16.485′ 105° 36.311′	3688	20	1.19 (133)	1.4 (781)	1.139 (4609)	**53.3 ± 5.4**	98	13		
	99LP05	Silver Plume Granite	40° 16.305′ 105° 35.175′	3383	20	1.12 (129)	1.44 (829)	1.151 (4609)	**49.2 ± 5.1**	98	13	13.5 ± 0.8 (26)	2.2
	99LP06	Silver Plume Granite	40° 16.276′ 105° 33.290′	2835	20	1.62 (186)	2.16 (1242)	1.149 (4609)	**47.3 ± 4.2**	>99	20		
	99CP01	pegmatite in schist	40°26.03′ 105°42.02′	3780	20	6.41 (739)	6.57 (3784)	1.074 (4609)	**57.6 ± 3.4**	55	64	13.7 ± 0.4 (53)	1.4
	99CP02b	mica schist	40°26.04′ 105°43.53′	3463	20	4.69 (435)	5.1 (2364)	1.078 (4609)	**54.5 ± 3.7**	85	49	13.8 ± 0.6 (37)	1.7
	99FF01	granodiorite in Silver Plume pluton	40°20.87′ 105°40.00′	2682	20	1.13 (134)	1.35 (797)	1.106 (4609)	**51.1 ± 5.2**	92	13	13.9 ± 1.2 (11)	2.0
Indian Peaks	00IP02	granitic gneiss	40°08.31 105° 40.44′	3389	20	0.69 (73)	0.835 (441)	0.901 (4603)	**41.0 ± 5.4**	83	10	N.D.	N.D.
	00IP03	granitic gneiss	40°08.45′ 105° 40.34′	3450	20	2.88 (207)	2.07 (744)	0.883 (4603)	**67.4 ± 6.0**	99	24	14.0 ± 0.8 (10)	1.3
	00IP04	granitic gneiss	40°07.96′ 105°40.14′	3548	20	3.07 (314)	2.59 (1327)	0.874 (4603)	**56.8 ± 4.3**	58	31	13.9 ± 0.6 (46)	2.0
	00IP05	granitic gneiss	40°07.53′ 105°40.32′	2926	20	2.12 (258)	1.90 (1155)	0.864 (4603)	**53.0 ± 4.3**	65	23	13.6 ± 0.4 (76)	1.9

TABLE 1—continued

Traverse name	Sample number	Rock type	Latitude (N) Longitude (W)	Elevation (m)	Number of grains dated	ρ_s x 10^5 t/cm^2	ρ_i x 10^6 t/cm^2	ρ_d x 10^5 t/cm^2	Central age (Ma) (± 1 S.E.)	P(χ)^2 (%)	Uranium content (ppm)	Mean track length (μm) (± 1 S.E.)	Standard deviation track length
Boulder Canyon	96BC01	granitic gneiss	40°00.79′ 105°18.10′	1675	20	8.21 (999)	1.86 (1131)	0.257 (1011)	**62.3 ± 3.8**	85	75	12.8 ± 0.4 (101)	1.9
Coal Creek	96COC01	granite	39°52.74′ 105°16.24′	2012	20	0.8 (88)	0.9 (496)	1.194 (3599)	**58.1 ± 7.1**	99	8	12.3 ± 1.2 (15)	2.4
	96COC02	metarhyolite	39°52.77′ 105°16.38′	2012	13	2.3 (131)	2.93 (845)	1.194 (3599)	**50.8 ± 5.2**	98	26	N.D.	N.D.
Von Bibber Creek and vicinity	97VB01	gneiss	39°48.23′ 105°15.52′	1951	20	2.27 (225)	2.82 (1400)	1.34 (4593)	**59.3 ± 4.9**	96	22	13.2 ± 0.4 (101)	2.3
	97VB02	gneiss	39°48.11′ 105°15.50′	2012	20	0.62 (61)	0.93 (462)	1.34 (4593)	**48.8 ± 6.9**	>99	7	13.3 ± 0.7 (37)	2.1
	97VB03	schist	39°49.32′ 105°17.06′	2256	20	2.27 (106)	2.65 (620)	1.34 (4593)	**63.1 ± 7.1**	90	20	14.2 ± 0.4 (19)	0.9
	97VB04	schist	39°48.89′ 105°17.44′	2469	20	5.91 (360)	6.49 (1973)	1.34 (4593)	**67.3 ± 4.8**	85	50	14.0 ± 0.3 (103)	1.5
	97VB05	gneiss	39°50.00′ 105°19.70′	2493	20	1.55 (104)	2.17 (728)	1.34 (4593)	**52.8 ± 5.9**	>99	17	13.7 ± 1.0 (22)	2.3
	97VB06	gneiss	39°50.83′ 105°21.27′	2310	20	3.42 (268)	4.84 (1899)	1.357 (4593)	**52.6 ± 4.1**	94	37	13.3 ± 0.4 (93)	1.9
	97VB07	monzonite	39°49.56′ 105°24.07′	2800	20	5.05 (404)	5.54 (2218)	1.357 (4593)	**67.8 ± 4.6**	32	43	13.5 ± 0.5 (105)	2.5
	97VB08	monzonite	39°49.64′ 105°23.84′	2896	20	3.74 (383)	3.73 (1907)	1.357 (4593)	**74.7 ± 5.2**	80	29	13.7 ± 0.3 (103)	1.6
Golden Gate Canyon	95GGC01	granitic lens in amphibolite	39°47.12′ 105°21.31′	2390	20	4.65 (454)	4.35 (2124)	1.04 (3825)	**60.1 ± 4.1**	88	44	14.2 ± 0.3 (53)	1.3
	95GGC02	schist	39°47.06′ 105°19.80′	2360	20	4.85 (473)	4.36 (2125)	1.04 (3825)	**62.5 ± 4.2**	92	44	14.0 ± 0.3 (90)	1.5
	96GGC03	phyllite/schist	39°47.09′ 105°14.54′	1859	20	16.68 (854)	1.68 (430)	0.272 (1011)	**142.8 ± 10.2**	90	66	11.3 ± 0.6 (104)	3.1
Golden/ Lookout Mountain	92GO01	gneiss	39°45.23 105°14.52′	1768	20	6.75 (689)	2.75 (1402)	1.28 (3900)	**149.7 ± 19.0**	<1	22	12.2 ± 0.6 (100)	2.9
	92GO02	gneiss	39°44.96′ 105°14.33′	1976	20	6.16 (702)	4.33 (2468)	1.31 (3756)	**100.8 ± 5.6**	40	35	12.4 ± 0.6 (80)	2.7
	92GO03	gneiss	39°44.83′ 105°14.63′	2036	20	7.99 (783)	2.91 (1426)	1.31 (3756)	**196 ± 13.2**	6	23	11.6 ± 0.6 (100)	2.8
	92GO04	gneiss	39°44.63′′ 105°14.49′	2152	15	11.74 (845)	3.16 (1139)	1.35 (3756)	**263.0 ± 17.6**	15	25	11.2 ± 0.4 (100)	2.3
Clear Creek	94CC01	migmatitic gneiss	39°44.85′ 105°15.02′	1770	20	4.13 (436)	2.18 (1152)	0.95 (3756)	**98.9 ± 7.0**	95	24	13.2 ± 0.4 (69)	1.8
	94CC02	gneiss	39°44.81′ 105°26.16′	2207	20	0.84 (70)	0.92 (385)	0.95 (3756)	**47.7 ± 6.5**	99	10	14.3 ± 0.6 (6)	0.8
	94CC03	gneiss	39°44.77′ 105°26.29′	2207	20	1.65 (124)	1.56 (585)	0.95 (3756)	**55.6± 5.9**	99	17	N.D.	N.D.
	94CC04	gneiss	39°44.58′ 105°24.39′	2140	20	1.03 (112)	1.03 (560)	0.95 (3756)	**52.4 ± 5.8**	>99	11	N.D.	N.D.
	94CC05	gneiss	39°44.48′ 105°19.66	2005	20	3.7 (332)	3.12 (1396)	0.95 (3756)	**62.3 ± 4.6**	98	34	14.1 ± 0.4 (47)	1.4

TABLE 1—continued

Traverse name	Sample number	Rock type	Latitude (N) Longitude (W)	Elevation (m)	Number of grains dated	ρ_s x 10^5 t/cm^2	ρ_i x 10^6 t/cm^2	ρ_d x 10^5 t/cm^2	Central age (Ma) (± 1 S.E.)	P(χ)^2 (%)	Uranium content (ppm)	Mean track length (μm) (± 1 S.E.)	Standard deviation track length
	96CC06	granitic gneiss	39° 45.25′ 105°14.22′	1755	20	1.05 (94)	0.13 (59)	0.266 (1011)	**115.7 ± 19.4**	99	5	N.D.	
	95CC07	granite	39°44.54′ 105°17.60′	1877	20	3.86 (482)	3.71 (2314)	1.04 (3825)	**59.7 ± 4.0**	92	37	14.0 ± 0.3 (76)	1.2
	95CC08	granitic gneiss	39°44.61′ 105°17.09′	1938	20	2.05 (262)	1.92 (1229)	1.04 (3825)	**61.0 ± 4.9**	99	19	14.2 ± 0.3 (31)	0.9
	95CC09	granitic gneiss	39°45.12′ 105°21.52′	2645	20	2.37 (265)	2.51 (1403)	1.03 (3825)	**54.0 ± 4.3**	95	25	14.6 ± 0.7 (7)	0.9
	95CC10	granitic gneiss	39°44.88′ 105°21.66′	2518	20	1.78 (128)	1.77 (638)	1.03 (3825)	**57.2 ± 6.0**	99	18	N.D.	N.D.
	95CC11	granitic gneiss	39°44.61′ 105°22.03′	2316	20	1.84 (212)	1.57 (902)	1.02 (3825)	**66.8 ± 5.8**	99	16	N.D.	N.D.
	95CC12	granitic gneiss	39°44.07′ 105°22.04′	2218	20	3.11 (329)	3.32 (1751)	1.02 (3825)	**53.3 ± 3.9**	98	33	14.4 ± 0.3 (57)	1.1
	96CC13	granitic gneiss	39°44.78′ 105°16.86′	2152	20	4.29 (536)	1.02 (635)	0.267 (1011)	**61.8 ± 4.5**	99	49	14.0 ± 0.3 (97)	1.6
	96CC14	granitic gneiss	39°44.71′ 105°16.94′	2097	20	7.54 (603)	1.99 (795)	0.269 (1011)	**56.0 ± 3.8**	96	77	14.0 ± 0.4 (100)	1.9
	96CC15	granitic gneiss	39°44.59′ 105°16.94′	2030	20	2.73 (297)	0.64 (349)	0.27 (1011)	**63.1 ± 5.6**	99	25	13.8 ± 0.3 (69)	1.4
	96CC16	granitic gneiss	39°44.56′ 105°16.97′	1951	20	2.96 (379)	0.74 (477)	0.271 (1011)	**59.4 ± 4.8**	99	28	13.9 ± 0.3 (108)	1.4
Grays Peak	00GP02	gneiss	39°38.15′ 105°48.67′	4139	20	1.93 (207)	2.36 (1266)	0.957	**43.0 ± 3.7**	93	26	14.1 ± 0.7 (28)	1.9
Deer Creek	99DC04	granite and biotite schist	39°32.77′ 105°09.60′	1829	20	1.14 (966)	3.44 (1461)	1.302 (4601)	**233.1 ± 13.3**	10	28	10.0 ± 0.9 (47)	2.7
	99DC05	granite	39°32.65′ 105°10.13′	1886	15	1.78 (111)	0.93 (292)	1.301 (4601)	**135.0 ± 15.6**	70	7		
North Fork South Platte River	94SPR07	granite	39°28.10′ 105°44.82′	2850	20	2.69 (179)	1.98 (659)	0.96 (3756)	**71.5 ± 6.9**	60	22	N.D.	N.D.
	94SPR08	granite	39°27.72′ 105°40.70′	2700	20	3.18 (376)	2.89 (1711)	0.96 (3756)	**57.6 ± 4.1**	99	32	13.0 ± 0.7 (25)	1.9
	94SPR10	granite	39°24.86′ 105°31.12′	2414	20	2.26 (159)	1.86 (656)	0.96 (3756)	**60.5 ± 6.8**	75	20	N.D.	N.D
	94SPR11	schist	39°23.00′ 105°26.71′	2353	20	6.67 (459)	2.93 (1010)	0.96 (3756)	**115.7 ± 9.3**	30	32	10.7 ± 0.6 (61)	2.4
	94SPR12	diorite	39°24.36′ 105°28.34′	2365	20	2.06 (81)	1.79 (352)	0.95 (3756)	**59.6 ± 7.7**	99	20	12.1 ± 1.0 (26)	2.6
	94SPR13	granite	39°25.44′ 105°27.98′	2521	20	7.23 (377)	2.61 (680)	0.95 (3756)	**117.1 ± 12.8**	<1	29	N.D.	N.D.
	94SPR14	granite	39°28.13′ 105°14.43′	2219	20	1.87 (228)	1.46 (889)	0.93 (3756)	**65.9 ± 5.7**	92	16	12.2 ± 0.6 (77)	2.8
	94SPR15	granite	39°26.33′ 105°13.58′	1999	20	5.16 (578)	2.31 (1292)	0.93 (3756)	**114.1 ± 7.6**	60	24	10.7 ± 0.4 (95)	2.2
	94SPR16	amphibolite	39°24.65′ 105°09.85′	1878	20	0.97 (115)	0.97 (576)	0.93 (3756)	**51.0 ± 5.6**	>99	11	13.1 ± 0.9 (12)	1.5
	94SPR17	granodiorite	39°29.11′ 105°06.45′	1708	20	6.73 (689)	1.71 (877)	0.92 (3756)	**197.4 ± 12.7**	>99	19	10.4 ± 0.5 (85)	2.5

TABLE 1—continued

Traverse name	Sample number	Rock type	Latitude (N) Longitude (W)	Elevation (m)	Number of grains dated	ρ_s x 10^5 t/cm^2	ρ_i x 10^6 t/cm^2	ρ_d x 10^5 t/cm^2	Central age (Ma) (± 1 S.E.)	P(χ)^2 (%)	Uranium content (ppm)	Mean track length (µm) (± 1 S.E.)	Standard deviation track length
	94SPR19	gneiss	39°26.33′ 105°07.42′	1798	20	1.52 (100)	1.66 (546)	0.92 (3756)	**47.1 ± 6.4**	55	19	N.D.	N.D.
	94SPR20	gneiss	39°26.77′ 105°07.30′	1768	20	3.45 (408)	2.67 (1578)	0.92 (3756)	**65.2 ± 4.5**	>99	30	12.7 ± 0.7 (34)	2.1
	94SPR21	granite	39°28.65′ 105°07.77″	1762	19	8.76 (841)	6.83 (3278)	0.9 (3756)	**64.4 ± 4.1**	10	78	12.0 ± 0.5 (80)	2.4
	95SPR22	gneiss	39°24.80′ 105°28.38′	2432	20	4.17 (322)	2.00 (771)	1.08 (3825)	**122.8 ± 10.1**	45	19	12.5 ± 1.1 (10)	1.8
	95SPR23B	granite	39°25.13′ 105°28.31′	2463	20	1.19 (149)	4.62 (288)	1.08 (3825)	**151.9 ± 16.1**	99	4	13.1 ± 1.0 (28)	2.6
	95SPR24	granite	39°22.15′ 105°32.81′	3554	20	4.86 (451)	1.83 (848)	1.08 (3825)	**155.8 ± 11.0**	96	18	12.8 ± 0.9 (30)	2.6
	95SPR25	granodiorite	39°22.95′ 105°32.56′	3042	25	5.67 (835)	2.4 (1768)	1.08 (3825)	**130.9 ± 9.4**	3	23	13.1 ± 0.7 (54)	2.6
	95SPR26	granitic gniess	39°23.62′ 105°31.83′	2749	20	18.61 (1429)	7.22 (2775)	1.08 (3825)	**149.9 ± 8.4**	22	70	12.7 ± 0.5 (100)	2.5
	95SPR27	granitic gniess	39°23.83′ 105°31.23′	2603	20	5.64 (233)	2.75 (568)	1.07 (3825)	**119.6 ± 10.7**	80	27	12.7 ± 1.2 (19)	2.7
	95SPR29	Granite	39°26.98′ 105°07.09′	2060	20	7.04 (811)	3.57 (2055)	1.07 (3825)	**111.9 ± 7.7**	8	35	12.5 ± 0.6 (73)	2.4
	95SPR30	granitic gniess	39°27.04′ 105°07.11′	2012	20	3.24 (405)	1.58 (984)	1.06 (3825)	**118.9 ± 8.8**	80	15	12.6 ± 0.7 (62)	2.8
	95SPR31	Granite	39°28.62′ 105°08.77′	2085	20	2.75 (308)	2.07 (1160)	1.05 (3825)	**76.8 ± 6.0**	94	20	13.1 ± 0.7 (45)	2.5
	95SPR32	granitic gniess	39°28.50′ 105°08.44′	1981	20	3.58 (378)	2.59 (1368)	1.05 (3825)	**79.8 ± 5.8**	93	26	13.2 ± 0.5 (100)	2.4
	95SPR33	Schist	39°28.32′ 105°08.07′	1719	20	1.82 (170)	1.6 (742)	1.05 (3825)	**66.1 ± 6.2**	99	16	14.3 ± 0.9 (5)	1.0
	95SPR34	granitic gniess	39°28.76′ 105°07.62′	1713	20	4.04 (452)	2.22 (1243)	1.05 (3825)	**93.4 ± 8.8**	1	22	12.6 ± 0.9 (26)	2.2
	95SPR35	gneiss/schist	39°29.00′ 105°07.15′	1707	20	4.23 (528)	1.96 (1225)	1.05 (3825)	**119.6 ± 12.2**	<1	20	11.8 ± 0.6 (80)	2.5
	96SPR37	sandstone dike float	39°26.02′ 105°07.11′	1813	20	4.31 (455)	0.96 (508)	0.282 (1011)	**69.3 ± 5.3**	99	36	13.0 ± 0.6 (78)	2.5
	96SPR38	gneiss	39°25.59′ 105°07.53′	2073	20	0.99 (68)	0.22 (76)	0.282 (1011)	**69.2 ± 11.8**	99	8	N.D.	
	96SPR39	gneiss	39°25.70′ 105°07.32′	2012	20	4.48 (516)	0.98 (565)	0.282 (1011)	**70.6 ± 5.2**	85	36	13.2 ± 0.8 (20)	1.8
	96SPR40	gneiss	39°25.54′ 105°07.27′	1963	20	1.17 (119)	0.37 (130)	0.282 (1011)	**70.8 ± 9.3**	>99	14	13.3 ± 1.0 (12)	1.7
	96SPR42	gneiss	39°25.71′ 105°07.09′	1902	20	6.54 (795)	1.36 (829)	0.282 (1011)	**74.2 ± 4.8**	>99	50	13.2 ± 0.4 (103)	2
	96SPR44	granitic gneiss	39°29.73′ 105°37.85′	3923	17	5.99 (364)	0.68 (208)	0.282 (1011)	**134.7 ± 12.7**	>99	25	n.d.	N.D.
	96SPR45	granitic gneiss	39°30.95′ 105°39.60′	3275	20	4.83 (618)	1.04 (667)	0.282 (1011)	**71.7 ± 5.0**	>99	38	13.2 ± 0.9 (29)	2.4
	96SPR47B	biotite gniess	39°30.11′ 105°41.00′	2875	20	8.4 (578)	2.22 (765)	0.282 (1011)	**58.5 ± 4.1**	80	82	13.1 ± 0.6 (51)	2.0

TABLE 1—continued

Traverse name	Sample number	Rock type	Latitude (N) Longitude (W)	Elevation (m)	Number of grains dated	ρ_s x 10^5 t/cm^2	ρ_i x 10^6 t/cm^2	ρ_d x 10^5 t/cm^2	Central age (Ma) (± 1 S.E.)	P(χ)^2 (%)	Uranium content (ppm)	Mean track length (μm) (± 1 S.E.)	Standard deviation track length
	96SPR48	granitic gneiss	39°28.97′ 105°41.56′	2750	20	5.4 (656)	1.26 (769)	0.282 (1011)	**66.0 ± 4.5**	>99	47	13.6 ± 0.4 (103)	1.8
	00BenTy01	gneiss	39°26.17′ 105°35.45′	2560	20	3.73 (388)	2.46 (1278)	0.948 (4600)	**78.9 ± 5.6**	20	27	14.6 ± 0.4 (31)	1.0
	00BenTy03	gneiss	39°24.80′ 105°39.36′	3560	20	3.27 (392)	1.61 (963)	0.938 (4600)	**104.5 ± 7.6**	20	18	12.2 ± 1.3 (19)	1.3
	00BenTy04	quartz monzonite	39°24.93′ 105°40.82′	3743	20	3.16 (404)	1.41 (903)	0.948 (4600)	**115.9 ± 8.4**	20	16	13.4 ± 0.5 (57)	2.0
	00BenTy05	gneiss	39°24.93′ 105°38.44′	3334	13	0.61 (30)	0.56 (137)	0.913 (4600)	**55.1 ± 11.2**	92	6		
Pikes Peak	92PP01	quartz monzonite	38°42.20′ 104°50.60′	1951	19	4.5 (666)	1.96 (1449)	1.35 (3900)	**171.0 ± 9.9**	77	15	11.1 ± 0.4 (161)	2.5
	92PP02	quartz monzonite	38°35.30′ 104°56.90′	2055	20	0.87 (133)	1.5 (1140)	1.37 (3900)	**44.5 ± 4.3**	99	11	13.4 ± 0.3 (100)	1.6
	92PP03	granodiorite	38°41.24′ 105°03.14′	2680	20	1.94 (186)	1.22 (584)	1.39 (3900)	**123.6 ± 11.2**	75	9	12.4 ± 0.5 (111)	2.8
	92PP04	granodiorite	38°42.16′ 105°07.48″	2963	20	1.97 (232)	5.81 (3429)	1.41 (3900)	**26.9 ± 2.0**	99	42	14.4 ± 0.3 (92)	1.6
	92PP05	granodiorite	38°39.24′ 105°06.95′	2771	20	1.07 (154)	0.4 (289)	1.47 (3900)	**211.7 ± 21.3**	99	3	11.1 ± 0.7 (37)	2.2
	92PP06	granodiorite	38°36.84′ 105°08.00′	2482	20	4.61 (470)	5.72 (2915)	1.51 (3900)	**66.2 ± 3.9**	99	40	12.1 ± 0.5 (100)	2.4
	92PP07	granodiorite	38°34.29′ 105°05.16′	2183	20	1.00 (142)	1.26 (895)	1.53 (3900)	**66.6 ± 6.3**	99	9	12.5 ± 0.4 (81)	2
	92PP08	migmatitic gneiss	38°32.92′ 105°06.22′	2054	20	0.33 (47)	0.55 (355)	1.55 (3900)	**56.8 ± 8.9**	99	3	10.8 ± 0.9 (21)	2.1
	92PP09	migmatitic gneiss	38°31.17′ 105°07.49′	1866	20	0.95 (148)	1.39 (1085)	1.57 (3900)	**59.7 ± 5.5**	99	9	12.6 ± 0.9 (34)	2.8
	92PP10	migmatitic gneiss	38°30.24′ 105°06.29′	1777	13	1.06 (76)	1.65 (595)	1.6 (3900)	**57.1 ± 7.1**	99	11	12.8 ± 0.9 (43)	2.8
Garden Park	93GP01	granodiorite	38°39.23′ 105°13.23′	2061	20	6.31 (669)	4.10 (2173)	1.28 (3719)	**110.9 ± 6.7**	20	33	11.8 ± 0.4 (107)	2.1
	93GP02	granodiorite	38°37.65 105°13.13′	1994	20	1.41 (141)	0.58 (290)	1.28 (3719)	**172.2 ± 17.9**	99	5	11.0 ± 0.5 (39)	1.7
	93GP03	granodiorite	38°36.55 105°11.92′	2512	20	0.85 (129)	0.35 (268)	1.28 (3719)	**170.5 ± 18.5**	99	3	11.7 ± 0.8 (34)	2.4
	93GP04B	granodiorite	38°36.59′ 105°12.24′	2329	20	2.58 (305)	1.17 (692)	1.28 (3719)	**156.3 ± 11.6**	99	9	12.7 ± 0.4 (100)	2.3
	93GP05	granodiorite	38°36.65′ 105°12.56′	2122	18	2.34 (197)	0.85 (358)	1.28 (3719)	**194.6 ± 17.7**	99	7	N.D.	N.D.
	93GP06	granodiorite	38°36.85′ 105°12.76	1994	20	3.95 (363)	4.21 (1937)	1.28 (3719)	**66.9 ± 4.4**	99	34	12.4 ± 0.4 (131)	2.4
	93GP07	granodiorite	38°36.37′ 105°13.13	1915	20	3.72 (402)	4.18 (2259)	1.28 (3719)	**63.6 ± 4.0**	96	33	12.2 ± 0.4 (153)	2.4
Elevenmile Reservoir	94SPR02	granite	38°55.86′ 105°29.82′	2615	20	3.05 (208)	2.01 (686)	0.98 (3756)	**80.9 ± 7.2**	99	22	12.1 ± 0.7 (42)	2.3
	94SPR03	pegmatite	38°57.13′ 105°28.27′	2758	20	8.17 (677)	3.02 (1251)	0.97 (3756)	**143.0 ± 9.0**	95	32	11.4 ± 0.6 (73)	2.6

TABLE 1—continued

Traverse name	Sample number	Rock type	Latitude (N) Longitude (W)	Elevation (m)	Number of grains dated	ρ_s x 10^5 t/cm^2	ρ_i x 10^6 t/cm^2	ρ_d x 10^5 t/cm^2	Central age (Ma) (± 1 S.E.)	P(χ)^2 (%)	Uranium content (ppm)	Mean track length (µm) (± 1 S.E.)	Standard deviation track length
	94SPR04	gneiss	38°58.44′ 105°26.87′	2643	20	4.28 (329)	1.63 (625)	0.96 (3756)	**138.7 ± 18.0**	95	18	11.0 ± 1.6 (10)	2.6
	94SPR06	gneiss	38°59.35′ 105°23.33′	2463	20	9.69 (992)	2.00 (1024)	0.96 (3756)	**252.1 ± 15.8**	50	22	11.1 ± 0.7 (52)	2.5
	11e	granite	38°56.05′ 105°33.52′	2670	20	4.45 (484)	0.73 (397)	0.282 (1011)	**94.1 ± 7.4**	90	28	11.8 ± 1.0 (28)	2.6
	11n	granite	38°56.00′ 105°33.60′	2650	8	6.19 (198)	0.36 (57)	0.282 (1011)	**264.7 ± 39.0**	97	13	12.0 ± 0.6 (39)	1.9
	11s	granite	38°54.12′ 105°30.13′	2639	20	4.18 (348)	0.5 (210)	0.282 (1011)	**127.6 ± 12.1**	99	19	12.2 ± 1.2 (23)	2.9
Agate Creek	CC-Ft	granite	38°50.30 105°46.63′	2880	10	2.22 (96)	0.35 (76)	0.282 (1011)	**97.5 ± 15.2**	95	13	N.D.	
Tarryall Reservoir	94TAR01	monzonite	39°13.35′ 105°37.64′	2743	20	1.5 (91)	1.05 (318)	0.95 (3756)	**74.9 ± 9.3**	99	11	N.D.	N.D.
	94TAR02	monzonite	39°14.15′ 105°36.25′	2737	20	5.28 (592)	3.53 (1976)	0.94 (3756)	**78.4 ± 4.9**	96	38	13.3 ± 0.5 (64)	2.1
Royal Gorge	93RG01	gneiss	38°26.01′ 105°15.89′	1650	20	4.24 (611)	2.62 (1890)	1.3 (3719)	**115.0 ± 6.8**	55	21	11.1 ± 0.5 (79)	2.4
Arkansas River	94ARK01	granodiorite	38°21.59′ 105°44.23′	1981	20	6.24 (659)	5.32 (2808)	1.22 (3756)	**77.5 ± 4.7**	90	46	13.3 ± 0.3 (102)	1.6
	94ARK03	granodiorite	38°22.28′ 105°40.98′	1951	20	2.74 (237)	3.34 (1445)	1.24 (3756)	**54.7 ± 4.5**	90	29	13.4 ± 1.0 (9)	1.6
	95ARK04	granite/ quartzite	38°24.52′ 105°35.60′	1920	20	1.42 (168)	1.06 (627)	1.02 (3825)	**75.8 ± 7.2**	92	10	12.6 ± 1.3 (19)	2.9
	94ARK05	gneiss	38°24.88′ 105°34.44′	1902	20	2.21 (212)	2.02 (968)	1.24 (3756)	**74.9 ± 6.5**	87	17	13.3 ± 0.6 (28)	1.5
	94ARK06	granite	38°26.35′ 105°32.35′	1877	20	3.21 (324)	1.33 (672)	1.25 (3756)	**164.0 ± 13.2**	91	11	12.8 ± 0.7 (20)	1.6
	94ARK07	gneiss	38°26.70′ 105°31.64′	1853	14	3.8 (124)	2.88 (470)	1.26 (3756)	**91.7 ± 9.9**	99	24	N.D.	N.D.
	95ARK07	granite/ pegmatite	38°26.84′ 105°31.25′	1853	20	4.22 (514)	1.83 (1113)	1.02 (3825)	**126.2 ± 10.0**	6	19	13.7 ± 0.7 (21)	1.6
	94ARK08	diorite	38°29.05′ 105°24.40′	1768	20	5.87 (517)	2.41 (1061)	1.26 (3756)	**169.8 ± 11.3**	99	20	11.7 ± 0.5 (83)	2.2
	94ARK09	diorite	38°29.21′ 105°22.24′	1756	20	8.53 (669)	3.47 (1359)	1.27 (3756)	**173.8 ± 11.9**	48	28	10.2 ± 0.5 (68)	2.1
	94ARK10	granodiorite	38°28.31′ 105°26.82′	1780	20	1.91 (220)	7.9 (455)	1.28 (3756)	**171.3 ± 15.3**	99	6	11.6 ± 0.9 (28)	2.4
	94ARK11	gneiss	38°27.28′ 105°30.00′	1841	17	3.86 (241)	2.05 (639)	1.29 (3756)	**134.0 ± 11.8**	85	16	N.D.	N.D.
	95ARK11	pegmatite	38°27.14′ 105°29.66′	1829	20	3.01 (356)	1.34 (793)	1.01 (3825)	**128.8 ± 10.8**	65	14	13.3 ± 0.7 (6)	0.9
	97ARK12	Garrell Peak granodiorite	38°26.22 105°39.98′	2515	18	7.72 (329)	8.83 (1881)	1.18 (3756)	**62.5 ± 4.6**	80	71		
	97ARK13	Garrell Peak granodiorite	38°26.33′ 105°40.62′	2362	20	8.82 (367)	11.01 (2102)	1.18 (3756)	**62.4 ± 4.4**	83	81	13.8 ± 0.4 (76)	1.8
	97ARK17	Garrell Peak granodiorite	38°29.54′ 105°45.73′	2865	20	5.87 (338)	9.00 (2591)	(3756)	**46.7 ± 3.3**	85	72	13.4 ± 0.8 (34)	2.5

TABLE 1—continued

Traverse name	Sample number	Rock type	Latitude (N) Longitude (W)	Elevation (m)	Number of grains dated	ρ_s x 10^5 t/cm^2	ρ_i x 10^6 t/cm^2	ρ_d x 10^5 t/cm^2	Central age (Ma) (± 1 S.E.)	P(χ)^2 (%)	Uranium content (ppm)	Mean track length (µm) (± 1 S.E.)	Standard deviation track length
	97ARK18	Garrell Peak granodiorite	38°29.78′ 105°47.16′	2633	20	3.31 (164)	4.34 (1077)	(3756)	**54.9 ± 5.1**	93	34	13.6 ± 0.4 (90)	2 0
	97ARK21	Garrell Peak granodiorite	38°26.17′ 105°42.99′	2512	20	3.51 (330)	4.28 (2015)	1.23 (3756)	**59.0 ± 4.3**	75	34	13.5 ± 0.3 (104)	1.5
	97ARK22	Pennsylvanian arkose	38°25.85′ 105°42.43′	2396	20	2.36 (242)	2.69 (1376)	1.24 (3756)	**63.9 ± 5.2**	80	21	13.3 ± 0.6 (44)	2.0
	97ARK24	qtz. monzonite	38°27.42′ 105°35.07′	2516	20	4.00 (435)	3.3 (1793)	1.31 (3756)	**87.9 ± 6.0**	20	26	10.9 ± 0.6 (79)	2.7
	97ARK25	gneiss	38°27.47′ 105°35.34′	2390	20	8.46 (921)	2.87 (1559)	1.35 (3756)	**212.1 ± 12.2**	<1	23	11.7 ± 0.4 (104)	2.2
	97ARK26	gneiss	38°27.17′ 105°35.54′	2219	20	4.31 (489)	3.25 (1847)	0.95 (3756)	**95.9 ± 6.3**	<1	26	12.3 ± 0.8 (54)	3
Currant Creek	Egd	granodiorite	38°33.56′ 105°25.39′	1999	20	12.67 (831)	0.84 (276)	0.282 (1011)	**230.0 ± 17.9**	99	31	12.0 ± 0.6 (60)	2.2
shear zone	Egn	gneiss	38°36.90′ 105°27.99′	2329	20	8.96 (631)	0.69 (242)	0.282 (1011)	**199.7 ± 16.7**	99	25	12.7 ± 0.6 (46)	2.1
	Wgn	gneiss	38°37.38′ 105°29.19′	2396	20	10.59 (542)	0.88 (226)	0.282 (1011)	**183.9 ± 16.0**	83	33	12.2 ± 0.3 (79)	1.5
	Eqd	quartz diorite	38°37.19′ 105°26.92′	2268	20	1.84 (141)	0.47 (180)	0.282 (1011)	**60.6 ± 7.2**	99	17	13.7 ± 2.2 (10)	3.6
	Wqd	quartz diorite	38°36.71′ 105°26.94′	2280	20	4.19 (295)	0.76 (267)	0.282 (1011)	**85.4 ± 8**	98	29	13.6 ± 0.6 (36)	1.8
	EGN2	gneiss	38°39.62′ 105°28.51′	2408	20	5.18 (514)	4.47 (2215)	1.334 (3756)	**84.8 ± 5.5**	10	35	13.6 ± 0.4 (101)	2.1
Wet Mountains	92WM01	granodiorite	38°20.7′ 105°14.0′	1911	20	5.08 (610)	1.37 (820)	0.97 (3900)	**195.1 ± 11.8**	97	15	11.0 ± 0.3 (103)	1.5
	92WM03	granodiorite	38°19.9′ 105°14.6′	2241	20	7.84 (502)	1.55 (496)	1.09 (3900)	**298.8 ± 20.1**	99	15	11.7 ± 0.5 (40)	1.5
	92WM04	granodiorite	38°19.8′ 105°14.1′	2108	20	7.91 (1234)	1.47 (1144)	0.97 (3900)	**290.2 ± 14.5**	99	15	11.3 ± 0.4 (67)	1.5
	92WM05	granite	38°17.8′ 105°15.65′	2311	7	0.47 (19)	0.32 (65)	1.00 (3900)	**80.8 ± 21.2**	65	3	N.D.	N.D.
	92WM07	migmatitic gneiss	38°13.6′ 105°20.7′	2414	20	4.59 (597)	1.35 (877)	1.00 (3900)	**188.6 ± 11.4**	97	14	12.9 ± 0.6 (32)	1.7
	92WM08	migmatitic gneiss	38°12.3′ 105°22.0′	2469	20	2.54 (366)	1.02 (732)	1.02 (3900)	**140.6 ± 10.2**	90	10	12.3 ± 0.4 (92)	2.0
	92WM09	migmatitic gneiss	38°10.9′ 105°24.4′	2411	20	6.97 (516)	2.18 (808)	1.02 (3900)	**180.8 ± 11.4**	99	22	13.0 ± 0.3 (104)	1.7
	92WM10	migmatitic gneiss	38°09.9′ 105°11.5′	2561	15	5.29 (360)	2.47 (841)	1.05 (3900)	**123.0 ± 8.8**	80	24	11.7 ± 0.5 (83)	2.4
	92WM11	granite	38°09.6′ 105°15.6′	2741	10	3.75 (150)	1.97 (394)	1.05 (3900)	**109.5 ± 11.2**	85	20	12.7 ± 0.6 (49)	2.0
	92WM12	migmatitic gneiss	38°10.5′ 105°08.9′	2256	20	1.71 (120)	1.97 (689)	1.1 (3900)	**53.4 ± 5.5**	95	18	11.2 ± 0.4 (142)	2.4
	92WM13	migmatitic gneiss	38°10.5′ 105°10.1′	2390	20	1.53 (181)	0.81 (478)	1.1 (3900)	**115.9 ± 10.6**	99	8	11.3 ± 0.4 (95)	2.1
	92WM14	migmatitic gneiss	38°06.9′ 105°07.6′	2687	20	2.39 (272)	1.05 (601)	1.1 (3900)	**138.4 ± 11.2**	85	10	11.8 ± 0.3 (95)	1.6

TABLE 1—continued

Traverse name	Sample number	Rock type	Latitude (N) Longitude (W)	Elevation (m)	Number of grains dated	ρ_s x 10^5 t/cm^2	ρ_i x 10^6 t/cm^2	ρ_d x 10^5 t/cm^2	Central age (Ma) (± 1 S.E.)	P(χ)^2 (%)	Uranium content (ppm)	Mean track length (µm) (± 1 S.E.)	Standard deviation track length
	92WM15	migmatitic gneiss	38°05.9′ 105°08.7′	2860	20	3.46 (346)	1.79 (894)	1.1 (3900)	**118.8 ± 8.6**	75	17	11.9 ± 0.5 (100)	2.5
	92WM16	migmatitic gneiss	37°54.0′ 105°01.4′	3564	20	4.89 (372)	1.31 (497)	1.11 (3900)	**228.3 ± 16.6**	99	12	12.3 ± 0.4 (45)	1.3
	92WM19	granite	37°53.6′ 105°02.4′	3506	20	5.71 (651)	1.59 (906)	1.11 (3900)	**219.8 ± 12.9**	99	15	12.5 ± 0.3 (103)	1.5
	92WM20	granite	37°56.0′ 105°04.0′	3445	20	3.17 (380)	1.04 (623)	1.12 (3900)	**187.4 ± 13.2**	99	10	12.5 ± 0.3 (102)	1.8
	92WM22	granite	38°00.05′ 105°10.95′	3171	20	4.89 (607)	1.43 (885)	1.13 (3900)	**210.7 ± 12.6**	96	13	12.5 ± 0.3 (100)	1.5
	92WM24	granite	37°54.05′ 105°00.8′	3116	20	5.05 (576)	1.57 (894)	1.13 (3900)	**199.1 ± 12.9**	60	14	12.2 ± 0.3 (100)	1.6
	92WM26	gneiss	37°54.95′ 104°59.7′	2521	20	6.09 (755)	2.27 (1406)	1.13 (3900)	**166.5 ± 9.4**	90	21	11.4 ± 0.4 (100)	2.0
	92WM27	migmatitic gneiss	37°55.1′ 104°58.4′	2329	20	0.64 (70)	0.77 (424)	1.13 (3900)	**51.7 ± 6.8**	99	7	11.6 ± 0.7 (43)	2.3
	93WM29	migmatitic gneiss	38°10.57′ 105°07.77′	2175	20	1.05 (554)	6.01 (1579)	1.3 (2719)	**122.3 ± 8.3**	15	48	12.2 ± 1.0 (15)	2.0
	93WM30	migmatitic gneiss	38° 04.59′ 104°59.49′	1940	20	0.1 (149)	2.19 (1706)	1.26 (3900)	**31.3 ± 2.9**	95	18	12.5 ± 0.4 (127)	2.6
	93WM31	migmatitic gneiss	38°02.78′ 105°00.24′	1900	12	2.16 (82)	4.96 (943)	1.25 (3900)	**31.1 ± 3.7**	95	40	12.0 ± 1.4 (15)	2.9